39

Coordinated Determination of Preventive and Curative Actions for Congestion Management in Power Systems

Tom Sennewald

Ilmenauer Beiträge zur elektrischen Energiesystem-, Geräte- und Anlagentechnik

TECHNISCHE UNIVERSITÄT
ILMENAU

Tom Sennewald

Coordinated Determination of Preventive and Curative Actions for Congestion Management in Power Systems

Ilmenauer Beiträge zur elektrischen Energiesystem-, Geräte- und Anlagentechnik (IBEGA)

Herausgegeben von
Univ.-Prof. Dr.-Ing. Dirk Westermann
(Fachgebiet Elektrische Energieversorgung) und
Univ.-Prof. Dr.-Ing. Frank Berger
(Fachgebiet Elektrische Geräte und Anlagen)
an der Technischen Universität Ilmenau.

Band 39

Tom Sennewald

Coordinated Determination of Preventive and Curative Actions for Congestion Management in Power Systems

Universitätsverlag Ilmenau
2024

Impressum

Bibliografische Information der Deutschen Nationalbibliothek
Die Deutsche Nationalbibliothek verzeichnet diese Publikation in der Deutschen Nationalbibliografie; detaillierte bibliografische Angaben sind im Internet über http://dnb.d-nb.de abrufbar.

Diese Arbeit hat der Fakultät für Elektrotechnik und Informationstechnik der Technischen Universität Ilmenau als Dissertation vorgelegen.

Tag der Einreichung:	03. November 2023
1. Gutachter:	Univ.-Prof. Dr.-Ing. Dirk Westermann (Technische Universität Ilmenau)
2. Gutachter:	Univ.-Prof. Dr.-Ing. Matthias Luther (Friedrich-Alexander-Universität Erlangen-Nürnberg)
3. Gutachter:	Hon.-Prof. Dr.-Ing. Rainer Krebs (Siemens AG)
Tag der Verteidigung:	07. Juni 2024

Technische Universität Ilmenau/Universitätsbibliothek
Universitätsverlag Ilmenau
Postfach 10 05 65
98684 Ilmenau
https://www.tu-ilmenau.de/universitaetsverlag

ISSN 2194-2838
DOI 10.22032/dbt.61594
URN urn:nbn:de:gbv:ilm1-2024000223

With great power comes great responsibility

(Benjamin Franklin Parker)

Acknowledgment

Die Fertigstellung dieser Dissertation wäre ohne die Unterstützung, Anleitung und Ermutigung vieler Menschen nicht möglich gewesen.

Zunächst möchte ich meinem Doktorvater, Herrn Univ.-Prof. Dr.-Ing. Dirk Westermann, meinen tiefsten Dank aussprechen. Seine Expertise, sein Verständnis und seine Geduld haben wesentlich zu meiner wissenschaftlichen Entwicklung beigetragen. Ich schätze alle seine zeitlichen und ideellen Beiträge, die meine Promotion produktiv und anregend gestaltet haben. Seine Freude und Begeisterung für Forschung und Lehre waren ansteckend und haben mich selbst in schwierigen Zeiten motiviert.

Ich möchte auch Herrn Univ.-Prof. Dr.-Ing. Matthias Luther von der Friedrich-Alexander-Universität Erlangen-Nürnberg und Herrn Hon.-Prof. Dr.-Ing. Rainer Krebs von der Siemens AG für ihre Rolle als Gutachter herzlich danken. Ihre wertvollen Kommentare und Anregungen waren entscheidend für die Verfeinerung dieser Arbeit. Ihr fachliches Wissen und ihre konstruktive Kritik haben die Qualität dieser Dissertation erheblich verbessert.

Ein besonderer Dank gilt meinen Kolleginnen und Kollegen des Fachgebiets Elektrische Energieversorgung. Dr.-Ing. Steffen Schlegel, Dr.-Ing. Robert Schwerdfeger and Dr.-Ing. Anne-Katrin Marten waren die ersten Ansprechpartner während meiner studentischen Tätigkeit und haben dafür gesorgt, mich als Teil des Teams zu fühlen. Weiterhin gilt mein Dank Dr.-Ing. Florian Sass, Dr.-Ing. Christoph Brosinsky, M.Sc. Franz Linke und M.Sc. Elisabeth Feldhoff, die mich durch inhaltliche Diskussion und auch Abenteuer abseits des Büroalltags auf meinem Weg begleiteten.

Mein herzlicher Dank gilt meiner Familie. Worte können nicht ausdrücken, wie dankbar ich meinen Eltern bin. Ihre unerschütterliche Liebe und Unterstützung haben mich während dieser Reise motiviert und fokussiert gehalten.

Diese Dissertation ist all denen gewidmet, die mich bei ihrer Fertigstellung unterstützt haben. Ohne euch hätte ich diesen Meilenstein nicht erreichen können.

Kurzfassung

Die Energiewende treibt die Entwicklung der Übertragungsnetze in Europa und weltweit entscheidend voran. Die Hochspannungs-Gleichstrom-Übertragung (HGÜ) ist der Schlüssel für die Fernübertragung und es entsteht ein vermaschtes HGÜ-Überlagerungssystem. Um den Netzausbau zu minimieren, müssen die bestehenden Anlagen in ihrem Betrieb optimiert werden, was neue Steuerungselemente wie Speichereinheiten und Regeltransformatoren erfordert. Ein effizientes Management dieser Steuerungsoptionen ist für die Systemsicherheit von entscheidender Bedeutung, wobei eine Verlagerung hin zu aktiver (N-1)-Sicherheit durch präventiv-kurative Maßnahmen wie HGÜ-Eingriffe eine unabdingbare Komponente der sich entwickelnden Energielandschaft darstellt. In dieser Arbeit wird ein innovativer Ansatz für die Koordination von präventiven und kurativen Engpassmanagementmaßnahmen in elektrischen Energiesystemen vorgestellt.

Die Arbeit enthält eine umfassende Analyse der aktuellen betrieblichen Planungslandschaft, die als Grundlage für die Entwicklung eines neuartigen Optimierungsmodells dient, das die Koordination von Engpassmanagementmaßnahmen erleichtern soll. Es wird eine Betrachtung von Optimierungsproblemen durchgeführt, die für die Betriebsplanung relevant sind, wobei diese Herausforderungen anhand ihrer Relevanz für verschiedene Planungsprozesse kategorisiert werden.

Ein besonderer Schwerpunkt liegt dabei auf dem Optimal Power Flow. Dieses Optimierungsproblem ist die Grundlage für die Ermittlung von Engpassmanagementmaßnahmen in der Betriebsplanung, insbesondere die Erweiterung der Methode im Hinblick auf Sicherheitsdefinitionen sowie deren Formulierung im Vor- und Nach-Fehlerzustand. Diese Formulierungen werden in ein BLP-SCOPF-Modell integriert und ermöglichen die Integration der kurativen Optimierung in den Rahmen der präventiven Planung durch den Einsatz der bilevel Programmierung. Dies ermöglicht eine koordinierte Bestimmung von präventiven und kurativen Maßnahmen.

Die Lösung des Bilevel-Modells stellt aufgrund seiner nicht-konvexen, nicht-linearen und $\mathcal{NP}$-schweren Natur eine erhebliche rechnerische Herausforderung dar. Um dieses Problem zu lösen, wird ein spezieller hybrider Lösungsalgorithmus vorgeschlagen, der auf dem Algorithmus der Differential Evolution basiert und die Anforderungen des komplexen Problems erfüllt.

Im weiteren Verlauf der Arbeit werden das vorgeschlagene Optimierungsmodell und der Lösungsalgorithmus anhand mehrerer Fallstudien untersucht. Diese Fallstudien bewerten die Auswirkungen der Berücksichtigung von kurativen Maßnahmen neben präventiven Maßnahmen im Planungsprozess und untersuchen die Priorisierung von präventiven oder kurativen Engpassmanagementmaßnahmen. Darüber hinaus werden die Folgen für die Kosten und die Komplexität der Berechnungen untersucht, um ein umfassendes Verständnis für die praktischen Auswirkungen des vorgeschlagenen Ansatzes zu erhalten.

Diese Forschungsarbeit leistet einen wichtigen Beitrag zum Bereich der Betriebsplanung von Stromnetzen, indem sie einen Rahmen für die Koordinierung von präventiven und kurativen Maßnahmen bietet, die letztlich die Zuverlässigkeit und die Widerstandsfähigkeit der Stromnetze angesichts der sich entwickelnden Herausforderungen gewährleisten. Es bietet ein wertvolles

Instrument für Netzbetreiber, um die Effizienz und Sicherheit ihres Systems zu verbessern und gleichzeitig die dynamische Natur der heutigen Energielandschaft effektiv zu bewältigen.

Abstract

The energy transition is driving significant developments in Europe and worldwide's transmission systems. High voltage DC (HVDC) technology is the key for long-distance transmission, with the emergence of a meshed HVDC overlay system. To minimize network expansion, existing assets must be optimized in their operation, requiring new control elements such as storage units and regulating transformers. Efficiently managing these control options is crucial for system security, with a shift towards active (N-1) security through preventive-curative measures like HVDC intervention, making it an imperative component of the evolving energy landscape. This thesis introduces an innovative approach for the coordination of preventive and curative congestion management measures in electrical power systems.

The thesis gives a comprehensive analysis of the current operational planning landscape, serving as a foundation for the development of a novel optimization model designed to facilitate the coordination of congestion management measures. A review of optimization problems relevant to operational planning is conducted, categorizing these challenges based on their relevance to different planning processes.

A special focus is on the Optimal Power Flow. This optimization problem is the basis for the determination of congestion management measures in operational planning, in particular the extension of the method with respect to security definitions as well as their formulations regarding the pre- and post-fault state. These formulations are integrated into a BLP-SCOPF model, enabling the integration of curative optimization into the preventive planning framework by the use of bilevel programming. This allows a coordinated determination of preventive and curative measures.

Solving the bilevel model poses a significant computational challenge due to its non-convex, non-linear and $\mathcal{NP}$-hard nature. To address this, a specialized hybrid solver based on the Differential Evolution algorithm is proposed, meeting the requirements of the complex problem.

The thesis proceeds to evaluate the proposed optimization model and solver through multiple case studies. These case studies assess the impact of considering curative actions alongside preventive measures in the planning process and explore the prioritization of either preventive or curative congestion management measures. Additionally, the research investigates cost implications and computational complexities, providing a comprehensive understanding of the practical implications of the proposed approach.

This research contributes significantly to the field of power system operational planning by offering a framework for the coordination of preventive and curative actions, ultimately ensuring the reliability and resilience of power systems in the face of evolving challenges. It provides a valuable tool for power system operators and planners to enhance the efficiency and security of their operations while effectively managing the dynamic nature of today's energy landscape.

Table of content

1 Introduction

1.1 Motivation

Power system operation is currently faced with challenges in regard of the change in the generation mix. Accelerated by the progression of the global climate change and events like the destruction of the nuclear power plant in Fukushima, political decision makers see the need to act and prepare the necessary frameworks to move to a more environmentally friendly energy supply [1–4]. As a result, conventional fossil and nuclear fueled power plant sare disconnected from the system and at national [5–7] and European level [8, 9], a rising share of renewable energy sources (RESs) is observed. According to [7, 10], 80 % of the German electric grid national power consumption (GNPC) has to be provided by renewables by 2050. Fig. 1.1 shows the development for Germany with the total amount of energy generation by RES and its share on the GNPC from 1996 (the beginning of the unbundling process) until 2022 [7, 11]. Compared to the increasing share of renewable energies, a slight decrease in the GNPC can be observed from 2007 onwards [12]. The GNPC peaked in 2007 with a total consumption of 614.6 TWh and was lowered to 546.5 TWh in 2022 [12]. When looking at the installed capacity of RES, the total volume almost tripled in the same time span from 89.4 TWh to 254.0 TWh with a threefold increase of wind energy and a twenty-fold increase in photovoltaics [7, 11]. As of the end of 2022, 66.2 GW of on- and offshore wind farms and 67.4 GW of solar power are installed in Germany [13].

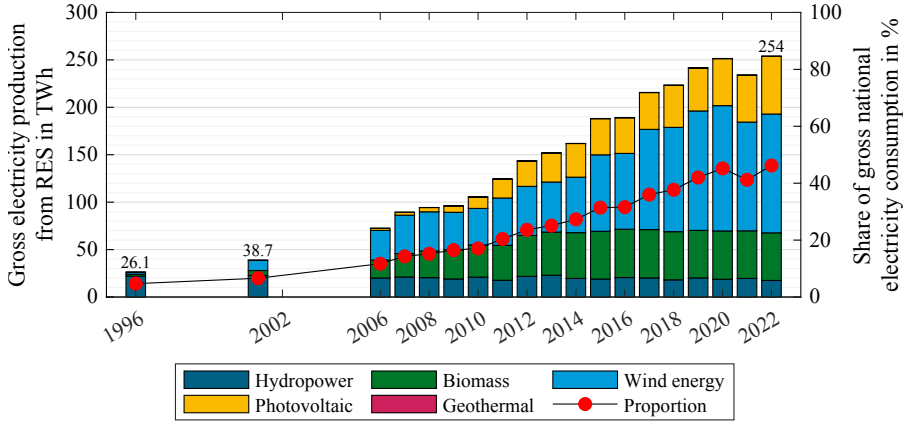

Figure 1.1: Development of energy generation by RES and its share on the GNPC in Germany from 1996 to 2022 [7, 11]

The change in the generation landscape leads to regional imbalances regarding the demand as the conventional generating units that are installed close to the demand centers are replaced by distributed RESs [14]. This leads to an increasing amount of congestions in the German transmission system, especially caused by the vast amount of offshore wind energy (8.1 GW as of 2022 [13]) and the missing load centers near the coast. To address this, all grid reinforcement and expansion measures determined by the federal requirements plan [15] are collected and described in the network development plan [16] and are pushed by political decision makers (cf. Energy Line Expansion

Act (German: EnLAG, Energieleitungsausbaugesetz) [17] and Grid Expansion Acceleration Act Transmission System (German: NABEG, Netzausbaubeschleunigungsgesetz Übertragungsnetz) [18]). At the European level, this happens in the Ten-Year Network Development Plan (TYNDP) [19].

Since the installation of additional transport capacities in the transmission system are delayed, TSOs must resort to preventive redispatch measures to ensure a reliable system operation. German TSOs are obliged to publish their redispatch measures [6]. The data are aggregated by [20] and used to visualize the total redispatch volume in TWh as well as the total duration of those measures (frequency of intervention) in hours in Fig. 1.2 from 2014 to 2022. After the spike in 2015 with 11.1 TWh, the redispatch volume decreased with the erection of the "Thüringer Strombrücke". This line, connecting the systems of 50Hertz and TenneT TSO Germany, provides additional capacities to reduce congestions in the north to south power transmission (wind energy generation in the north and load centers in the south). Following the initial reduction, since 2019 the volume of redispatch measures is on a rise with a total volume of 10.7 TWh as well as the frequency of intervention for 315, 508 h in 2022.

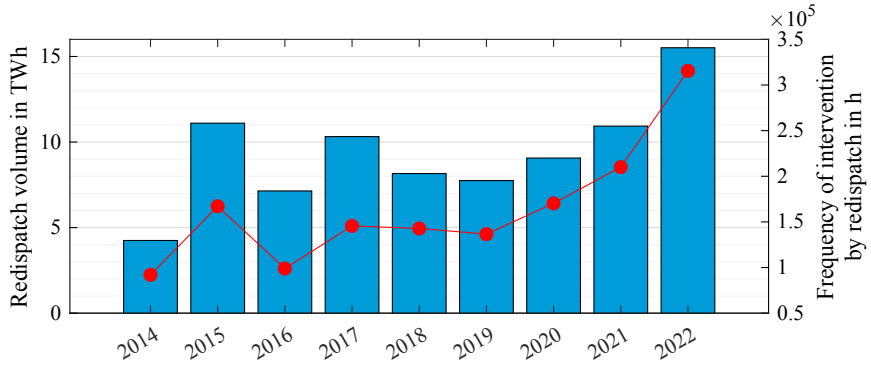

Figure 1.2: Time course of the volume and frequency of intervention of preventive redispatch measures in the German transmission system based on [20]

Besides the reinforcement and expansion measures needed to ensure a secure transmission system operation, the network development plan also describes actions in regard to the optimization of system operation called the NOVA criterion (German: Netzoptimierung vor Verstärkung vor Ausbau, grid optimization before reinforcement and expansion) [16]. The NOVA criterion describes that additional transmission capacities should first be enabled by optimizing already existing equipment (e.g. by overhead line monitoring or topological measures) before reinforcing existing transport corridors and before erecting new lines. One aspect to optimize system operation that is currently discussed by TSOs is the curative system operation or rather the establishment of (N-1) security by enabling curative congestion management measures (CMMs) that are triggered after a fault event.

Currently, the establishment of (N-1) security is realized purely by preventive actions. This means an electrical power system is operated in a way that the loss of any kind of equipment does not

lead to a violation of operational security constraints such as the maximum line loading or voltage range and cascading outages are prevented. To enable this, the power flow in the system is adjusted preventively to reserve enough transmission capacities to, e.g., prevent congestions after a line outage. Simultaneously, preventive power flow controlling measures also inhibit a full utilization of existing equipment. Therefore, the current definition of *preventive (N-1) security* can also be labeled as *passive (N-1) security*, as the systems automatically switches into a (N-0) secure state without any further actions taken. A report from the "System Protection and Dynamics" subgroup of the European Network of Transmission System Operators for Electricity (ENTSO-E) states that "it is not economical to design a power system arbitrarily redundant" and "it is necessary to find a technical and economical trade-off between investment cost, operation cost and power system security needs" [21]. The subgroup concludes that new instruments are needed and proposes the use of curative or corrective CMMs, especially a special protection scheme (SpPS) to address those issues. The general use of such actions is already defined at the European level in the system operation guideline (SO GL). German TSOs are also aware of the necessity of incorporating curative actions in their system operation and investigate the necessary framework e.g. in research projects [22, 23]. Following the labeling of preventive (N-1) security, a system operation scheme incorporating curative actions can be called *active (N-1) security*. Thus, the default system state is in an (N-0) secure state initially. After an event, an automatic action is triggered which leads the network to an (N-0) safe state.

The general operation principle of curative measures compared to preventive ones is depicted in Fig. 1.3 using the transition of system states after a critical contingency event, i.e., an event that leads to the violation operative security constraints. After the occurrence of the event, the operating state leaves the (N-1) secure area. Here, the difference between the preventive and curative approach lies in the area the system state lands in. In a system a passive (N-1) security, the system state transitions in a (N-0) secure state and is then transferred back to the (N-1) secure state with a restoration measures. In an active (N-1) secure concept, a temporary insecure system state is allowed where, e.g., a short-term line overloading is permitted. A suitable curative action then transfers the system state from the (N-0) violation state to the (N-0) secure state.

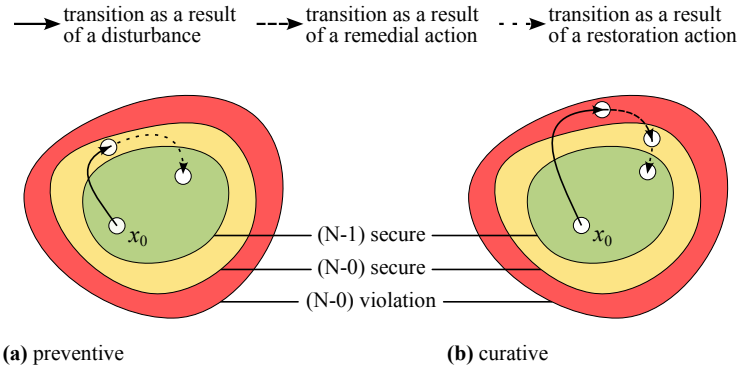

Figure 1.3: State diagram for (a) preventive and (b) curative measures for an outage in the system

Curative actions can be distinguished in continuous and event-based actions [24]. Continuous actions are based on control systems which continuously and automatically support the system. In [25], such a continuous curative action is presented by utilizing an angle control scheme with a voltage source converter (VSC) based high voltage direct current (HVDC) system, as presented by [26]. As such actions are foremost realized with power electronic equipment, due to their small time constants they are especially useful in addressing events endangering the stability of the system [27]. Event-based actions on the other hand are activated after the occurrence of specific events such as line trip signals or signals from overcurrent protective devices. They enable a precise intervention in the system operation to cure the constraint violation. The SO GL [28] defines various degrees of freedom, such as power flow control (e.g. by phase-shifting transformers (PSTs)), topological measures, redispatch of generation units, adjusting the power flow of HVDC systems or load shedding.

1.2 Scope and Scientific Contribution of the Thesis

Within the scope of this thesis, an approach to coordinate the determination of preventive and curative CMMs is proposed. Based on a status-quo analysis on the current landscape of operational planning and optimization in the context of power systems, an optimization model to allow CMM coordination is introduced. A European perspective on operational planning, especially in regard to ensuring system security, is given by detailing the framework described in the SO GL. Based on the European perspective that dictates the realization of the transmission system operators (TSOs) in the participating countries, the implementation in Germany is highlighted. For further details on the status-quo of the operational planning landscape, the planning processes defined by the German TSOs are described. Thus, the requirements for the CMM coordination can be deduced. To propose a new optimization model, the state-of-the-art review gives an overview of the common optimization problems and assigns them to the planning processes. Formulations for the Preventive Security Constrained Optimal Power Flow (PSCOPF) and Corrective Security Constrained Optimal Power Flow (CSCOPF) optimization problems are derived and combined in a bilevel programming (BLP) model to nest the curative optimization into the preventive model. As the BLP-SCOPF is a non-convex and non-linear problem, strict requirements on the solver are given. Therefore, a hybrid solver is proposed based on the differential evolution (DE) algorithm. An evaluation of the proposed optimization model and solver is given by multiple case studies. The focus is on the effect of for once respecting the determination of curative actions while calculating preventive measures and furthermore on prioritizing either preventive or curative CMMs. Besides the impact on the level of system security, cost aspects and computational complexity are also investigated.

The scientific contributions of this thesis can be summarized as follows:

1. Overview of the framework of system security from the perspective of Europe and Germany and localization of the presented approach in the German operational planning processes

2. Definition of an enhanced, active (N-1) security

3. Classification of the common optimization problems in the operational planning processes
4. Proposal of a BLP-SCOPF to enable the optimization of preventive and curative CMMs in a holistic model
5. Design of a hybrid Differential Evolution solver to solve the proposed bilevel optimization model
6. Demonstration of the capabilities of coordinating and prioritizing preventive and/or curative CMMs

Parts of the scientific contributions of this work have been published previously in international publications. For reasons of transparency and scientific integrity, the most relevant are listed below. A full list of the author's published publications are given in Appendix A.1.

T. Sennewald, F. Linke, and D. Westermann, "Preventive and Curative Actions by Meshed Bipolar HVDC-Overlay-Systems", *IEEE Transactions on Power Delivery*, vol. 35, no. 6, pp. 2928–2936, 2020, ISSN: 1937-4208. DOI: 10.1109/TPWRD.2020.3011733.

F. Sass, T. Sennewald, and D. Westermann, "Automated Corrective Actions by VSC-HVDC-Systems: A Novel Remedial Action Scheme", *IEEE Transactions on Power Systems*, vol. 35, no. 1, pp. 385–394, 2020, ISSN: 1558-0679. DOI: 10.1109/TPWRS.2019.2928887.

F. Linke, T. Sennewald, and D. Westermann, "Derivation-free Steady State Power Flow Calculation Approach for HVDC Systems with Distributed DC Voltage Control and Arbitrary p-v-Characteristics", in *2020 IEEE Power Energy Society General Meeting (PESGM)*, 2020, pp. 1–5. DOI: 10.1109/PESGM41954.2020.9281821.

A. Raab, T. Sennewald, P. Wiest, S. Schlegel, *et al.*, "Implementation of closed-loop Adaptive Power Control for VSC-HVDC in a Power System Control Center Demonstrator", in *CIGRÉ 2022 Kyoto Symposium*, Kyoto, 2022.

F. Sass, T. Sennewald, F. Linke, and D. Westermann, "System security of hybrid AC-HVDC-systems challenges and new approaches for combined security assessment, preventive optimization and curative actions", *Global Energy Interconnection*, vol. 1, no. 5, pp. 585–594, 2018, ISSN: 2096-5117. DOI: 10.14171/j.2096-5117.gei.2018.05.008.

1.3 Research Questions and Structure

The effectiveness of curative CMMs is highly dependent on the preventive actions. Based on the pre-fault generation landscape, the determination of feasible curative measures may be hindered or inhibited. Therefore, both kind of actions need to be coordinated to encompass an optimal congestion management. Within this thesis, the question for the design of such a coordination is discussed. The following research questions are formulated:

Q1 *What are the specifics of operational planning in terms of a coordinated determination of preventive and curative measures?*

Q2 *By using a coordinated congestion management measure determination, what must be taken into account in the modeling?*

Q3 *To what extent must a prioritization of preventive or curative system management be enabled?*

Derived from the example of Germany but developed for universal use, the research questions addressed are not limited to the German power system. This thesis is dedicated to answering the research questions in five chapters. **Chapter 1** opens with a brief introduction in the topic and motivates the lead question of this thesis. Subsequently, the scientific contribution is given and detailed research questions formulated.

To answer the question regarding the operational planning specifics, **Chapter 2** dissects the (legal) framework at the European and German level given by the SO GL and the German Energy Industry Act respectively in Section 2.1. Therefore, first a general description of the security definition is given as well as a depiction of the coordination framework of TSOs in the establishment of (N-1) security. Then, the concept of curative system operation is introduced and the most relevant requirements are shown. At last, the current landscape of the German planning processes is given. Especially Section 2.1.4.1 goes into more detail regarding the actual processes and shows them based on a timeline. Furthermore, Section 2.2 presents the basics regarding the mathematical formulation of optimization problems, followed by a classification of optimization problems based on its class and its applicable solvers. Afterwards, the most common optimization problems in the context of electrical power system are presented and assigned to the different time horizons of the planning processes shown in Section 2.1.

In **Chapter 3**, the structure of a BLP-SCOPF is described, allowing the coordination of preventive and curative CMMs. Followed by the introduction of CMM technologies, research question Q2 is answered by showing their implementation in an optimization model are presented such as HVDC systems and grid boosters. The structure of a preventive and curative optimization model is shown and combined in a bilevel Security Constrained Optimal Power Flow (SCOPF) model, which nests the calculation of curative actions in the preventive determination. Subsequently, the implementation of the novel optimization model into a solver based on a hybrid intelligent search algorithm is depicted.

An evaluation of the approach is substance of **Chapter 4** through numerical case studies. Starting point is the description of a suitable test system. For this, a system dedicated to test SCOPF applications using overlay HVDC systems is used as a base and further adapted, e.g., to incorporate more technologies. To broaden the scope of the evaluation, different scenarios are compiled. The scenarios comprise permutations of high and low wind generation and load respectively. For an answer to the last research question, the proposed optimization model is compared to a simple staggered optimization approach. Thereby, differences in the coordination of CMMs can be identified. Furthermore, the prioritization of preventive measures against curative ones is simulated and vice versa.

Chapter 5 summarizes the results and evaluates them in relation to the research questions formulated. Finally, based on the findings, an outlook is derived with regard to further research fields and recommendations for action.

2 State of the Art and Categorization of the Research Questions

2.1 Current State of Operational Planning

2.1.1 System Security in Power Systems

The central aspect of system security in electrical power systems is to establish a reliable system operation with a minimal interruption of supply, e.g., as a result of cascading faults. To ensure this in the heavily meshed power system of continental Europe, uniform operational regulations are required. Of particular importance is compliance with the (N-1) criterion. The (N-1) criterion is defined for the European area in Article 3 (2) (14) of the system operation guideline (SO GL):

> *'(N-1) criterion' means the rule according to which the elements remaining in operation within a TSO's control area after occurrence of a contingency are capable of accommodating the new operational situation without violating operational security limits;* [28]

Accordingly, the power system must be continuously robust against the failure of a single equipment (transmission line, generation unit, etc.) and must not involve cascading failure events. When such a failure event occurs, the power system changes from the *N-situation* (all network resources are available; Article 3 (2) (3) SO GL) to the *(N-1)-situation* (situation with one failure occurred in the failure variant list; Article 3 (2) (15) SO GL). Within the (N-1)-situation, the power system may be in one of the network states defined in Article 3 (2) (18) SO GL.

A first classification of the states of an electric power system came from [29] in 1968. He defined the three states *normal*, *emergency* and *restoration*. The normal state describes the state in which the supply of all consumers on the network is ensured and no operational limits are violated. If the operational limits are violated, the system switches to the emergency state. Here, the exceeding of protective currents, for example, can lead to cascading switching actions and finally to a blackout. To get from the emergency state back to the normal state, the transition is made via the restoration state. This describes the state in which parts of the overall system are not yet supplied again, although the areas already supplied are back in the normal state. Based on this classification, [30] has subdivided the normal state again into the states *secure-normal* and *insecure-normal*. This further subdivision is intended to provide a more fine-grained transition between the normal and emergency states. The secure-normal state corresponds to the original normal state, while the unsafe-normal state is added as a link. This state occurs when all operational limits are complied with in the current operating case, but one of these limits is violated as a result of a failing operating equipment.

The transition between the network states according to Debs is shown in Fig. 2.1. The transition to a worse state occurs in each case by the occurrence of a disturbance, such as a resource failure. The return to a better state happens through remedial actions. Of these, Debs defines four different

ones: the preventive measure, the curative measure, the emergency measure, and the restoration measure.

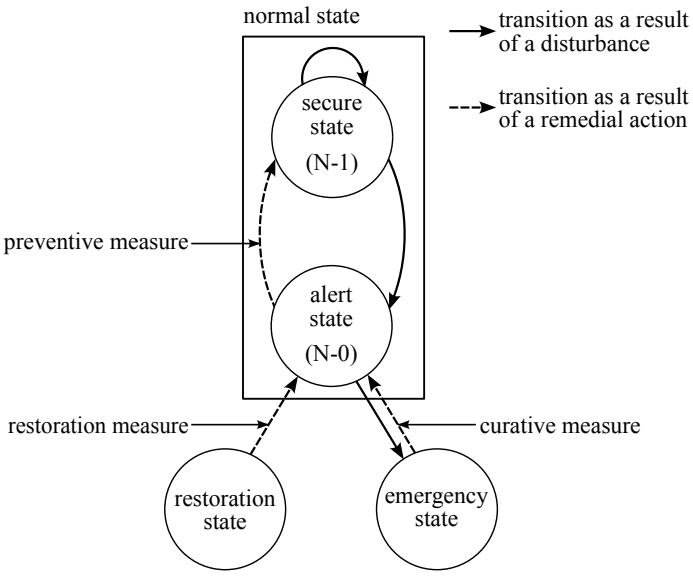

Figure 2.1: Transitions between system station caused by disturbances and remedial actions according to [30]

For the operation of electric power systems in Europe, system states are defined in Article 18 of the SO GL [28]. In general, the nomenclature corresponds to the one proposed by [30]. Differences are made in the naming of the secure-normal and insecure-normal state which the SO GL defines as normal state and alert state respectively. Furthermore, the SO GL introduces the blackout state as a separate system state as it was included within the emergency state by [30].

As already shown by Fig. 2.1, the transition from one system state to a worse state is caused by the occurrence of a disturbance or by a failure event from the system operator's contingency list. In order to return to a secure system state, the responsible system operator must use remedial actions. According to Article 20 SO GL, remedial actions are such measures that serve the purpose of maintaining a transmission system in a *normal* state. transmission system operators (TSOs) are therefore obliged to establish, prepare and activate appropriate remedial actions upon detection of potential operational security violations. On the one hand, they are to restore the *normal* state of the network, and on the other hand, they are to prevent the extension of the *alert* and *emergency* state beyond the borders of their own control area. Provided that the effect of the outage variant as well as the measure provided for it do not affect adjacent TSOs, the responsible TSO may perform the tasks on its own. Otherwise, the measures must be coordinated with all TSO involved (see Article 76 (1) (b) SO GL) and the recommendations of the regional safety coordinator (TSO) must be taken into account.

The SO GL defines ten types of congestion management measures (CMMs). There is no explicit order given for their activation, only stating a preference for those with the largest possible cross-zonal capacity available for capacity allocation. The defined actions are as follows:

1. Change of planned unavailability
2. Power flow control
3. Voltage regulation and reactive power management
4. Recalculation of cross-zonal day-ahead and intraday capacity according to Commission Regulation (EU) 2015/1222 [31]
5. Redispatch of network users connected to the transmission or distribution network within the control area between two or more TSO
6. Countertrading between two or more bidding zones.
7. Adjustment of active power flows of high voltage direct current (HVDC) systems
8. Use of balancing power
9. Restriction of already allocated cross-zonal capacities according to Article 16 (2) Regulation (EC) No 714/2009 [32]
10. Manually controlled load shedding (if necessary also in normal state or in alert state)

For Germany, system security of electrical energy systems is defined in the German Energy Industry Act (EnWG; German: Energiewirtschaftsgesetz). According to § 12 (3) EnWG [6] in conjunction with § 14 (1), system operators have the task of contributing to security of supply by providing a reliable system. Additionally, the European regulations of the SO GL are transferred into application guidelines [33, 34]. In the German context, an order is given by § 13 (1) of the EnWG. According to sentence 1, the TSO has to prepare a catalog of measures consisting of:

1. network-related measures,
2. market-related measures, and
3. the use of network reserves (cf. § 13d EnWG) and capacity reserves (cf. § 13e EnWG).

Analogous to the regulation in the SO GL, the maxim that the measures are to be selected according to the lowest probable total costs also applies here. Accordingly, the grid-related measures named in sentence 1 number 1 are always the ones to be preferred due to their cost neutrality. In addition to the classic network circuits, the network-related measures also include the use of HVDC systems or other measures influencing the power flow. If these are not sufficient in terms of their effectiveness or availability, a distinction must be made between market-related measures and reserve systems based on their cost advantage. The market-related measures include both the use of balancing power and measures under § 13a (1) and the connection and disconnection of contractually committed loads. As a last resort, the emergency measures described under § 13 (2) are available. The TSO

may dispose of these if the measures defined in § 13 (1) do not take effect or are not available in time. The emergency measures thereby include intervention in power generation, transits, and purchases. This adjustment, or request for adjustment, affects not only facilities or customers connected to the respective transmission system, but also neighboring or subordinate system operators within the framework of cooperation under § 12 (1).

2.1.2 Curative System Operation

In addition to the categorization of the type of remedial action (network-related or market-related), the differentiation with regard to the activation timing is also relevant. The Union for the Coordination of Transmission of Electricity (UCTE) Operation Handbook [35] introduces the differentiation between preventive and curative actions. Preventive actions take effect before the actual failure event occurs. Therefore, the dimensioning of the action is done by anticipating the event. Since it is not tailored to a specific failure event, but the total set of all possible failures, the preventive remedial action is not efficient with respect to a single event. However, it ensures that the electric power system remains in the normal state only, since the remedial action is already effective at the time of the fault occurrence. The curative measure, on the other hand, refers to a relief measure that is triggered only after a failure has occurred. Referring to the state diagram in Fig. 2.1, the failure causes a transition of the system state from the normal state to the emergency state, and the return to a safe state is then performed by means of the curative action. Compared to the preventive measure, the curative measure is very efficient in resolving a congestion, since it is exclusively dimensioned for a specific event.

Curative actions enable new possibilities in regard to higher line utilization in the (N-0) state of the power system. As shown in Fig. 2.2 based on an exemplary line, a preventive system operation scheme curtails the available transport capacity of any transport corridor by the amount of the highest (N-1) overloading, so the system remains congestion free in the event of a contingency.

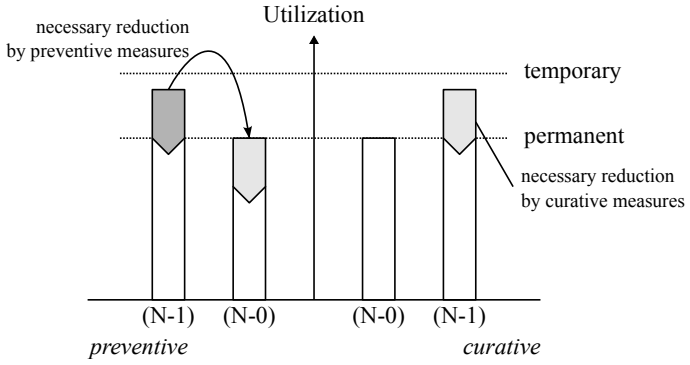

Figure 2.2: Principle higher utilization through curative measures using an exemplary representation of the line load in the (N-0) and (N-1) states, following [36]

Fig. 2.3 shows a simplified example, depicting a system consisting of two busses with a generation unit at bus d and a load at bus e. Both busses are connected via two transmission branches that run in parallel. A preventive operation scheme would limit the maximum line loading of both lines to 50 % of their rated current (see Fig. 2.3a) so that, in the event of a line outage, the parallel line will not exceed its respective permanent admissible transmission loading (PATL) value, as is seen in Fig. 2.3b. Over the whole process, the system state remains within the (N-0) secure state without any further intervention by the system operator necessary. Thus, the preventive establishment can also be interpreted as a *passive (N-1) security*.

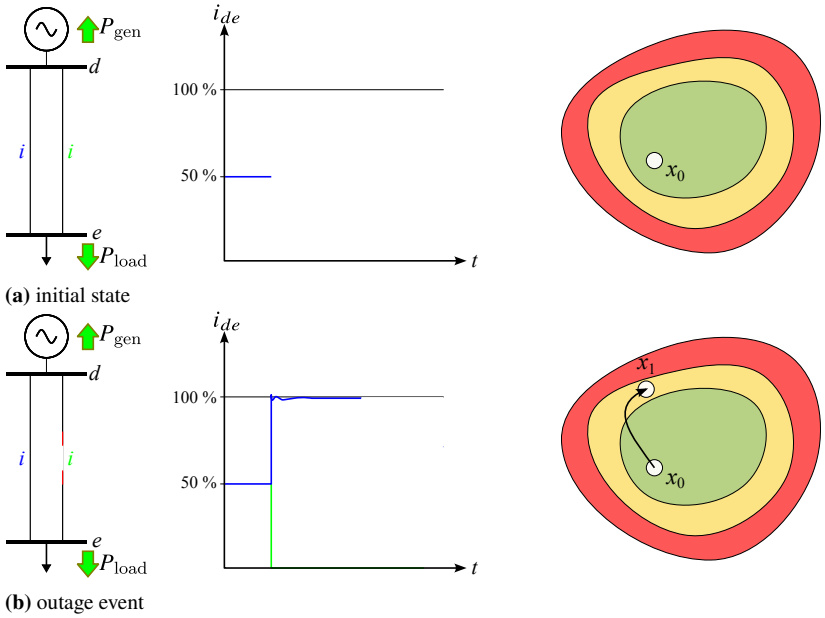

Figure 2.3: Exemplary depiction of the passive (N-1) security showing from left to right the simplified network, line utilization and state diagram for (a) the initial state of the system and (b) the outage event

The general concept of including curative actions into system operation stems from [37] and is further described in [38]. Curative system operation is applicable by utilizing the thermal inertness of electric conductors and thereby exploiting their thermal reserves. The idea is to allow a temporary overloading of the congested line, while in the meantime, a fast acting curative action is activated to return the system back to a normal system state [24, 39, 40]. Two limiting values for lines must be considered for the congestion management: PATL and temporary admissible transmission loading (TATL) [35]. In normal operation, lines are operated up to the PATL, the rating at which a line can be operated at for an infinite time without exceeding the thermal reserves and thereby risking, e.g., a line sag leading to a pole-to-ground-failure. After the contingency event occurs, congested lines can be operated up to the TATL value.

This is further visualized in Fig. 2.4 using the same simplified network as in the previous depiction. As the line utilization in the (N-1) secure state is above the 50 % threshold, a line outage as shown in Fig. 2.4b leads to an overloading of the remaining healthy branch and the system transitions into the (N-0) violated state. To prevent further faults due to an insecure system state, a curative action is activated (see Fig. 2.4c) and the (N-0) secure state is reached. As the curative operation of the power system requires an active intervention of the system operator, the established (N-1) security using curative means can also be called *active (N-1) security*[1].

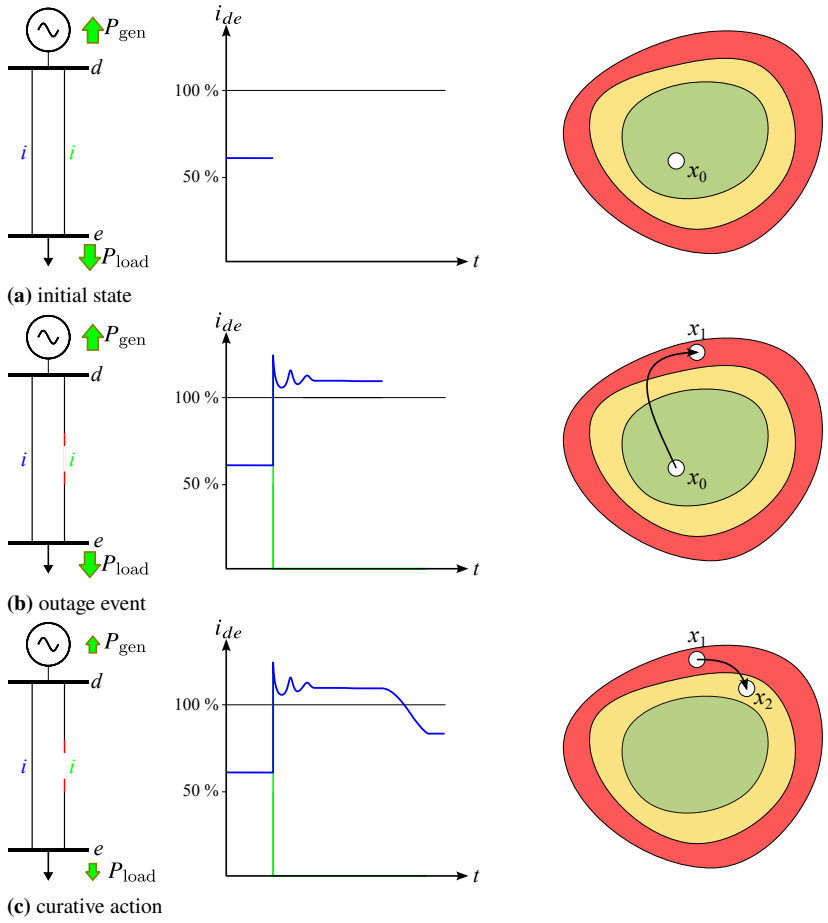

Figure 2.4: Exemplary depiction of the active (N-1) security showing from left to right the simplified network, line utilization and state diagram for (a) the initial state of the system, (b) the outage event and (c) the curative action

While the PATL often is defined by the vendor, the TATL is not a constant value. In [41], the initial loading, heat capacity/thermal inertia of the conductor and ambient weather conditions are lists as

[1] Please note that both for the passive and active (N-1) security, the system needs further restoration measures to be transitioned back the (N-1) secure state.

restricting factors defining the TATL. The thermal inertia also defines the time frame the congestion current can flow through the asset, e.g., the transmission line. By differentiating between the level of the congestion current, multiple TATL time frames can be defined. For higher current levels, shorter time windows have to be defined to not exceed the thermal reserves. Fig. 2.5 illustrates this relation. It shows three different current levels with $I_{\text{congestion},1}$ being the highest and $I_{\text{congestion},3}$ as the lowest. The higher the congestions current, the quicker the rise in temperature of the electric conductor, leading to a shorter time window before the thermal reserves are exhausted.

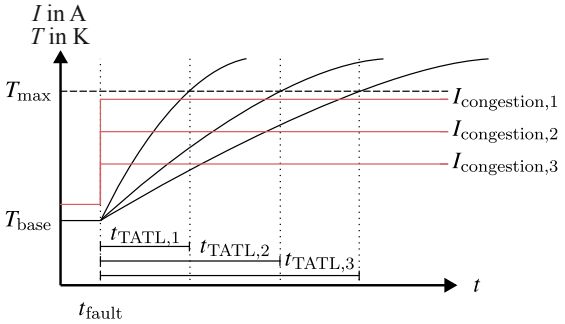

Figure 2.5: Conductor temperature and impact on thermal reserves dependent on different levels of congestion currents following [41]

Besides the thermal load of a congested transmission branch, the overall congestion current is limited by additional systemic factors [42]. For once, system protection has to be considered. The German TSOs define the protection congestion current $I_{\text{lim,prot}}$. For all $I < I_{\text{lim,prot}}$ under normal conditions ($V > 360$ kV, $\cos(\varphi) > 0{,}8$) it is ensured a tripping will not happen. In the context of temporary overloading, the TATL current cannot exceed the protection congestion current to avoid any unwanted line tripping. Another aspect is the time constants defined for protection devices. Typically, the devices energizes after 200 ms and trips after 2 s. A curative action therefore has to be fully realized after 1.5 s [43].

Curative actions aim at lowering the congestion current fast enough that the maximum thermal capacity of a conductor is not exceeded. Fig. 2.6 shows the operating principle of curative actions by exploiting the thermal reserves of an electric conductor. Up to the point of $t < t_{\text{outage}}$, the line is loaded with a current just below its PATL. With the contingency event happening at $t = t_{\text{outage}}$, a line in the system is tripped, leading to a rise of the current to the TATL. Along with a rise in current levels, the temperature of the line rises quickly. After a short reaction time frame t_{reaction}, a curative remedial action gets activated and ramps its active power infeed to P_{cur}. As the curative action reaches its target value within the $t_{\text{activation}}$ time frame, the congestion current is relieved until it reaches the PATL value. Furthermore, by lowering the congestion current the rise in temperature is also slowed down so that the maximum line temperature $\vartheta_{\text{line,max}}$ is neither reached nor exceeded. Therefore, the total time window t_{TATL} is the sum of the reaction time t_{reaction} and the activation time $t_{\text{activation}}$.

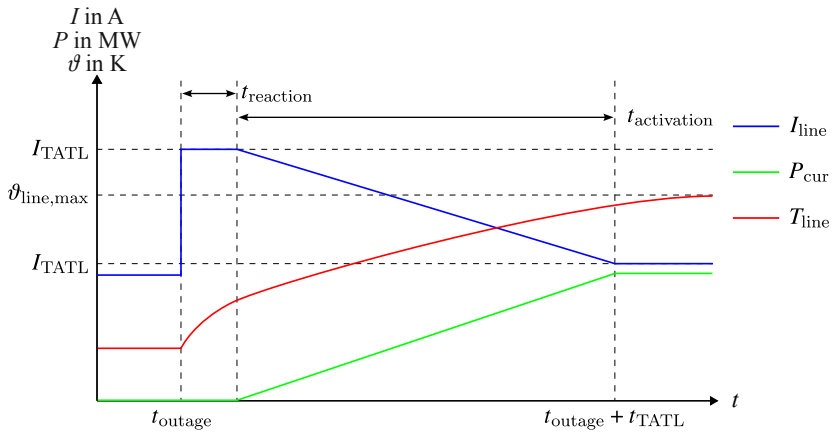

Figure 2.6: Operating principle of curative actions by [38]

2.1.3 Activation of Curative Measures

Quick response times are necessary to enable a secure and reliable curative system operation scheme. The crucial factor in ensuring a secure operation is to not exceed the thermal reserves. Control schemes centered around the control room are not in all cases fast enough to detect the congestion and then prepare and activate the curative action giving the need to faster, decentralized concepts [23]. To guarantee a fast activation, system automations are needed like the usage of special protection schemes (SpPSs). SpPS are special solutions to avoid unfeasible systems states by automatically executing appropriate counter measures [24, 44]. As part of the iTesla research project [45], a survey was conducted among the participating TSOs regarding the three most frequently installed SpPS in 2016. The results are published in [46] and list: load shedding (46 %), generator rejection (25 %) and islanding (10 %). SpPSs generally refer to controllers following certain characteristics [47]:

- can be armed and disarmed based on the current condition of the system
- are "normally dormant", i.e., they are activated seldom
- usually employ discrete, feed-forward control laws
- use predetermined control actions
- have a need of some kind of communication

The general structure of an SpPS is shown in Fig. 2.7. Following a disturbance in the power system, certain electric variables like nodal voltages and branch currents change. Those measurements are forwarded towards the SpPS where they are further analyzed by the implemented decision logic. The implementation of the decision logic can either be centralized in the control center (separated from the energy management system) or decentralized at the substation level [48]. A key criterion

of an SpPS is to ensure a reliable activation of the (curative) actions. This is secured by linking the arming of the SpPS with certain criteria like minimum line loadings [49].

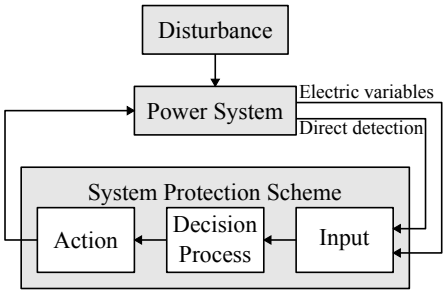

Figure 2.7: General structure of an SpPS [49]

In regard to the implementation of curative actions in system operation in Germany, the TSO TransnetBW is currently working on an implementation with the project name KAI (German: Kurative Ausführungsinstanz; curative execution instance) [50]. The KAI is to be implemented in the control center of TransnetBW to coordinate the necessary steps of monitoring and managing curative actions. This also comprises the SpPSs that are implemented to trip the remedial actions. Initially, the KAI is used to control the pilot grid booster project (see Section 2.1.5.3) and will be expanded once the proof of concept succeeds. The actual determination of the curative actions is not part of the KAI but will take place within the operational planning.

In general, the same CMM are available for the curative system operation as for the preventive one. Accordingly, the hierarchy from § 13 (1) EnWG is imposed on curative actions. An additional boundary constraint is given by the time requirements regarding t_{TATL}. Therefore, technologies based on power electronics are more favorable compared to synchronous generators, as their capabilities to change their set-points are greater. In [24, 41, 43], the following technologies are listed:

- switching actions,
- tap changing of transformers,
- power flow control (HVDC, phase-shifting transformer (PST), grid booster, fast AC transmission system (FACTS) devices),
- control actions by power plants (thermal, hydro, renewable),
- load shedding and
- emergency power control functions.

Fig. 2.8 shows an exemplary curative concept, utilizing SpPS for the activation. The system consists of three busses, four transmission lines and incorporates various degrees of freedom: an HVDC system, a synchronous generator, a battery energy storage system (BESS) and a wind park as viable

curative actions. For the curative operation scheme, an SpPS is installed to monitor the current on line L2 via an amperemeter as well as the operating state of L1 by observing the status of its circuit breakers (shown by the blue arrows). The tripping action of the SpPS is triggered when both circuit breakers on line L1 are opened and the amperemeter detects a congestion current above its PATL value. If the tripping conditions of the SpPS are fulfilled, a curative action is activated. Based on the grid situation, a combination of the available degrees of freedom is feasible, e.g., an adaptation of the HVDC set-points to replace the lost AC line or an infeed of the BESS. Please note that as this is an exemplary representation, only a single protection scheme is shown. The concept can be expanded at will.

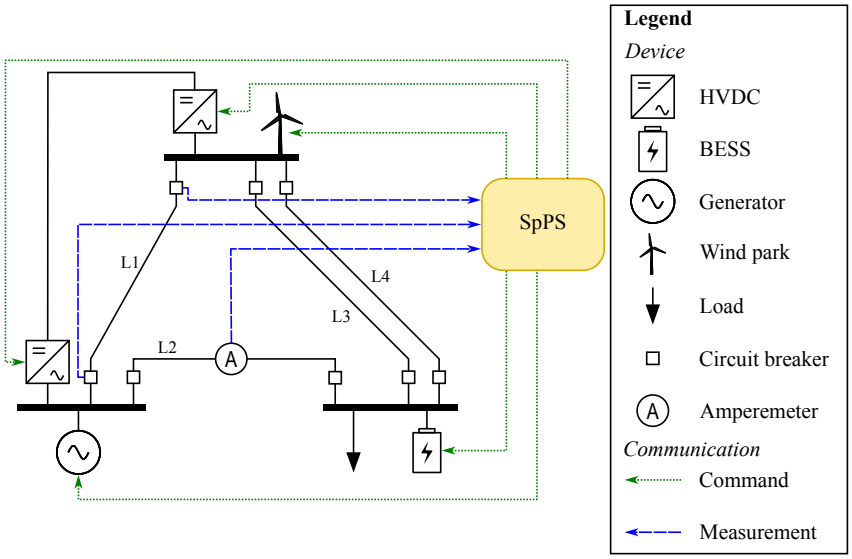

Figure 2.8: Three bus system using an SpPS to monitor a transmission line and activate a curative CMM in case of a congestion

2.1.4 Landscape of Operational Planning Processes in Germany

This section is meant to give a general overview of the landscape of operational planning. The structure is divided into a more detailed look on the German perspective in subsection 2.1.4.1 and a small outlook on the framework of determination of CMM. Operational planning in regard of determining preventive actions for system security is a lengthy process and can be clustered in four main processes, shown in Fig. 2.9. The overview was first presented by [51] based on the regulations imposed by NERC for the North American power system. Due to the unbundling in Europe, the presentation is split in grid and generation planning. Within the long-term planning, e.g., a scope of five to 15 years, available and needed transmission capacities are anticipated based on generation forecasts. The mid-term planning process looks at a yearly or monthly maintenance scheduling of equipments as well as an optimal allocation of resources. Short-term planning, where the actual focus of this subsection lies in, starts at the forecast of generation and demand on the one hand

and expected topological changes on the other. This data merged into consolidated preview data models in regular update intervals. Following the regulations of the SO GL, in Europe the model is further validated by the regional security coordinator, who also performs joint steady-state security assessments (SSAs). Consequently, the results of the SSA calculation build the data basis for the TSOs for their capacity calculation and planning of reserve power plant call-up and redispatch demand. Those are needed on the one hand, to provide the actual capacities of the interconnectors on the market and for scheduling of redispatch resources to address congestion-related findings within the bid zone. The focus here is especially on planning redispatch resources: if there are too few available in real-time operation more far-reaching measures from § 13 (2) EnWG are needed.

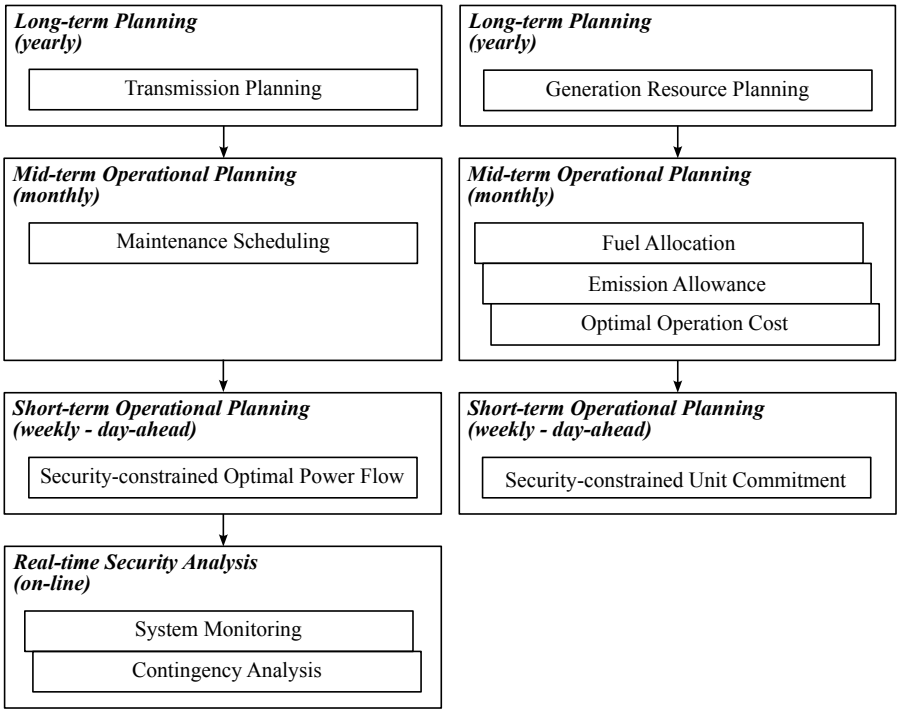

(a) grid planning **(b)** generation planning

Figure 2.9: Hierarchical power system security analysis in context of operational planning, following [51]

2.1.4.1 Operational Planning Processes in Germany

Operational planning processes in Germany are performed with a lead time of one week with the goal of preparing the power system for the actual real-time operation, e.g., by determining CMM and activating preventive measures. The general landscape of operational planning is clustered into several processes, each with their own specialized goal and boundary conditions, e.g., differences in forecast uncertainty and start-up periods of thermal power plants. Also, the scope of each process

varies. The week ahead planning process (WAPP) and preventive redispatch 1 (pRD1) are mainly meant to secure redispatch reserves due to longer start-up times and are marked-based [52]. On the other hand, the day-ahead congestion forecast (DACF) and intraday congestion forecast (IDCF) are purely focussed on determining CMM and averting congestions. In each process, different optimization problems are addressed [38]. Section 2.2.3 goes into more detail regarding the optimization problems. Fig. 2.10 gives an overview of the temporal classification of the planning processes in Germany.

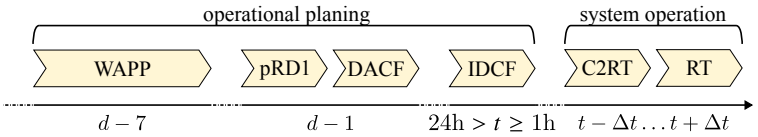

Figure 2.10: Overview of operational planning processes in Germany following [38, 53, 54]

In [38, 55–57], an overview of the schedule of the German operational planning processes is given and shown in Fig. 2.11. In the morning, the coordination processes start with the WAPP which is split into two separate sessions that continue until the early afternoon, right after the closing of the day-ahead market [57]. At 4:30 pm, the pRD1 takes places, followed by the DACF process at 6 pm and the IDCF at the end of the day. The IDCF is a rolling process, coordinating CMMs up to the close to real-time (C2RT) time frame (roughly one hour prior to real-time). In the following, the mentioned planning processes are discussed in more detail.

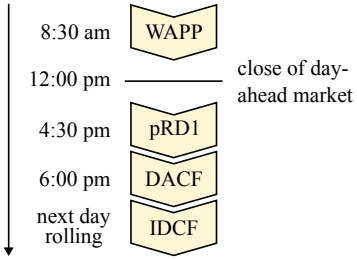

Figure 2.11: Schedule of operational planning processes in Germany [38, 55]

Week ahead planning process and pRD1

The WAPP is a planning process taking place twice a day at the German level [57] with the aim to determine the demand for grid reserve power plants, i.e., plants solely for providing CMM and not participating at the market. As the data basis of the network model on which the planning is consists of the market and power flow forecasts available to date, power flow limits as well as more detailed information of relevant power plants. The result of the WAPP is an optimization of the redispatch volume and setting of the tap changers of PSTs by the reserve power plant deployment forecast. Network reserve requirements exceeding those already ordered to date will be reported and ordered after coordination of the German TSO [52]. The preventive redispatch 1 (pRD1)

process is, analogous to the WAPP, an established process on the German level and continues the planning process of the WAPP from the morning with an updated data situation after the close of the day-ahead market at 12 pm [57].

Day-ahead Congestion Forecast

The DACF is a planning process established at the European level in which the need for CMM is coordinated at the international level and is the continuation of the pRD1 process [38]. In the zone relevant for Germany, the moderation is done by the regional security coordinator TSCNET[2] [58]. The regional security coordinator is responsible for the coordinated security assessment. Within this process, the individual grid models of each TSO (including network- and market-related measures) are combined to a combined grid model of the entire regional security coordinator zone [59]. In this process, 24 data sets are available in hourly resolution for the entire following day [60, 61]. As a result of the assessment process, a congestion-free network model is produced [52], incorporating the coordination of additionally required CMM that have an influence on neighboring TSO in each case [59]. If the regional security coordinator identifies further findings for which there are no CMM, a conference call with all participating TSOs is organized at 9 pm [60, 61]. In the conference it is then discussed which TSO will be responsible for providing a suitable CMM.

Intraday Congestion Forecast

The last planning process is the IDCF. In order to take into account the decreasing forecast uncertainty of the power plant deployment forecast data as well as the feed-in of renewable energy plants, the IDCF process runs an hourly update of the congestion forecast with the updated forecast data. Accordingly, the goal of the IDCF is to evaluate the results of the DACF as uncertainty decreases. According to [61], the individual grid models of each TSO are to be provided one hour and a half prior to allow a verification by the other TSOs and the regional security coordinator. Analogous to the DACF, further measures must be dimensioned should unmanaged congestion be identified during the congestion forecast [62].

2.1.4.2 Determination of Remedial Actions

To prepare their remedial actions, TSOs shall, in accordance with Article 23 SO GL, review the effects thereof. In case of determination of effects on the circuits of neighboring system operators, these shall be included in the evaluation of remedial actions. During the normal state and alert state, TSOs must also evaluate the impact of their actions on significant grid users and distribution system operators connected to the transmission system. The selection of remedial actions must ensure the maintenance of the normal state and the operational safety of all parties involved. Outside these two states, the TSO must coordinate its actions with the stakeholders in order to continue

[2] TSCNET is the regional security coordinator among others for the German TSOs (`www.tscnet.eu`).

to ensure the operational security and integrity of the system. If the measures taken by the TSO include instructions to significant grid users and distribution system operators, they must carry out the instructions when the relief measure is activated.

To coordinate the determination of remedial actions across the German TSOs, a new IT system is deployed. It consists of two separate platforms: the redispatch determination server (German: Redispatch Ermittlungsserver) and redispatch settlement server (German: Redispatch Abwicklungsserver) as can be seen in Fig. 2.12. The redispatch determination server is meant for power flow calculations, analyses and determination of CMM [63]. The congestion management measure calculation is modeled as a nonlinear Security Constrained Optimal Power Flow (SCOPF) [38] (cf. Section 2.2.3.3 for more details regarding the SCOPF problem). To actually activate the measures of the redispatch determination server, the redispatch settlement server is used. Its application comprises the activation and monitoring of the proposed measures and is capable to directly communicate with all market participants. Also, all downstream processes like billing and obligation of transparency are supported by the redispatch settlement server platform [64]. Both system are planned to be implemented across all planning process from WAPP to IDCF and C2RT.

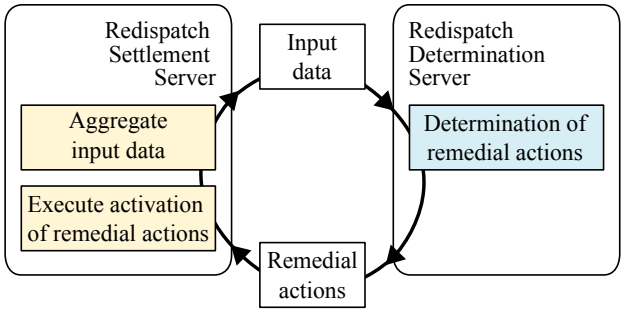

Figure 2.12: Interaction of the redispatch settlement and determination server

A similar methodology is planned at the European level with the implementation of a regional operational security coordination (ROSC) for the capacity calculation region of the Core TSOs called Core-ROSC-method [55, 65, 66]. The goal of the Core-ROSC-method is to deploy a platform similar to the redispatch determination server where CMMs are determined across all TSOs. Thereby, the need for the daily DACF conference calls at 9 pm (cf. Section 2.1.4.1) is omitted to discuss how to handle the new identified findings.

2.1.5 Degrees of Freedom of Congestion Management

As stated in Section 2.1.1, the SO GL lists several options regarding CMMs while the EnWG categorizes them based on their relation to network and market as well as the usage of reserves. Furthermore, a grouping of remedial actions according to where in the network they act is missing. Thereby, measures can be categorized into the two groups of branch-based and node-based measures. With the former, the congestion is directly addressed by changing the power flow on a branch by

power flow controlling devices such as PSTs. Node-based measures on the other hand affect the power flow indirectly by changing the power infeed on at least two busses in the system, e.g., by redispatch of conventional generating units. Tab. 2.1 assigns the measures of SO GL according to the two introduced categories. In the following, a brief characterization of node-based technologies is given. Please note that the usage of balancing power is not actively presented. The working principles are analogous to redispatch actions while balancing power falls in the category of network or capacity reserves (cf. § 13d and § 13e EnWG).

Table 2.1: Categorization of congestion management measures in branch- and node-based actions

Branch-based	Node-based
Power flow control	Redispatch
Planned unavailability	Countertrading
Capacity recalculation	HVDC systems
Restriction of capacity	Grid booster
Switching actions	Balancing power
PST	Load shedding

2.1.5.1 Redispatch and Countertrading

Redispatch and countertrading are among the most used measures today to establish (N-1) security as they are historically one of the few viable CMMs available to system operators. A generator redispatch utilizes the available upward and downward capacities in the system, changing the power flow through additional power injections [67]. Thereby, the intervention in the generation-load-profile of the power system must be balance-neutral. Countertrading is a purely market-based action where system operators purchases or sells energy at the intraday market to counter the initial congestion power flow. In Germany, countertrading accounts for a small part of CMMs, especially compared to redispatch. For the year 2022, countertrading and redispatch amounted to € 371 million and € 2,689 million respectively [68].

In regard to the classification of § 13 (1) EnWG, redispatch is a market-based action as power plant operators, participating at redispatch, get compensation. Therefore, redispatch is always associated with additional costs compared to the normal system operation.

Due to the large time constants associated with the thermal inertia of conventional power plants, redispatch is used in most cases as part of preventive congestion management. Taking into account the higher lead times of thermal generators, a preventive operating point can be set within the time limits. The time constants required for a curative scheme are too small to be effectively used by redispatch.

Synchronous generator provide two degrees of freedom to congestion management: their active and reactive power output. Both factors are dependent on each other and cannot be controlled separately.

For further visualization, Fig. 2.13 shows the capability curve of a synchronous generator. Often, synchronous generators are equipped with a voltage control function. In such cases, the reactive power output is not a viable degree of freedom

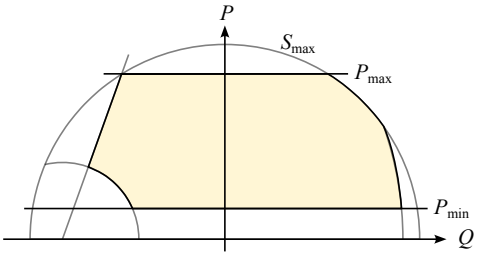

Figure 2.13: Capability curve of synchronous generators

2.1.5.2 HVDC Systems

HVDC systems can be differentiated in line commutated converter (LCC) and voltage source converter (VSC) based systems. LCC systems are discussed since 1914 and were based on mercury arc valves [69]. Since 1972, LCC systems using thyristor valves are build [70], either as six- or twelve- pulse bridges. Today's projects are mainly focused around the connection of offshore wind farms, as the LCC technology is most suited for bulk power transmission. Insulated-gate bipolar transistor (IGBT) based VSC HVDC systems are around since 1997 with the experimental Hellsjön–Grängesberg project [71]. The VSC technology has seen multiple evolutionary steps. Early versions were realized using two-level converters, using two IGBT modules per phase. Building on this, three-level converters were developed and resulted in the currently used modular multi-level converter (MMC) technology, first proposed in [72]. MMCs are composed of multiple IGBT based submodules in series for each phase. VSC based HVDC systems are not as suitable for bulk power transmission as LCC based ones. Today commercial applications of VSC based transmission are used up to approximately 3 GW per system whereas the LCC technology can achieve a multiple of this rating. Yet, VSC technology is flexible for system operation as they can provide ancillary services such as black start capabilities or reactive power provision, even when no active power is being transmitted.

In general, there are a variety of possible converter topologies in HVDC systems, which are shown in Fig. 2.14. One can distinguish between a monopole and bipolar topology. In the context of this work, the focus is on the symmetrical bipole with metallic return conductor. The configuration here consists of two independent inverters per head station, of which inverter 1 is connected to a conductor with positive polarity and inverter 2 to a conductor with negative polarity. The two inverters are controlled independently of each other. In normal (symmetrical) operation, both converters are operated with identical set points for active and usually also for reactive power, so that both poles carry equal currents and no current flows through the ground system [73]. Only in

the case of an active power imbalance between the two poles can a current be detected through the metallic return conductor.

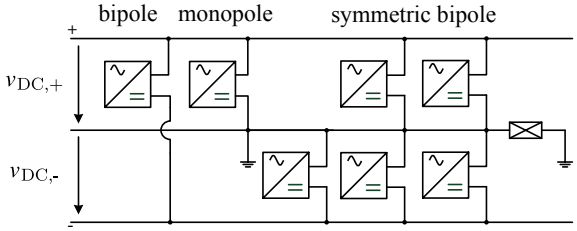

Figure 2.14: Examples of inverter topologies [74]

Regarding the number of transmission corridors, the configurations range from back-to-back (B2B), point-to-point (P2P), multi-terminal and meshed. A B2B system only consists of two converters without an actual transmission link in between. Most applications are the coupling of two asynchronous areas, such as the Shin-Shinano frequency converter in Japan coupling the 60 Hz and 50 Hz area [75]. P2P systems consist of two converter stations connected by a single transmission corridor. In Germany, two P2P links are planned, SuedLink and SuedOstLink. If multiple points are connected by the same HVDC link, it is called a multi-terminal link. Lastly, meshed HVDC systems are erected when at least one mesh is formed. To date, only one meshed HVDC systems is in operation. It is the Zhangbei DC system [76] in China, a four terminal bipolar system with a voltage of ±500kV and a total capacity of 9,000 MW.

The use of HVDC systems as part of congestion management has already been described in the literature in several facets. In [77, 78], the first applications of HVDC systems in OPF formulations is presented, whereas [79] expanded the model for multi-terminal systems and [80, 81] applied it to the SCOPF problem. Since then, multiple contributions can be found extending the scope by new frameworks [82, 83], degrees of freedom [84] and applications to preventive or curative system operation [40, 85–94] and as measure to stabilize power systems [27, 95, 96].

An important aspect in the operation of multi terminal (MT) or meshed HVDC systems is the control scheme of the DC system, called the DC voltage control. DC voltage control is similar to the frequency containment reserve of the AC system, where frequency is an indicator of power imbalances. In both systems, the injected power must match the demand and transmission losses at all times. An energy imbalance in the AC system results in a change in frequency. Here, the rotating mass of the turbines and generators acts as the main energy storage. In the DC system, the main energy storage is the network capacitance C_{DC} and an energy imbalance causes a change in the DC voltage v_m. This effect is described in (2.1).

$$v_m = \frac{1}{v_m C_{\mathrm{DC}}} \int_{t_0}^{t_1} \left(p_{\mathrm{in}}(\tau) - p_{\mathrm{out}}(\tau)\right) \mathrm{d}\tau \tag{2.1}$$

The energy storage capacity of the DC grid is very small compared to the transmitted power [97]. This results in the need for DC voltage control to operate in the range of milliseconds to maintain

voltage limits within the operating range in the presence of large energy imbalances. The short time range to balance the DC system affects local DC voltage control at each converter. Therefore, each converter station is given a control function that provides active power ($\Delta p_{\mathrm{conv},m}$) as a function of the deviation of the locally measured voltage v_m and the set-point $v_{m,\mathrm{ref}}$ (2.2).

$$\Delta p_{\mathrm{conv},m} = f(v_m - v_{\mathrm{ref},m}) \tag{2.2}$$

Two concepts of DC voltage control are discussed in the literature: the centralized and decentralized control. The centralized voltage control, sometimes referred to as master-slave-control, is focused around one converter with a droop value of infinity and therefore acting as a DC slack bus (or master). Other converters in the system operate in a constant P control mode corresponding to a droop factor of zero. This is depicted in Fig. 2.15, with Fig. 2.15a and Fig. 2.15b showing the slack and constant P control modes respectively. This concept is capable for large systems under normal operating condition. As disturbances or fluctuations are balanced by a single converter, the usability is only ensured for small fluctuations around the operating point. Another problem with the centralized voltage control is its possible impact on the AC system.

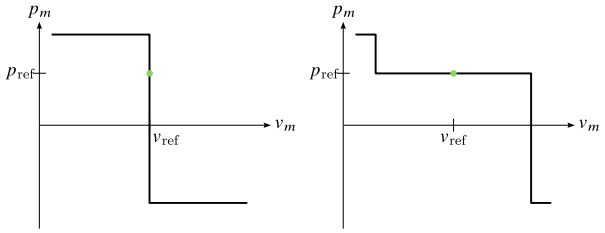

(a) slack **(b)** constant P

Figure 2.15: Control modes for centralized DC voltage control

Analogous to frequency containment reserve, where a distributed balancing control is applied to the AC system, the idea of a distributed decentralized voltage control in the DC system is a logical conclusion [98]. Most applications in the literature [99–102] dealing with decentralized DC voltage control use single linear droops as depicted in Fig. 2.16a. Here, the gain factor k_{droop} defines the fraction of active power adaptation due to DC voltage control. The set-point adjustment is calculated according to (2.3).

$$\Delta p_{\mathrm{conv},m}(v_m) = k_{\mathrm{droop},m} \cdot (v_m - v_{m,\mathrm{ref}}) \tag{2.3}$$

The linear control function can be extended, for example, by a tripartite P domain [103], as shown in Fig. 2.16b, or by sigmoid functions [104] in Fig. 2.16c.

For system operation, VSCs contribute both their active and reactive power output as feasible degrees of freedom. Due to VSCs being based on power electronics, they are not imposed by the same constraints as synchronous generators (cf. Fig. 2.13). Fig. 2.17 illustrates the range of action of an ideal VSC. They are capable of setting their active and reactive power operating point

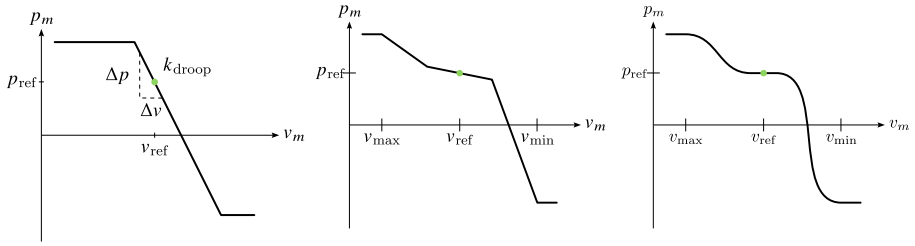

(a) linear droop **(b)** tripartite **(c)** sigmoid

Figure 2.16: Decentralized control functions applicable for DC voltage control, following [103–105]

independently of each other. The behavior of the DC system in case of sudden imbalances can also be controlled by implementing the droop parameter of the DC voltage control as seen in Fig. 2.16a as is a viable degree of freedom for the preventive security.

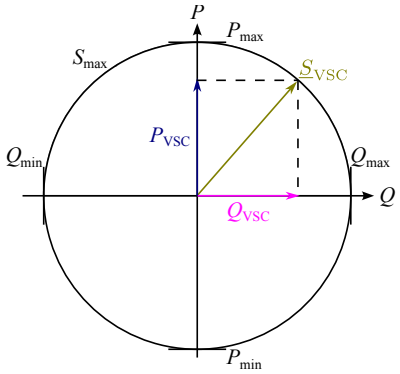

Figure 2.17: Capability curve of VSCs

2.1.5.3 Grid Booster

The concept behind the grid booster was proposed for the first time in [106]. In [107], it was initially introduced as component for a curative system operation and was discussed at length as part of the research project *InnoSys 2030* [22, 23] as viable technology for a curative system operation scheme. A grid booster functions like a sink on one end of a congested line and a source at the other end, inducing an inverted power flow to the actual congestion current. Please note that a grid booster refers to a set of individual grid booster units. In [43], the grid booster concept is summarized as a load at the beginning and a generator at the end of a transmission branch that gets switched on in the event of a contingency and a congestion on the branch. A broad variety of loads is deployable as long as its controllable, i.e., controllable loads, power-to-x plants or curtailment of renewables. Similar to the redispatch, the grid booster concept is an action that is neutral to the generation-load-profile. Meaning, the amount of load and generation at the beginning and

end of the line have to be identical to not impose an additional power flow. Due to the strict time requirement for curative actions, the generation unit at the end of the branch needs to be a device connected via power electronics.

Furthermore, a differentiation can be made between the pilot grid booster, as shown in Fig. 2.18a, and the systemic grid booster shown in Fig. 2.18b. The systemic grid booster is the extension of the pilot project as it does not comprise single pairs of grid booster units but coordinates multiple units across different control areas, giving more flexibility in regard to the contingencies that can be addressed. It should be noted that in its early stage, the grid booster is used to control one transmission corridor. If the concept proofs its functionality, the systemic grid booster is capable of addressing multiple congestions within the system. On the one hand, this raises the applicability of the grid booster but simultaneously complicates the operational planning as multiple units have to be orchestrated.

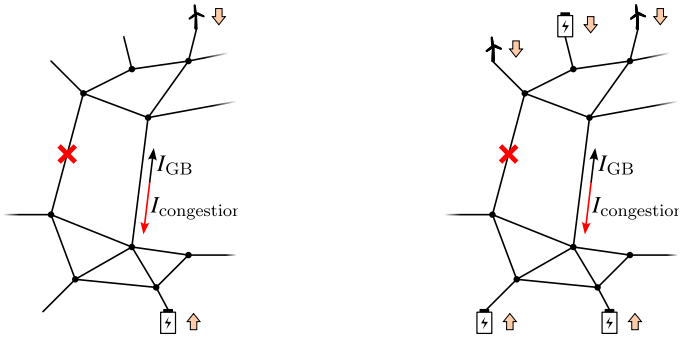

(a) Pilot grid booster with one BESS and wind park

(b) Systemic grid booster consisting of a combination of BESSs and wind parks

Figure 2.18: Configurations of grid boosters, according to [23, 108]

The grid development plan 2037/2045 [16] describes the framework data of the planned pilot system. The construction of a BESS in the system of TenneT TSO Germany is planned for 2023. Both storage facilities are planned with a nominal capacity of 100 MW and a capacity of 100 MWh. The designated locations for the two units are Audorf (Bavaria) and Ottenhofen (Schleswig-Holstein). In 2025, the second pilot system is to be completed. This pair consists of an energy storage, operated by TransnetBW in Kupferzell, and an offshore wind farm of TenneT TSO Germany. The feed-in point of the wind farm is at the Dörpen/West substation. The BESS is specified with a power of 250 MW.

The general operation scheme of the grid booster was substance of the research project *InnoSys 2030* [22, 23]. Some discussions regarding the grid booster resulted in the paper of Lindner *et al.* [108]. Fig. 2.19 shows the separate phases associated with the concept. They are described in the following except the performance measurement and the deployment of redundancy actions. Those phases are solely needed for completeness of the operation concept to address the possibility of a fault within the grid booster system, e.g., a component associated with the grid booster.

1. **Monitoring and activation** In this stage, the actual need for a curative deployment of the grid booster is determined. Activation in this context means to put the grid booster in a state of awareness to be ready to use in the event of a contingency. Conversely, this means a deployment is not possible if the grid booster was not activated prior to the failure. The actual activation is a result of the operational planning where the grid booster usage is determined exclusively for a specific contingency. This whole process is meant to prevent an unwanted triggering based on false data or human mistakes.

2. **Triggering** When the necessary trigger criteria (i.e. a circuit breaker trip or measurement of a congestion current) are fulfilled during the monitoring phase, the set-point adaptation of the relevant grid booster units has to be initiated as soon as possible. To satisfy the tight time constraints, SpPSs are utilized to detect the necessity of a deployment as well as send the commands to the grid booster units. The realization of a curative measure can happen in two ways. For the pilot projects, where the grid booster is used to secure selected circuits, the set-point adaptation is fixed, e.g., a hard-wired implementation. In a coordinated operation, as thought for the systemic grid booster, a decision matrix will be used. The decision matrix maps the needed units to the corresponding trigger criteria.

3. **Deployment** The phase of actual deployment of the grid booster pair (pilot) or units (systemic). This state of operation can only be maintained for a short duration for as long as the storage capacities of the BESSs are available. According to the use case of the gird booster concept, a prolonged operation mode is not needed as the grid booster only needs to bridge the time until slower units can act.

4. **Substitution** Before the storage capacities of the BESSs are exhausted, the relief of the congested branch has to be taken over by a different unit. Typically, conventional generation units can assume those roles. While the substitution actions are ramped up, the BESS reduce their power infeed or demand accordingly and are transitioning to a stand-by state. Based on their state of charge (SoC) they can either participate in subsequent curative actions or have to be restored to their initial SoC.

5. **Restoration** The restoration phases serves two purposes. For once, the initial SoC of the BESS has to be restored to enable a further deployment of the unit. The SoC restoration is accompanied by certain constraints such as a need for cost optimality. Additionally, the violated (N-1) security also needs to be restored as the power system is still in a vulnerable system state after the curative action.

Fig. 2.20 shows an exemplary process of a successful grid booster deployment with a BESS as grid booster unit and a conventional power plant as substitution measure. Across the first three phases, the activation, triggering and actual deployment of the BESS is shown. With the fourth phase, the substitution, the rate of discharge of the BESS slows down as the power plant is activated and starts to adopt the curative action. When the infeed of the BESS reaches zero, it switches into a standby state for an indefinite period until the restoration phase starts. Then, the BESS recharges

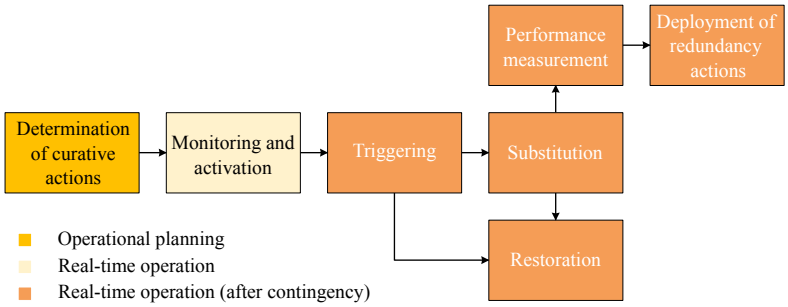

Figure 2.19: Phases associated with the grid booster concept for curative deployment

with additional power provided by the power plant. At the end of the cycle, the grid booster unit is available for further deployment.

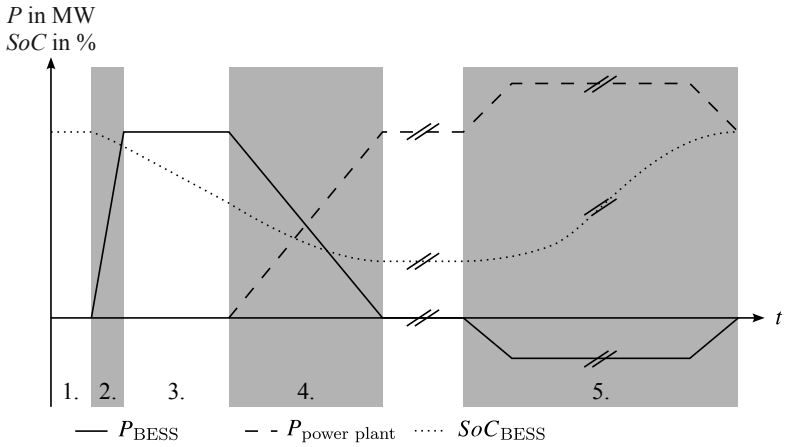

Figure 2.20: Phases of the grid booster operation scheme, following [108]

In the proposed concepts, the grid booster is unspecific regarding the utilized technologies, with the only condition being the compliance with the strict time requirements needed for a curative system operation scheme (cf. Section 2.1.2). The function of a power sink can be assumed, i.e., by a controllable load or a curtailed renewable energy source (RES). Conversely, the power source is more difficult as conventional energy source have a comparatively long ramping speed. Lindner *et al.* [108] gives an overview of possible technologies, leaving only BESS as viable technology as source or sink and large (offshore) wind parks as sinks. In the scope of this work, only BESS-based grid booster will be considered.

As the idea of the grid booster is a rather new and mainly pursued in the German context, not many studies discussing the use of grid booster as a part of congestion management can be found in the literature. In [109], the dynamics of a curative action by a BESS-based grid booster is studied. Lastly, [48] discusses the use of an SpPS using the example of a grid booster.

2.1.5.4 Utilization of Flexibility of Underlying Systems

As energy generation capabilities are shifted towards lower voltage level due to the energy transition and the thereby increased installation of RESs, those capacities need to be made available for congestion management. In Germany, this is done by the implementation of the so-called Redispatch 2.0 process expanding the regulations to consider units bigger than 100 kW and remote-controlled assets of lower levels for congestion management [110–112]. The capabilities of underlying systems to provide active and reactive power flexibility are already studied and shown (e.g. [53]). Current challenges revolve around establishing a suitable process in which the TSO who needs the flexibility potentials, the system operators of the underlying systems who provide those potentials as well as the operators of the RESs are incorporated.

2.1.5.5 Load Shedding

As mentioned in Section 2.1.1, § 22 (1j) SO GL and § 13 (2) EnWG define the option of shedding controllable loads. Load shedding is at most an emergency measure available to the system operator as it implicates a violation of their supply task and are therefore associated with immense compensatory payment. In the literature, load shedding is often included solely to guarantee the solvability of the optimization problem.

2.1.6 Summary of Operational Planning Principles

This section outlines the framework of the operational planning processes at the European and German level. The SO GL, which sets the framework for TSOs at the European level, is open to technology in regard to the time of activation of a remedial action and defines a list of applicable degrees of freedom for congestion management. On the German level, the measures are classified and set in order for their activation in the EnWG. Hence, a priority is laid on network-related measure before market-related ones and lastly the use of network or capacity reserves.

Following this, the principles of a curative system operation scheme is presented. A prerequisite for curative actions is the exploitation of thermal reserves of electrical conductors. The actual critical value in congestion management is not its congestion current but the thermal rating at which the line sag becomes so large that a pole-to-ground-fault occurs. Since the temperature of the conductor does not increase abruptly but uniformly, a temporary overloading of the transmission branches is permissible. Here, two definitions are made: the PATL and TATL value which both define the maximum loading for a permanent and a short-term period. While the PATL can be defined as a constant value, the TATL is dependent on weather conditions, initial loading and most importantly the intensity and duration of the congestion current. As the overloading of lines can only be for short amounts of time, quick response times are necessary for the activation of curative actions and are best implemented by decentralized concepts such as SpPSs.

Since the SO GL is open to technology with respect to the type of remedial action, its definition for integration into operational planning processes is also. The dimensioning of remedial actions happens as of the short-term operational planning phase. Starting with the WAPP, TSOs identify critical contingencies within their systems and prepared CMMs. From the day-ahead processes, the regional security coordinator is involved to coordinate the efforts of the individual system operators to create an overall picture at European level and to identify control area crossing contingencies.

This sets requirements for the implementation of curative actions:

- Thermoelectrical model of electrical conductors (both overhead transmission lines (OHTLs) and cables)
- Monitoring systems in the transmission grid to accurately depict TATL time windows
- Uniform exchange formats for operational planning (cf. DACF)
- Devices and systems for an automatic activation of curative actions
- Sufficient amount of controllable power flow controlling assets
- Holistic coordination of preventive and curative measures
- Maximum computation time of 60 minutes (for IDCF) or 15 minutes (close to real-time)

An important prerequisite for curative system operation is the modeling and monitoring of the thermal reserves of transmission branches. Therefore, a suitable thermoelectrical model is needed to calculate the available reserves. Additionally, a monitoring system needs to be installed to measure the current temperature of affected branches and fully allow a dynamic thermal line rating. First proposals for thermoelectrical models are already presented (e.g. [41]) but not yet validated in actual operation. Accordingly, monitoring systems are installed in pilot projects to collect data of conductor temperatures.

Also, when looking at the operational planning processes, the need for uniform exchange formats is seen. Starting from the DACF, the regional security coordinator collects the determined CMMs from all participating TSOs to prepare a holistic snapshot of its region. As preventive actions are currently the state of the art, this process needs to be extended to allow curative actions as well as their replacement measures in the SSA. Devices or assets for an automatic activation of curative actions are already available in principle such as SpPSs. Pilot projects such as the KAI project from TransnetBW also show the attention and interest of system operators in the problem. Lastly, curative actions must be dimensioned with preventive measures as they greatly impact the post-contingency power flow state of the system. This is especially the case, as curative actions are only for a short-term activation and are to be replaced by other measures. Those replacement measures also need to be respected in the planning processes. A coordination of both actions is therefore irrevocable. This is currently not implemented by TSOs.

2.2 Status-quo of Optimization in Power Systems

Regarding operational planning processes, especially the determination of CMMs are typical optimization problems. In this context, Fig. 2.21 shows the most common applications of optimization problems within the aforementioned planning processes based on their temporal occurrence starting from the week-ahead process to intraday and online processes. For the week-ahead planning, the Unit Commitment problem is used to schedule the most Economic Dispatch of generation units, although it is not applied in the European context due to the unbundling. Simultaneously, the Economic Dispatch is used for allocating the scheduled generating units up to the day-ahead process. The actual determination of remedial actions is done by an Optimal Power Flow (OPF) as it is the first formulation to consider the electrical grid whereas the previous method adopt a power grid similar to a copper plate.

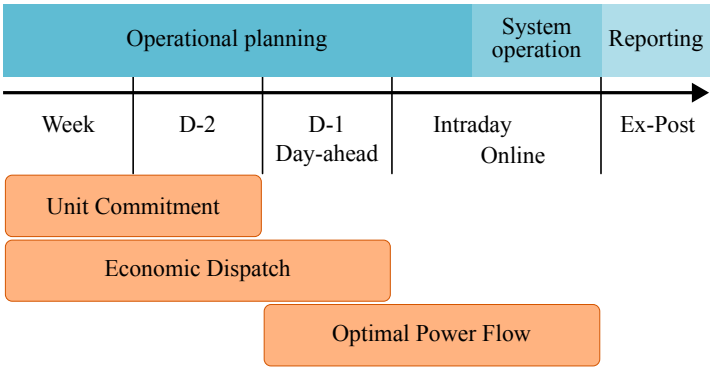

Figure 2.21: Applications of optimization problems in power system operation classified by time domain

As this thesis is centered around discussing the aspect of the determination of CMMs, this section is meant to briefly outline the mathematical basics of optimization. According to the explanation of [36, 113, 114], optimization consists of the elements:

- Modeling,
- Solution and
- Application problem.

Therefore, this list gives the structure of this section. The mathematical foundation to optimization is presented first by going into detail of how to define a model for optimization in Section 2.2.1 and subsequently outlines solution techniques in Section 2.2.2. Typical application problems in the power system context are already mentioned and classified in Fig. 2.21. Thus, Section 2.2.3 details those problems in regard to their mathematical modeling.

2.2.1 Modeling of an Optimization Problem

The goal of the modeling is to give an abstraction and representation of the application problem in form of a purely mathematical formulation [36]. The general goal of an optimization consists of minimizing (or maximizing) a specific parameter of the actual application problem. In the general context of optimization in power system operation or planning, where the reliability of the system is the focus, the objective should be the minimal global socio-economic cost [115]. A maximization can be achieved by formulating a minimization problem with an inverted sign. In the following, all problem formulations are written as minimization problems. In its most basic form, an optimization problem is defined as the minimization of an objective function f, with the mathematical model shown in (2.4). Here, the vector $\boldsymbol{x}$ represents the decision variables of the optimization problem and $\boldsymbol{u}$ the state variables respectively.

$$\min_{\boldsymbol{x}} f(\boldsymbol{x}, \boldsymbol{u}) \tag{2.4}$$

The common form of (2.4) is also called an unconstrained optimization problem, as the objective function is not dependent on any other conditions. In contrast, constrained optimizations are formulated with constraint functions to restrict the solution space of the objective function. The standard formulation of a constrained optimization problem is given by (2.5) by adding (2.5b) and (2.5c) as equality and inequality constraints to the overall problem formulation.

$$\min_{\boldsymbol{x}} f(\boldsymbol{x}, \boldsymbol{u}) \tag{2.5a}$$

$$\text{subject to} \quad g(\boldsymbol{x}, \boldsymbol{u}) = 0 \tag{2.5b}$$

$$h(\boldsymbol{x}, \boldsymbol{u}) \leq 0 \tag{2.5c}$$

2.2.1.1 Problem Classes

Optimization problem classes can be roughly classified into [116]:

- Linear programming (LP),
- Non-linear programming (NLP) and
- Dynamic programming.

The names of the problem classes give an insight about the properties of the optimization formulation. LP models are made up solely of linear equations whereas NLP have at least one non-linear part. All categories have further subclasses like the mixed-integer programming (MIP) or mixed-integer non-linear programming (MINLP) as derivates of the LP and NLP respectively to optimize integer values, i.e., when optimizing on-off-variables or positions of transformer tap changers. The term "programming" finds its origin in the beginning of optimization algorithms in the course of military programs and was established also for future works [117].

Convexity is an important factor in the solution process of optimization problems. As it can be seen in Fig. 2.22, there is a clear difference in the number of stationary points. The more stationary points

that exist in the problem formulation, the harder it gets for the optimization algorithm to identify the global solution. This is especially the case for conventional methods that rely on differentiation.

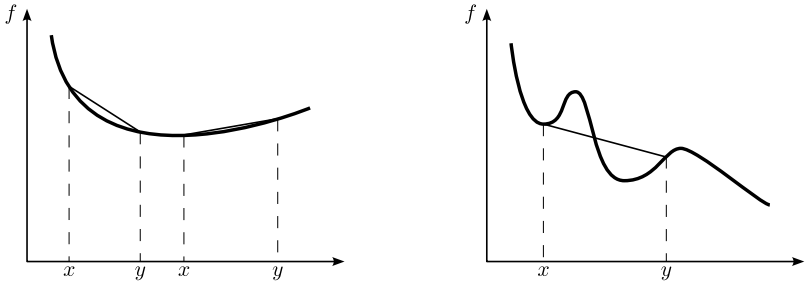

(a) Convex **(b)** Non-convex

Figure 2.22: Exemplary function graphs showing convexity on $\mathbb{R}$

According to [118], convexity for two point $x, y \in X$ of a function $f : X \to \mathbb{R}$ is given by the Jensen's inequality [119] in (2.6).

$$\forall x, y \in X, \mu \in [0,1] : \quad f((1-\mu)x + \mu y) \leq (1-\mu) f(x) + \mu f(y) \tag{2.6}$$

This means, a function f is convex if the function graph runs under each of its secants as is shown in Fig. 2.22a whereas the graph of a non-convex function, as shown in Fig. 2.22b, (partially) runs under its secants. Another definition of a convex continuously differentiable function is that its graph runs above the graphs of each of its linearization [120], which can be defined by (2.7).

$$\forall x, y \in X : \quad f(y) \geq f(x) + \langle \nabla f(x), y - x \rangle \tag{2.7}$$

Due to the non-linearity of the power flow equation, AC representations of power system optimization problem fall into the class of NLP problems. Often, non-linear problems also have a non-convex nature. Lesieutre and Hiskens [121] proofed this for the OPF problem and Lavaei *et al.* [122] partially attributed it to the non-linear physical parameters P, Q and $|V|$. Because of this, non-linear power system optimization poses a challenge for conventional solving techniques [123] as they are local optimizers by nature. This means that they will converge towards a local optimum, instead of a global one, when the starting point is near a local solution [124]. For most commercial non-linear solvers, this is a general problem [125] as they are based on the Karush-Kuhn-Tucker necessary optimality conditions [126]. To ease up the tight non-linear optimization problem, one possibility is the use of convex relaxation techniques [127] to transform the model to a convex problem. Exemplary representatives for such relaxations are semi-definite programming [128], second order cone [129], Convex DistFlow [130], quadratic convex [123] and the moment-based relaxation [131, 132].

2.2.1.2 Optimization with Multiple Objectives

Multi-Objective Function

The optimization problem described in (2.4) and (2.5) formulate a single objective problem each, e.g., the optimization minimizes a single parameter of the application problem, and can be described mathematically by (2.8) [133].

$$\min_{\boldsymbol{x}}\{f_1(\boldsymbol{x},\boldsymbol{u}), f_2(\boldsymbol{x},\boldsymbol{u}), \ldots, f_k(\boldsymbol{x},\boldsymbol{u})\} \tag{2.8}$$

Even though, multi-objective optimization enables the optimization of multiple parameters it is not possible to find a single solution that would be optimal for all objectives simultaneously. A holistic optimal is the so-called Pareto optimality. A Pareto efficient solution is achieved, when no objective can be improved without deteriorating another objective. The set of all Pareto efficient solutions is called Pareto front [134].

Another way of defining a multi-objective problem is shown by (2.9). Here, each single objective is provided with a weighting factor w_l and summed over all N_{OF} functions. Through the proper dimensioning of the weighting factors, specific objectives can be prioritized where the optimum deviates from the Pareto front.

$$\min_{\boldsymbol{x}} f(\boldsymbol{x},\boldsymbol{u}) = \min_{\boldsymbol{x}} \sum_{l}^{N_{\mathrm{OF}}} w_l f_l(\boldsymbol{x},\boldsymbol{u}) \tag{2.9}$$

Based on the idea of multi-objective optimizations, there exists also the definition of a many-objective problem. However, no clear definition for a many-objective function can be found in the literature. In [135], many-objective is defined as an objective function with more than two to three individual objectives, while [136] refers to more than four objectives and [137] more than three.

Bilevel Programming

Besides the application of multi-objective functions to solve optimization problems with different goals, the literature also discusses the use of bilevel programming (BLP). The BLP problem goes back to the description of oligopoly situations in economy markets by [138] in 1934. The Stackelberg competition, or Stackelberg leadership model, describes a strategic economy game in which a leading company takes action first and following companies move upon it.

In a broader sense, BLP, or two-level optimization, handles problems with an upper and lower level optimization problem where the optimality of the upper level problem is dependent on the lower level. Variables defined in the upper level problem are then considered parameters in the lower level and the solution lower level optimization problem are a part of the objective function of the upper level optimization. The very first actual introduction of BLP problems was in 1973 by Bracken and

McGill [139, 140]. In [141] the general form of the BLP optimization problem is given according to (2.10).

$$\min_{\boldsymbol{x},\boldsymbol{y}} F(\boldsymbol{x},\boldsymbol{y},\boldsymbol{u}) \tag{2.10a}$$

$$\text{subject to} \quad G(\boldsymbol{x},\boldsymbol{u}) = 0 \tag{2.10b}$$

$$H(\boldsymbol{x},\boldsymbol{u}) \leq 0 \tag{2.10c}$$

$$\min_{\boldsymbol{y}} f(\boldsymbol{y},\boldsymbol{u}) \tag{2.10d}$$

$$\text{subject to} \quad g(\boldsymbol{y},\boldsymbol{u}) = 0 \tag{2.10e}$$

$$h(\boldsymbol{y},\boldsymbol{u}) \leq 0 \tag{2.10f}$$

The variables of (2.10) are structured in the same way as the individual optimization problems: $\boldsymbol{x}$ represents the vector of upper level variables and $\boldsymbol{y}$ the vector of lower level variables. Accordingly, the functions F and f are called upper and lower level objective function while G and H define the upper level constraints and g and h the lower level constraints. Even though, first works on the BLP started in the 1970s, its usefulness became more apparent in the 1980s [141]. In [142], one of the first literature review on the topic was presented. Regarding their properties, BLP problems are generally non-convex and non-differentiable and was proven by [143] to be $\mathcal{NP}$-hard[3] in its simplest form (a linear–linear problem). A formal proof, showing the non-existence of an algorithm solving a linear BLP problem to a global solution was provided by [144]. Even evaluating the optimality of a solution was proven to be an $\mathcal{NP}$-hard task. Another aspect of BLP problems is their asymmetry. While the leader usually has complete knowledge of the follower's problem, the follower can only observe the leader's decisions and optimize its own strategies. Conventional algorithms to solve the BLP problem are:

- single level reduction,
- descend methods,
- penalty methods and
- trust-region methods.

Real world problems, such as non-linearities and discreetness, make it difficult for conventional methods to solve complex bilevel problems, leading [145] to suggest the application of intelligent search algorithms. Through the usage of intelligent search algorithms, multiple ways to solve bilevel problems arise, such as a single level reduction, metamodeling-based methods or nesting multiple optimization algorithms. Nested methods are usable in two ways, either by applying an intelligent search algorithm for the upper-level problem and a conventional method for the lower level or by

[3] Informally speaking, an $\mathcal{NP}$-hard problem is defined as a problem whose time to solve a problem scales badly with its size and are therefore hard to solve. Taking the Traveling Salesman Problem for example, finding the shortest route for 20 cities may be solvable but expanding this to a whole country, an exact solution may not be found and can only be approximated reasonably close to the optimum.

using an intelligent search algorithm for both levels [145]. One of the first application of a nested bilevel optimization was presented by [146].

2.2.2 Optimization Solvers

The solution of an optimization problem is directly dependent on its modeling and is needed to make suitable adjustments to the problem formulation. Based on the model, certain requirements on the usable solving techniques arise. Based on [116], optimization algorithms can be structured in:

- Conventional methods,
- intelligent search algorithm and
- Fuzzy search theory.

Conventional methods are those that are purely based on exact mathematical modeling and incorporate complex operations such as the use of gradients, Hessian matrices and matrix inversions. For industrial applications, they are the state of the art as they are very fast and deliver reproducible results due to their exact mathematical formulation. Common representatives of conventional solvers are:

- Interior Point [147, 148],
- Simplex Method [149],
- Newton Raphson,
- Barrier Method or
- Trust Region Method [150].

Based on their use of complex operations, tight restrictions on, e.g., the objective functions imposed such as differentiability, continuity and convexity. Especially the aspect of convexity, which is accompanied by non-linear optimization problems, is a problem for conventional solvers that is often addressed by convex relaxation (cf. Section 2.2.1). Another approach to address the non-convex nature of AC optimization problems is the use of intelligent search algorithms. Instead of determining the optimality through complex mathematical operations, metaheuristics are applied to measure the optimality by a fitness value. Thereby, some restrictions on the objective function are relieved [124].

Intelligent search algorithms renounce of an exact mathematical formulation by using heuristics in the modeling process. Therefore, they are more practical in the application on large and complex optimization problems as the risk of, i.e., non-convergence due to a badly chosen start value or convergence to a local solution is reduced [151]. Initially, intelligent search algorithms were designed for unconstrained optimization problems thus lacking in any inbuilt constraint handling techniques like the Lagrange multiplier method used by most conventional methods. In [152, 153],

an overview of different techniques is given, such as the penalty function. The penalty function adds a penalty term to the objective function value. Thereby, a differentiation between death penalties [154], static penalty factors [155] and penalty functions [156].

Another design approach is the use of a hybrid optimizer. In [157], an intelligent search algorithm was combined with an interior point method, where the intelligent search algorithm optimized the upper and lower limits of the control variable of the interior point. Other proposals combine properties of two or more different intelligent search algorithms, i.e., [158–160].

As proven by the No Free Lunch theorem [161], there is no perfect algorithm that is applicable to every optimization problem. Consequently, intelligent search algorithms also come with certain drawbacks. One is that, as there is no complete mathematical model, there is also no evidence on optimality of the result. Furthermore, as most methods rely on stochastic processes and are not deterministic, results are not reproducible. And lastly, most optimizers introduce new parameters to control their behavior. This introduces a new problem of finding the most optimal set of parameters for each optimization problems. It should be noted that there are efforts to design algorithms with self adaptive parameters and penalty functions (e.g. [154–156, 162–166]).

2.2.3 Application Problems in Power System Operation and Planning

2.2.3.1 Unit Commitment

Unit Commitment [167] is a combinatorics problem of the MIP class. The objective is to find an optimal dispatch schedule, including production level, for each generating unit to meet the forecasted consumption. Therefore, decisions have to be made about which generating unit to deploy at which times within a given planning horizon [168–170]. For a comprehensive literature review from 2004 as well as 2012, see [168] and [171].

The objective function is usually the minimization of generation costs C_{total} for the planning horizon under consideration (2.11) or the maximization of profit C_{profit} in the context of a liberalized energy market (2.12) [172]. For the last objective function, the binary decision variable $\boldsymbol{o}_{\text{on/off},t}$ is introduced and controls the operating condition of the asset, i.e., if it is turned on or off, for the time frame $t \in T$.

$$\min_{\boldsymbol{p}_{\text{gen}}} C_{\text{total}} = \sum_{t=1}^{T} C_{\text{fuel},t}(\boldsymbol{p}_{\text{gen},it}) + C_{\text{maintenance},t}(\boldsymbol{p}_{\text{gen},t}) + \boldsymbol{C}_{\text{start},t} + \boldsymbol{C}_{\text{stop},t} \tag{2.11}$$

$$\max_{\boldsymbol{p}_{\text{gen}},\boldsymbol{o}_{\text{on/off},t}} C_{\text{profit}} = \sum_{t=1}^{T} (\boldsymbol{p}_{\text{gen},t}\boldsymbol{C}_{\text{price},t})\boldsymbol{o}_{\text{on/off},t} \tag{2.12}$$

A list of possible constraints is given in Tab. 2.2. It can be noted that all constraints neglect the actual power system. For the Unit Commitment, the power system is assumed to be a copper plate.

Table 2.2: List of common constraints of the Unit Commitment problem [171, 173]

Constraint	Description
Minimum operation time	A generating unit must run for a certain amount of time before shutting down.
Minimum downtime	A generating unit must be switched off for a certain time before it can be switched on again (e.g. to cool down components).
Ramp speed	The limit on how fast the active power feed-in can change within a certain time range.
Power balance	To balance the power between generation and consumption.
Necessary running generation units	Certain units that must run due to operational reliability and/or economic considerations.
Necessary idle generation units	Idle units due to maintenance or (temporary) shutdown
Reserve power	Limitation due to necessary provision of balancing power or keeping balancing power reserve capacity free
Personnel constraints	Limitations due to the limited amount of personnel within a power plant/power park.

2.2.3.2 Economic Dispatch

Economic Dispatch, or optimal dispatch, describes the problem of allocating power generation quantities to appropriate generating units within a mix so that all consumers in a network are supplied as economically as possible [174]. The Economic Dispatch optimization problem dates back as early as the 1920s [175–177]. A historical development up to the year 1988 can be found in [174], where the work builds on the research results of [175, 178, 179] and supplements them from the year 1977. The Economic Dispatch is very much related to the Unit Commitment problem, as they are both MIP combinatorics problems. The difference between the two optimization problems is that the Economic Dispatch assumes that a set of generating units N_{gen} is already connected to the grid. It is therefore up to the Unit Commitment to select this quantity for the Economic Dispatch.

[173] describes the Economic Dispatch optimization problem as the minimization of the power generation cost to meet the demand (2.13a). Constraints are the active power balance (generated power equals consumed power) in (2.13b) and the power limits of the generating units in (2.13c). Here, the scalars N_{gen} and N_{load} describe the total number of generators and loads in the system respectively.

$$\min_{\boldsymbol{p}_{\text{gen}}} \quad C = \sum_{i=1}^{N_{\text{gen}}} C_i(p_{\text{gen},i}) \tag{2.13a}$$

$$\text{subject to} \quad \sum_{i=1}^{N_{\text{gen}}} p_{\text{gen},i} - \sum_{i=1}^{N_{\text{load}}} p_{\text{load},i} = 0 \tag{2.13b}$$

$$p_{\text{gen,min},i} \leq p_{\text{gen},i} \leq p_{\text{gen,max},i} \tag{2.13c}$$

The total costs as well as the plant-specific costs are represented here by C and C_i, respectively. A striking feature of Economic Dispatch is that the model is built without information of the underlying network. Accordingly, power losses or limitations due to transmission capacities are neglected. Such aspects are considered in the so-called Security Constrained Economic Dispatch [180, 181] which will not be discussed further here.

2.2.3.3 Optimal Power Flow

The OPF goes back to work of the 1960s [182, 183]. It describes the logical continuation of Economic Dispatch by extending the optimization problem to include considerations of the underlying power system and incorporating power flows. The equality constraint of the OPF is given by the power equilibrium. Compared to the mathematical formulation from (2.13b), it is extended by the net node apparent power. Using Kirchhoff's current law (2.14), Ohm's law (2.15) as well as the formulation to calculate the complex apparent power, the formulation of the net node apparent power is seen according to (2.20).

$$\underline{i}_{\text{generation},d} - \underline{i}_{\text{demand},d} = \sum_{(d,e)} \underline{i}_{de} \tag{2.14}$$

$$\underline{i}_{de} = \underline{y}_{de}(\underline{v}_d - \underline{v}_e) \tag{2.15}$$

$$\underline{s}_{de} = \underline{v}_d \underline{i}^*_{de} \tag{2.16}$$

$$\underline{y}_{de} = g_{de} + j b_{de} \tag{2.17}$$

$$\underline{s}_{de} = \underline{y}^*_{de} \underline{v}_d \underline{v}^*_d - \underline{y}^*_{de} \underline{v}_d \underline{v}^*_e \tag{2.18}$$

$$\underline{s}_{\text{generation},d} - \underline{s}_{\text{demand},d} = \sum_{(d,e)} \underline{s}_{de} \tag{2.19}$$

$$\underline{s}_{\text{generation},d} - \underline{s}_{\text{demand},d} = \sum_{(d,e)} \underline{y}^*_{de} \underline{v}_d \underline{v}^*_d - \underline{y}^*_{de} \underline{v}_d \underline{v}^*_e \tag{2.20}$$

As optimization solvers are not able to use complex numbers as control variables, the power equilibrium is split in the active (2.21) and reactive power (2.22). Please note that the depiction uses the trigonometric form. Thereby, g_{de} and b_{de} indicate the conductance and susceptance of the branch admittance $\underline{y}_{de}$ respectively. The angle θ_{de} is the voltage angle difference between bus d and e.

$$p_{\text{generation},d} + p_{\text{demand},d} = v_d \sum_{\substack{j=1 \\ j \neq i}}^{N_{\text{bus}}} v_e (g_{de} \cos\theta_{de} + b_{de} \sin\theta_{de}) \tag{2.21}$$

$$q_{\text{generation},d} + q_{\text{demand},d} = v_d \sum_{\substack{j=1 \\ j \neq i}}^{N_{\text{bus}}} v_e (g_{de} \sin\theta_{de} - b_{de} \cos\theta_{de}) \tag{2.22}$$

For the inequality constraints, in addition to the resource limits of the generators, other technical and regulatory limits are included in the problem description, such as the voltage band or PATL

and TATL values of transmission lines. With respect to the objective function, modifications to the OPF can also be seen. Minimization of total cost, analogous to (2.13a), is one of the most common objective functions in the literature, along with minimization of network losses [184]. A comprehensive literature review regarding modeling and solution approaches can be found in [184–187].

Based on the initial definition of the OPF problem, several sub-problems are derived over time, expanding its original scope, such as the SCOPF. The SCOPF dates back to initial work around 1987 [188, 189]. Developments in research through 2011 are summarized in [190]. As an extension to the OPF, the SCOPF integrates the consideration of possible fault variants within the power system in the form of additional constraints, see (2.23), and seeks a solution to prevent or cure limit violations due to the resource failures. Here, the index k describes the corresponding failure variant from the set of all possible contingencies C with its cardinality NC. A special case represents the scenario $k = 0$ and describes the base case of the power system without failed resource.

$$g_k(\boldsymbol{x}_k, \boldsymbol{u}_k) = 0 \qquad k \in [0, NC] \tag{2.23a}$$

$$h_k(\boldsymbol{x}_k, \boldsymbol{u}_k) \leq 0 \qquad k \in [0, NC] \tag{2.23b}$$

Depending on the application of SCOPF, whether in the prevention or the curation of a critical failure, a distinction is made between Preventive Security Constrained Optimal Power Flow (PSCOPF) and Corrective Security Constrained Optimal Power Flow (CSCOPF). The PSCOPF (in [188] also introduced as Contingency Constrained Optimal Power Flow) goes back to the work of [191] and focuses solely on computing a preventive solution by superimposing all contingencies as well as the base case on the optimization problem. On the other hand, the CSCOPF described in [189] computes a specific action to correct an unsafe system state.

2.2.4 Summary of Optimization in Power Systems

The determination of remedial actions is a classic task of optimization. To formulate requirements on the optimization model to allow a coordination of preventive and curative CMMs, this section provides a brief introduction to mathematical optimization and its common applications to power systems. A basic optimization model encompasses the elements of modeling, solution and the application problem. In regard to the modeling, optimization problems are generally clustered in LP and NLP problems (with various subcategories) which only depend on the presence of non-linear equations in the modeling. LP formulations tend to be easier to solve as convexity of the problem is given more often, whereas NLP problems are non-convex by nature and need convex relaxation to be solvable by certain algorithms.

For optimization solving algorithms, conventional methods and intelligent search algorithms are introduced and discussed regarding their advantages and limitations. Conventional methods (e.g. Interior Point, Simplex Method, Newton Raphson) are the state of the art for industrial applications and operate on complex mathematical operations such as gradients, Hessian or matrix inversions.

Therefore, they impose strict requirements on the objective function, i.e., differentiability or continuity. Intelligent search algorithm on the other hand renounce such exact mathematical formulations and approach optimization problems by heuristics. Yet, as stated by the No Free Lunch theorem (cf. Section 2.2.2), every method comes with its own drawbacks and the optimal solving technique depends on the modeling and application problem.

In the context of operational planning and system operation in electrical power systems, the optimization problems of Unit Commitment, Economic Dispatch and OPF are presented as the most common application problems and assigned to the corresponding planning processes. Whereas Unit Commitment and Economic Dispatch are more economically oriented problems with no real regard to the underlying power system, OPF is a diverse problem with many variations. The determination of remedial actions for congestion management is an OPF problem or rather a problem of its subcategory the SCOPF as it expands the OPF formulation by operational security constraints needed in congestion management. Within the scope of the SCOPF problem, a further specialization regarding the determination of preventive and curative measures is made by defining the PSCOPF and CSCOPF respectively. To address the scope of this thesis of designing a coordinated determination approach of preventive and curative CMMs, the optimization problem must combine the PSCOPF and CSCOPF problems.

2.3 Conclusion and Gap Analysis

By current implementations, system security is established via a *passive (N-1) security*. This means, congestions are averted solely by preventive means while curtailing transmission capacities and therefore pushing the need for grid reinforcement and expansion. The state-of-the-art research shows the capabilities of the inclusion of curative actions into the current system operation landscape, shifting system security towards a more *active (N-1) security*. Unlike preventive actions, curative CMMs are activated after the actual failure occurs, as shown in Fig. 2.23. A curative operation of the system is based on exploiting the thermal reserves of the transmission lines, which is the actual critical factor in congestion management. Simultaneously, this sets strict requirements on the activation time of curative actions so that the thermal reserves are not exhausted. Thus, by employing an active (N-1) strategy, transmission lines can be utilized at a higher level in the base case of the system compared to when operating the system in a passive (N-1) secure state.

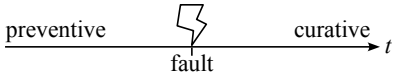

Figure 2.23: Temporal order of preventive and curative actions

Several studies have been carried out to investigate the prerequisites to enable a curative operation scheme as well as its general feasibility and effectiveness. First and foremost is the *InnoSys 2030* research project [22, 23]. Over the course of three years, the impact of curative system operation on the need for grid reinforcement and preventive redispatch was investigated. Parts of the research project have been published in individual publications.

- In [192], first investigations of the impact on the volume of preventive CMMs were published. A MIP model was used to show how the curative use of HVDC systems, PSTs, offshore wind farms and BESSs can reduce the preventive redispatch volume by up to 69 % (depending on the scenario) for the German power system in the target year 2030.
- The study framework of [192] is extended by [41] by incorporating a thermal line model into the optimization problem. The model used precise constraints for the PATL and TATL of the transmission lines, allowing for an accurate exploitation of the thermal reserves needed for a safe deployment of curative measures.
- In [193], using a similar framework, the potential of the grid booster technology as a curative CMM is investigated and a heuristic approach for an ad-hoc determination of curative measures is introduced. In contrast to [41, 192], a coordination of preventive and curative measures is discussed. A ratio, indicating how many curative actions correspond to one preventive action, is defined by a parameter but no extensive investigation of the implications of the ratio is presented.
- A NLP formulation is presented in [36]. Here, the capabilities of power flow controlling devices, especially HVDC systems, for curative system operation have been investigated.
- The capabilities of distribution systems to provide curative actions for the transmission system are discussed by [194].

Thus, there is a gap regarding the modeling of a coordinated determination of preventive and curative measures as well as the investigation of its benefits on system security. Therefore, this thesis proposes an optimization problem combining the unique aspects of the PSCOPF and CSCOPF. Section 2.2.1 outlines two approaches for this with the application of multi-objective functions and bilevel programming. A bilevel SCOPF model thereby enables capabilities in the distinct separation of the preventive and curative model, both in regard to the available degrees of freedom and the problem class itself.

3 Design of a BLP-SCOPF

The preceding considerations have shown the theoretical benefits an active (N-1) security scheme can have on system operation, especially considering the need for grid reinforcement measures. At the European level, scattered implementations of curative actions in system operation are done by TSOs but no uniform application is found. This comprises for once the comprehensive use of curative actions but also the missing exchange formats that are needed in operational planning. In addition, previous research has addressed the general modeling of curative actions in optimization problems, but there have been few to no approaches regarding the coordination of these with the necessary preventive measures. Due to the strong interactions of the preventive set-point of the power system with the capabilities of curative CMMs, this poses a big gap that this thesis addresses. Therefore, an optimization problem is formulated to enable the coordination of preventive and curative actions.

Fig. 3.1 shows two possible process structures how a coordination of those two measures is possible. The first variant, shown in Fig. 3.1a, describes a staggered coordination in which the preventive and curative optimization takes place in an iterative process. In a staggered process, a preventive solution is determined and remaining fault cases are addressed by a curative optimization. If unresolved scenarios remain, an adjustment must be made to the preventive model via a feedback loop. The process is repeated until all contingency cases have been addressed and the total number of critical contingencies N_{cc} is reduced to zero. Another approach to coordination is the holistic optimization approach shown in Fig. 3.1b. Contrary to the staggered approach, the modeling of preventive and curative action determination is not done in separate steps. Instead, both models are merged into a joint optimization model so that the coordination becomes part of the optimization problem itself.

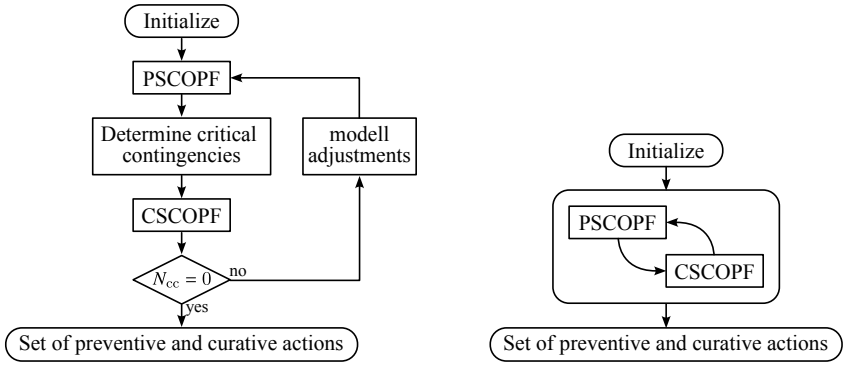

(a) Staggered **(b)** Holistic

Figure 3.1: Coordinated determination approaches by (a) staggering the optimizations or (b) combining them in a single model

Both approaches allow an independent modeling of the PSCOPF and CSCOPF with regard to the problem class as well as the degrees of freedom. While the staggered approach is solvable by current state-of-the-art means, the actual importance and scientific significance lies in the adjustment of

the PSCOPF model based on the CSCOPF results. Additionally, due to the iterative nature, some kind of convergence criterion has to be defined to prevent the optimization to run continuously.

On the contrary, the holistic approach does not need an explicit feedback loop or an extra convergence criterion and is therefore more straightforward. As the holistic optimization means the combination of the PSCOPF and CSCOPF in one optimization problem, the actual challenge to this is the formulation of a model with different objectives. Section 2.2.1.2 introduces two concepts to realize this requirement with the multi-objective function and the BLP model. While the usage of multi-objective functions is well tested and established in the literature, it omits the possibility of separating the PSCOPF and CSCOPF models. Hence, a bilevel SCOPF algorithm is proposed in the scope of this thesis to enable a coordinated optimization of preventive and curative CMMs.

3.1 Bilevel SCOPF Model

As mentioned previously, the proposed SCOPF model is designed as a BLP problem. The upper level describes the determination of preventive actions and the curative ones are determined at the lower level, thereby incorporating the determination of preventive and curative actions in a combined optimization process.

Opposed to the conventional approach, where preventive and corrective measures are determined consecutively, the BLP-SCOPF combines the calculation of curative measures into the PSCOPF problem. A formal problem definition is given by (3.1) where (3.1a)-(3.1e) define the upper level (i.e. the PSCOPF) and (3.1g)-(3.1i) the lower level (the CSCOPF).

$$\min_{\boldsymbol{x},\boldsymbol{y}} F(\boldsymbol{x}, \boldsymbol{y}_c, \boldsymbol{u}_c) \tag{3.1a}$$

$$\text{subject to} \quad G_0(\boldsymbol{x}, \boldsymbol{u}) = 0 \tag{3.1b}$$

$$H_0(\boldsymbol{x}, \boldsymbol{u}) \leq 0 \tag{3.1c}$$

$$G_c(\boldsymbol{x}, \boldsymbol{y}_c, \boldsymbol{u}_c) = 0 \tag{3.1d}$$

$$H_c(\boldsymbol{x}, \boldsymbol{y}_c, \boldsymbol{u}_c) \leq 0 \tag{3.1e}$$

$$c \in C \tag{3.1f}$$

$$\min_{\boldsymbol{y}} f(\boldsymbol{y}_c, \boldsymbol{u}_c) \tag{3.1g}$$

$$\text{subject to} \quad g_c(\boldsymbol{y}_c, \boldsymbol{u}_c) = 0 \tag{3.1h}$$

$$h_c(\boldsymbol{y}_c, \boldsymbol{u}_c) \leq 0 \tag{3.1i}$$

The optimization problem describes the minimization of an objective function F subject to equality constraints G, inequality constraints H and a secondary optimization problem min f. The vectors $\boldsymbol{x}$, $\boldsymbol{y}$ and $\boldsymbol{u}$ describe the upper and lower level optimization variables as well as the state variables. A characteristic of the PSCOPF is to consider the constraints of the base case of the system in addition to the contingency scenarios as the preventive action is initially activated in the base state, and therefore must not violate any of the operational limits even in the initial state. This is reflected in the model by (3.1b) and (3.1c), using zero as index to indicate the base case constraints. In

(3.1d) and (3.1e), the index c is used to indicate the corresponding contingency scenarios where c corresponds to a scenario in the set of all possible scenarios $C = \{1, \ldots, NC\}$. Here, the complexity of the preventive optimization problem becomes apparent. The CMM must satisfy the equality and inequality constraints of the base case and all NC scenarios. Accordingly, the complexity also increases with the size of the electric power system under consideration and the associated length of the contingency list.

In the next step, the specific functions of the devices to be used for CMM or power flow control must be modeled so that they can be formulated into the optimization problem. Within the scope of the proposed BLP-SCOPF, the technologies and their usable degrees of freedom are presented in Tab. 3.1. As mentioned in Section 2.1.5, based on their method of intervening with the power flow CMMs can be grouped in node- and branch-based actions. Here, the modeling focuses solely on node-based actions and comprise VSC-based HVDC systems, conventional generators and BESS-based grid boosters.

Table 3.1: Viable degrees of freedom in congestion management by electrical equipment

Technology	Degree of freedom
Conventional generator	Active power P_{gen}
VSC-based HVDC system	Active power P_{VSC}
	Reactive power Q_{VSC}
	Droop factor k_{droop}
BESS-based grid boosters	Active power P_{GB}
	Reactive power Q_{GB}

Conventional generator contribute primarily to the preventive operation stage as they do in the current system operation framework. Its available degree of freedom is the active power provision P_{gen}. The reactive power is neglected as it is assumed that conventional generators are equipped with some kind of voltage control where the reactive power is a function depending on the target voltage.

As both, VSC-based HVDC systems and BESS-based grid boosters, are building on power electronic technology, their active and reactive power infeed can be controlled independently thus making them viable degrees of freedom for the proposed BLP-SCOPF. In [195], multiple reactive power control modes are defined HVDC systems can be operated in, such as voltage or power factor control mode. In the scope of this work, a reactive power control mode is assumed for all HVDC converters, specifying a fixed reactive power set-point Q_{VSC}. The same is assumed for grid booster units. Additionally, the gain factor of the DC voltage control k_{droop} is utilized as degree of freedom. By doing so, the reaction of the HVDC system on any kind of DC disturbances can be influenced and a preventive action for, e.g., converter outages are feasible. To fully facilitate the capabilities of an HVDC system in system operation, a meshed HVDC overlay system is recommended. For once, this allows for more flexibility in changing the set-point of individual converters and secondly is a necessity to utilize the droop constant as degree of freedom.

As the operation of grid boosters is dependent on the available storage capacity, the grid booster have to be substituted by other equipment (ideally conventional generators) that must be respected in the planning process. By current considerations, the substitution of grid booster units is taken over by fully integrated network components during the pilot phase[4].

3.1.1 Upper Level SCOPF

The upper level optimization variable $\boldsymbol{x}$ comprises the degrees of freedom of the VSCs and generators, as can be seen in (3.2). BESS-based grid booster are omitted as a preventive action, as their active power provision is time-dependent due to the SoC of the BESS and would lead to an increase of the complexity of the problem. Provided that there is always enough storage available for the period under consideration, the BESS-based grid booster can be included in the preventive optimization. However, since this is a large assumption, it is not included here.

$$\boldsymbol{x} = \begin{bmatrix} \boldsymbol{p}_{\text{gen}} & \boldsymbol{p}_{\text{VSC}} & \boldsymbol{q}_{\text{VSC}} \boldsymbol{k}_{\text{droop}} \end{bmatrix}^{\mathsf{T}} \tag{3.2}$$

3.1.1.1 Upper Level Objectives

The objective function of the optimization describes the general goal, which is aimed by the computation. For the upper level optimization, a many-objective objective function is used (see Section 2.2.1.2) as shown in (3.3). This consists of N_{OF} individual objective functions F_l, which are multiplied by a weighting factor w_l and summed up to a final objective function value. In the scope of this work, two sub-objectives are implemented for the upper-level problem, hence $N_{\text{OF}} = 2$.

$$F(\boldsymbol{x}, \boldsymbol{y}_c, \boldsymbol{u}_c) = \sum_{l}^{N_{\text{OF}}} w_l F_l(\boldsymbol{x}, \boldsymbol{y}_c, \boldsymbol{u}_c) \tag{3.3}$$

The first sub-objective function (3.4) is the minimization of the number of critical contingency scenarios by the preventive and curative CMMs, represented by the function $N_{\text{cc,opt}}(\boldsymbol{x}, \boldsymbol{y}_c, \boldsymbol{u}_c)$. The function considers only the contingency scenarios and not the base case. The behavior of $N_{\text{cc,opt}}$ is discrete. For each contingency scenario c in which an operational limit is not met, the function value increases by one. Thus, the function F_1 has its optimum at 0 and its maximum at NC, where NC is the cardinality of C. In section 3.2.3, the computation of $N_{\text{cc,opt}}$ is discussed in more detail.

$$F_1(\boldsymbol{x}, \boldsymbol{y}_c, \boldsymbol{u}_c) = N_{\text{cc,opt}}(\boldsymbol{x}, \boldsymbol{y}_c, \boldsymbol{u}_c) \qquad c \in C \tag{3.4}$$

Since unbundling, the use of conventional generator is associated with a monetary cost, as power plant operators must be additionally compensated for their intervention. The resulting costs are shown in (3.5), where the parameters a_2, a_1, and a_0 are costs depending on the primary energy

[4] [196] defines fully integrated network components as network components "used for the sole purpose of ensuring a secure and reliable operation of the transmission or distribution system, and not for balancing or congestion management".

source and Δp_{gen} the set-point deviation of the generating unit. This deviation is indicated by (3.6) and is the absolute change in the set-point generating unit from its scheduled value by the optimization.

$$F_2(\boldsymbol{x}, \boldsymbol{y}_c, \boldsymbol{u}_c) = \sum_{l=1}^{N_{\text{gen}}} a_2 \Delta p_{\text{gen},l}^2 + a_1 \Delta p_{\text{gen},l} + a_0 \tag{3.5}$$

$$\Delta p_{\text{gen}} = \left| p_{\text{gen,schedule}} - p_{\text{gen,optimization}} \right| \tag{3.6}$$

3.1.1.2 Equipment Modeling

An important part of the formulation of the optimization problem is the modeling of the existing equipment as their operational security limits serve as inequality conditions. In particular, system operation limits (e.g. voltage band and PATL/TATL) and unit-specific limits are applied. Accordingly, in the following the mathematical representation of the utilized equipment is described as well as the constraints they contribute to the model.

AC Branches

AC transmission branches are modelled as π models in series with an ideal PST on end of the branch, shown in Fig. 3.2.

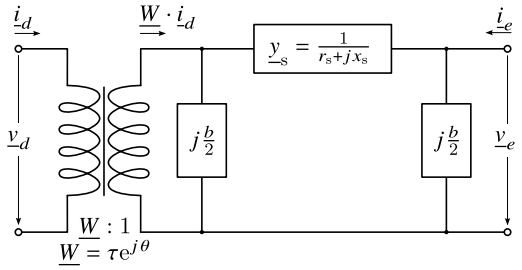

Figure 3.2: Representation of an AC branch segment, following the model of [197]

The series admittance of the π element (3.7) is described by its series admittance $\underline{y}_{\text{s}} = \frac{1}{r_{\text{s}} + i x_{\text{s}}}$ and susceptance b, assuming the shunt conductance g is negligible in comparison to b. To model the ideal PST, its tap ratio is described by the magnitude τ and phase shift angle θ.

$$\underline{\mathbf{Y}}_{\text{br}} = \begin{bmatrix} (\underline{y}_{\text{s}} + j\frac{b}{2})\frac{1}{\tau^2} & -\underline{y}_{\text{s}}\frac{1}{\tau e^{j\theta}} \\ -\underline{y}_{\text{s}}\frac{1}{\tau e^{j\theta}} & (\underline{y}_{\text{s}} + j\frac{b}{2})\frac{1}{\tau^2} \end{bmatrix} \tag{3.7}$$

The complex current injection (3.8) at node d and node e of a branch can be expressed by a multiplication of the branch admittance matrix $\underline{\mathbf{Y}}_{\text{br}}$ and the respective nodal voltages. To limit the power flow across the branch element between nodes d and e, the inequality constraint (3.9) is

added to the optimization model. Thereby, $i_{\max,de}$ corresponds to the PATL value of the branch element.

$$\begin{bmatrix} \underline{i}_d \\ \underline{i}_e \end{bmatrix} = \underline{\mathbf{Y}}_{\text{br}} \begin{bmatrix} \underline{v}_d \\ \underline{v}_e \end{bmatrix} \tag{3.8}$$

$$|\underline{i}_{de}| \leq i_{\max,de} \tag{3.9}$$

DC Branches

As the DC system uses bipolar transmission lines, a single π model is not sufficient. Instead, the transmission corridors are modelled according to the model shown in Fig. 3.3 which is basically two π models mirrored at the dedicated metallic return (DMR).

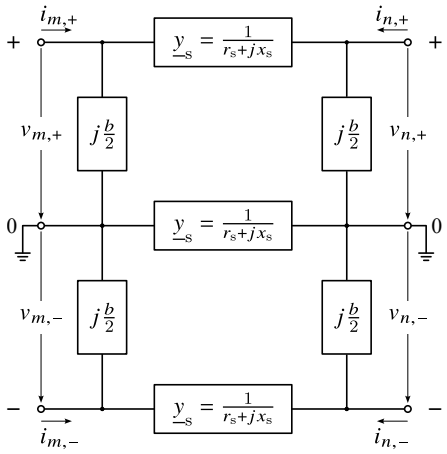

Figure 3.3: Modeling of a bipolar transmission section consisting of DMR, positive and negative conductor

Note that in steady-state power flow calculations the influence of conductance x_{s} and susceptance b can be neglected. Thereby, only the ohmic part remains, and the matrix representation is accordingly to (3.7) without the part of the ideal PST. Similarly to the AC branches, the power flow of the DC branches is also limited by its corresponding PATL value. The inequality constraint is given by (3.10).

$$i_{mn} \leq i_{\max,mn} \tag{3.10}$$

HVDC Converter

For the modeling of VSC-based HVDC converters, [198–200] propose the use of two generators, each at the AC and DC side as shown in Fig. 3.4a. On the AC side, the VSCs provide an active and reactive power output. To respect the technological limitations, the power provision is constrained following (3.11). Due to the rectification of the active power to the DC side, active power losses are represented by p_{loss}.

$$p^2_{\text{VSC},m} + q^2_{\text{VSC},m} \leq s^2_{\text{VSC,max},m} \tag{3.11a}$$

$$p_{\text{VSC,min},m} \leq p_{\text{VSC},m} \leq p_{\text{VSC,max},m} \tag{3.11b}$$

$$q_{\text{VSC,min},m} \leq q_{\text{VSC},m} \leq q_{\text{VSC,max},m} \tag{3.11c}$$

As stated in Section 2.1.5.2, voltage control schemes are recommended for the operation of meshed DC systems to address power inequalities. Therefore, a linear droop function is used for the DC voltage control at each VSC, as depicted in Fig. 3.4b. Additionally, as the droop constant $k_{\text{droop},}$ is an optimization variable, (3.12) is added as inequality constraint.

$$k_{\text{droop,min},m} \leq k_{\text{droop},m} \leq k_{\text{droop,max},m} \tag{3.12}$$

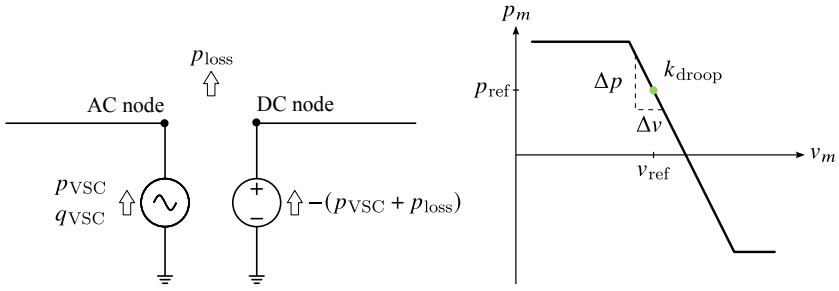

(a) equivalent circuit diagram of converters [201] **(b)** linear droop voltage control function

Figure 3.4: Modeling of VSC-based HVDC converters with (a) the equivalent circuit diagram and (b) the implemented DC voltage control characteristic

Generators and Loads

For generators and loads, their modeling corresponds to the state-of-the-art representation and is depicted in Fig. 3.5. Accordingly, their complex power injection is given by (3.13) and (3.14) respectively.

$$\underline{s}_{\text{gen},d} = p_{\text{gen},d} + jq_{\text{gen},d} \tag{3.13}$$

$$\underline{s}_{\text{load},d} = p_{\text{load},d} + jq_{\text{load},d} \tag{3.14}$$

The operating point of synchronous generators is given by the capability curve shown in Fig. 2.13. Therefore, active and reactive power are not controllable independently as the generator is voltage controlled. To accommodate for this, RESs are modelled as conventional loads to respect their capability to uncouple the active and reactive power provision.

Accordingly, the technical limitations of the equipment imposes constraints to the upper level optimization problem given by (3.15).

$$s_{\text{gen,min},d} \leq s_{\text{gen},d} \leq s_{\text{gen,max},d} \tag{3.15a}$$

$$p_{\text{gen,min},d} \leq p_{\text{gen},d} \leq p_{\text{gen,max},d} \tag{3.15b}$$

$$q_{\text{gen,min},d} \leq q_{\text{gen},d} \leq q_{\text{gen,max},d} \tag{3.15c}$$

As can be seen, only constraints from the synchronous generators are considered. Loads are not controlled by the optimization as load shedding is often included only to improve the solvability of the OPF problem (cf. Section 2.1.1 – emergency actions pursuant to § 13 (2) EnWG) or artificial load ('Load Management') and dummy units at each bus [193]. Thus, loads do not impose additional constraints to the problem.

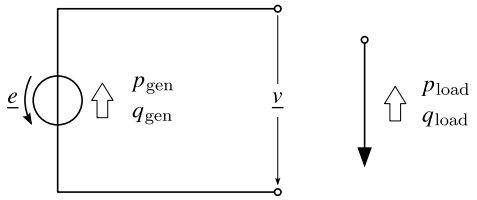

(a) Synchronous generator **(b)** Load

Figure 3.5: Equivalent circuit diagram of (a) synchronous generators and (b) loads

By using the generators as a preventive degree of freedom, another equality condition arises in the context of a preventive redispatch. As noted in Section 2.1.5.1, a preventive redispatch must be neutral to the generation-load-profile. This is ensured by (3.16) so that the sum of all set-point adaptions of the generators equals to zero.

$$\sum_{l=1}^{N_{\text{gen}}} \Delta p_{\text{gen},l} = 0 \tag{3.16}$$

3.1.1.3 AC-DC Network Formulation

The set of equality constraints of the upper level optimization problem (3.1d) in the context of electric power systems is typically described as satisfying the power equilibrium. Thus, the equality constraints can be divided into constraints of the AC and the DC system. For the AC system, the

power equilibrium is divided into the active (3.17a) and reactive power (3.17b) at each AC node.

$$p_{\text{gen},d} + p_{\text{load},d} + p_{\text{VSC},d} = v_d \sum_{\substack{e=1 \\ e\neq d}}^{N_{\text{bus,AC}}} v_e (g_{de}\cos\theta_{de} + b_{de}\sin\theta_{de}) \tag{3.17a}$$

$$q_{\text{gen},d} + q_{\text{load},d} + q_{\text{VSC},d} = v_d \sum_{\substack{e=1 \\ e\neq d}}^{N_{\text{bus,AC}}} v_e (g_{de}\sin\theta_{de} - b_{de}\cos\theta_{de}) \tag{3.17b}$$

The susceptance and conductance here are the congregation of the individual instances and correlate to the simplified branch model shown in Fig. 3.6.

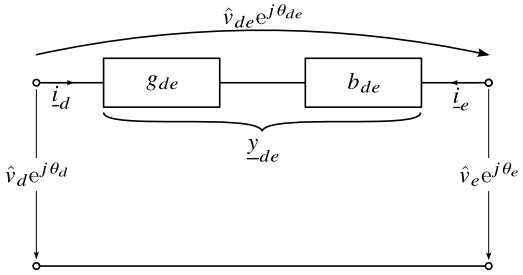

Figure 3.6: Simplified branch representation

To formulate the power equilibrium in the DC system, first the active power injection by the VSCs with DC voltage control is described by (3.18). The power balance of the DC system is described by (3.19) [202].

$$p_{\text{VSC},m}(v_m) = p_{\text{VSC},m,\text{ref}} - k_{\text{droop},m}\cdot(v_m - v_{m,\text{ref}}) \tag{3.18}$$

$$p_{\text{VSC},m,\text{ref}} - k_{\text{droop},m}\cdot(v_m - v_{m,\text{ref}}) = v_m \sum_{\substack{n=1 \\ n\neq m}}^{N_{\text{bus,DC}}} g_{mn}(v_m - v_n) \tag{3.19}$$

To comply with the operational voltage range, the voltages of the AC and DC system are limited by (3.20a) and (3.20b) respectively.

$$v_{\min,d} \leq v_d \leq v_{\max,d} \tag{3.20a}$$

$$v_{\min,m} \leq v_m \leq v_{\max,m} \tag{3.20b}$$

3.1.2 Lower Level SCOPF

In the lower level optimization problem described by (3.1g)-(3.1i), the determination of a curative CMM is modeled for all emergency scenarios that cannot be covered by the preventive measures. Therefore, the lower level SCOPF corresponds to the third stage of decision periods of a TSO. According to the design of a BLP problem, the upper level variable $\boldsymbol{x}$ is fixed at its current iteration for the lower level optimization. In the context of the BLP-SCOPF, this means that the injection of

the conventional generators and VSCs is set to an initial level as well as the gain factor of the DC voltage control.

For the curative action, the usable degrees of freedom $\boldsymbol{y}$ is changed compared to the preventive stage. Firstly, conventional generators are not a viable CMM for curative system operation due to their time constraints. Furthermore, in an attempt to reduce the costs for the corrective measures or even design them cost-neutral (except for costs for maintenance etc.) cost-extensive curative redispatch is not a viable variable. In its stead, BESS-based grid booster units are utilized. Thereby, it is assumed that the capacity of all BESS is sufficient so that the grid booster can be deployed. Regarding the VSC-based HVDC system, the droop gain factor is omitted for the optimization as the frequent change of a control variable is not considered useful at this point.

A BLP optimization problem is complex and computationally extensive (cf. Section 2.2.1.2). To address the topic of complexity, a LP formulation is chosen for the lower level problem and not the same NLP formulation as in the upper level. Consequently, the lower level problem corresponds to a DC power flow model, as described by [203], which assumes a flat voltage profile of 1 pu at all nodes and neglects losses and reactive power flows. Due to the linearization of the power flow model, a consideration of reactive power is not possible. Therefore, only the active power injection of the HVDC systems and grid booster are used as optimization variables as shown in (3.21).

$$\boldsymbol{y}_c = \begin{bmatrix} \boldsymbol{p}_{\mathrm{VSC},c} & \boldsymbol{p}_{\mathrm{GB},c} \end{bmatrix}^{\mathsf{T}} \tag{3.21}$$

3.1.2.1 Lower Level Objectives

Other than the upper level optimization problem, the lower level objective is a single objective function, see (3.22). The function is used for controlling the optimization variables of the VSCs. The equation describes a minimization of the curative set-point adaptation. Therefore, the VSCs set-points of the preventive optimization $\boldsymbol{p}_{\mathrm{VSC,PSCOPF}}$ are needed which are given by $\boldsymbol{x}$.

$$f(\boldsymbol{y}_c, \boldsymbol{u}_c) = \sum |\Delta \boldsymbol{p}_{\mathrm{VSC}}| = \sum \left| \boldsymbol{p}_{\mathrm{VSC,PSCOPF}} - \boldsymbol{p}_{\mathrm{VSC,CSCOPF}} \right| \tag{3.22}$$

The set-point adjustment of an HVDC system can be considered cost-neutral, since there is no intervention in the generation balance. According to [204], a monetary evaluation of the HVDC system deployment is possible to represent the potential wear and tear of the converter technology and the associated rising losses. Based on the assumption that technical wear is a ubiquitous problem that is not characteristic only of converter-based systems, it is not considered within the scope of this work. The objective function pursues two specific intentions. On the one hand, it gives the optimization a general search direction. Furthermore, especially with regard to the adjustment of the active power injection of the HVDC system, an excitation of the underlying AC system is reduced. Theoretical, a VSC-based CMM could result in a power flow reversal of a transport corridor. Using the example of the SuedOstLink with a transport capacity of 2 GW [205], a set-point adjustment of 4 GW is possible in an extreme case. This set-point change can be done within one to two seconds [206].

As the grid booster units are inactive in their initial state and only get activated in the event of a curative action, phenomena like power reversal are not bound to occur. Therefore, no objective function is associated with the grid booster units as they are also cost-neutral.

3.1.2.2 Linearized Network Formulation

The LP problem formulation reduces the set of constraints of the CSCOPF. The equality constraints (3.23) only consider the active power equilibrium of the AC and DC system respectively. According to the assumptions of the DC power flow model, (3.23a) neglects the contribution of the voltage magnitude v_d/v_e and conductance g_{de}. The CMM of the CSCOPF is designed to be in a balanced system state. Therefore, the DC voltage control is not considered as part of the curative action help in balancing the system and (3.23b) considers the active power of the VSCs not as function of the nodal voltage but a constant value.

$$p_{\text{gen},d} + p_{\text{load},d} + p_{\text{VSC},d} = -\sum_{\substack{e=1 \\ e\neq d}}^{N_{\text{bus,AC}}} b_{de}\theta_{de} \tag{3.23a}$$

$$p_{\text{VSC},m} = v_m \sum_{\substack{n=1 \\ n\neq m}}^{N_{\text{bus,DC}}} g_{mn}(v_m - v_n) \tag{3.23b}$$

3.1.2.3 Linearized Modeling of Electrical Equipment

Just like the equality constraints, the inequality constraints are limited to the constraints addressing active power when compared to the upper level modeling. Regarding the constraints imposed by equipment, (3.11) gets reduced to a single constraint addressing the active power limits of the VSCs in (3.24).

$$p_{\text{VSC,min},m} \leq p_{\text{VSC},m} \leq p_{\text{VSC,max},m} \tag{3.24}$$

Grid Booster

As the grid booster is added as new device and degree of freedom, constraints to limit its power output are necessary.

$$p_{\text{GB,min},d} \leq p_{\text{GB},d} \leq p_{\text{GB,max},d} \tag{3.25}$$

As stated in Section 2.1.5.3 and seen in Fig. 3.7, the grid booster contributes a freely controllable active and reactive power output. Due to the linearized model, only the active power is respected in the optimization and the only degree of freedom that needs to be limited by (3.25).

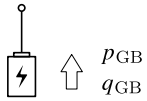

Figure 3.7: Modeling and available degrees of freedom of BESS-based grid boosters

Transmission Lines

Regarding the consideration of transmission line PATL value, the work of [93] pointed out possible problems due to the mixing of non-linear and linear problem formulations. In the proposed model of [93], the same PATL values were used for the non-linear upper and linear lower level optimization. Due to the neglected reactive power flow, the line utilization in the lower level problem was below the PATL threshold. Therefore, in some instances the upper level optimization result $\boldsymbol{x}$ matches the optimality conditions of the lower level linearized CSCOPF. In those cases, the optimization process is skipped as no congestion is present which in turn leads to an unfeasible lower level problem solution $\boldsymbol{y}$ from the perspective of the superimposed problem.

This problem is addressed in this thesis by curtailing the PATL value of the LP model. To realize this, the method used to reduce the PATL value of a transmission branch presented in [207] is applied. The approach of [207], was initially designed to reduce the complexity of a PSCOPF model. In the implementation in this work, the terminology is changed.

The methodology to calculate the PATL values of the linearized model is shown in Fig. 3.8 and presented as follows. For the current preventive set-point, an SSA is performed. This identifies congestions for each transmission branch based on (3.26). Thereby, congested branches have a negative value for ΔS_{de} while it is positive for non-congested branches.

$$\Delta S_{de} = S_{de,\mathrm{PATL}} - S_{de,\mathrm{load,(N\text{-}1)}} \tag{3.26}$$

The new PATL values used for the optimization are calculated by (3.27). For branches affected

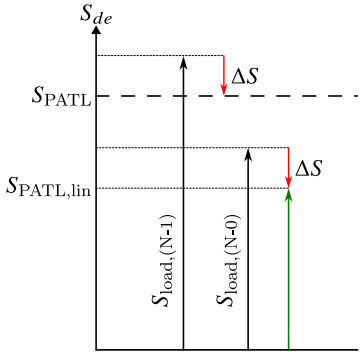

Figure 3.8: Schematic calculation of TTC of a transmission branch in the linearized CSCOPF model for a branch with and without a congestion, following [207]

by a congestion, the new PATL value $S_{de,\text{PATL,lin}}$ is the loading of the (N-0) state, reduced by the amount of the (N-1) overload ΔS_{de}. Branches without a congestion, and therefore a positive ΔS_{de}, simply use the original PATL value $S_{de,\text{PATL}}$.

$$S_{de,\text{PATL,lin}} = \begin{cases} S_{de,\text{load,(N-0)}} + \Delta S_{de}, & \Delta S_{de} \leq 0 \\ S_{de,\text{PATL}}, & \text{otherwise} \end{cases} \tag{3.27}$$

The PATL constraints of the AC and DC branches for the lower level optimization are changed accordingly to the updated PATL values and are given by (3.28) and (3.29) respectively. Please note that the shown concept of curtailing the PATL is only applied to the AC branches.

$$|i_{de}| \leq i_{de,\text{PATL,lin}} \tag{3.28}$$

$$|i_{mn}| \leq i_{mn,\text{max}} \tag{3.29}$$

3.2 Design of the Optimization Solver

To solve the optimization problem, a differential evolution (DE) algorithm is applied for the previously described BLP optimization model. Section 2.2.2 briefly mentions the advantages and disadvantages of optimization techniques based on heuristics. The DE has for once a better robustness for large-scale optimization problems at the expense of reproducibility and is therefore chosen for this thesis. Furthermore, the algorithm is more adaptable for the use of bilevel models than conventional gradient-based solvers, especially for non-convex problems such as non-linear OPF problems. On the downside, the total computational effort and reproducibility are worse and less reliable when compared to conventional methods due to the usage of stochastic functions and other factors. Additionally, intelligent search algorithm, such as DE, rely on further parameters, making its performance reliant on an optimal parameterization of the solver.

3.2.1 Differential Evolution Algorithm

The DE algorithm, as first described in [208], belongs to the class of evolutionary algorithms and as such utilizes methodologies inspired by Darwin's theory of evolution [209]. The iterative process of optimization, as shown in Fig. 3.9, is structured into three core elements:

- Mutation,
- Cross-over and
- Selection.

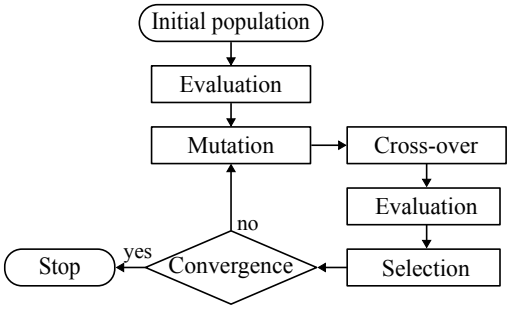

Figure 3.9: Process of DE method

The design of the DE method is as such that in each generation (iteration step) a population of individuals (multiple set-point combinations $\boldsymbol{x}$ in the set of X) is considered[5]. This population undergoes the aforementioned basic steps of evolution.

At the start of the algorithm, an initial population is constructed and consists of NP individuals, each comprising D variables. The construction of the individual $\boldsymbol{x}_v$ of the population, see (3.30), is based on a uniform random distribution within the limits of the variables.

$$\boldsymbol{x}_v = \boldsymbol{x}_{v,\min} + \text{rand}(0,1) \cdot (\boldsymbol{x}_{v,\max} - \boldsymbol{x}_{v,\min}) \qquad v \in [1, D] \tag{3.30}$$

To assess the optimality of each individual, a numerical evaluation is performed. Thereby, the value of the objective function is calculated as well as all constraints checked. Existing constraint violations are added up with the objective function value as the fitness of the individual.

The next step is the mutation to generate an offspring population or so-called mutation population $\boldsymbol{v}^G$ for generation G. There are numerous ways a mutation can be conducted. The original strategy, proposed by [208], is the DE/rand/1/bin mutation. Each individual of the mutation population v is generated by three randomly chosen individuals of the parent population according to (3.31)

$$\boldsymbol{v}_g^G = \boldsymbol{x}_{\text{r1}}^G + F \cdot (\boldsymbol{x}_{\text{r2}}^G - \boldsymbol{x}_{\text{r3}}^G) \tag{3.31}$$

with $g \in [1, NP]$, the indices r1 $\neq$ r2 $\neq$ r3 represent the three randomly chosen individuals of the current population and $F \in [0, 1]$ as a real constant weighing factor that scales the influence of the random individuals.

In this thesis, the self adaptive DE approach by [210] is used. This approach uses a set of mutation strategies (see Tab. 3.2) and uses each strategy based on a uniform distribution. By keeping track of the performance of each mutation strategy, i.e., which strategy produces offsprings with a better fitness value, the distribution is adapted in favor of the better performing strategies.

[5] Please note that in the context of application in congestion management, the individuals $\boldsymbol{x}$ comprise the total of all CMMs for a given time frame.

Table 3.2: Mutation strategies utilized by the self adaptive DE approach

Name	Formulation
DE/rand/1/bin	$\boldsymbol{v}_g^G = \boldsymbol{x}_{\mathrm{r1}}^G + F \cdot (\boldsymbol{x}_{\mathrm{r2}}^G - \boldsymbol{x}_{\mathrm{r3}}^G)$
DE/best/1/bin	$\boldsymbol{v}_g^G = \boldsymbol{x}_{\mathrm{best}}^G + F \cdot (\boldsymbol{x}_{\mathrm{r1}}^G - \boldsymbol{x}_{\mathrm{r2}}^G)$
DE/rand-to-best/1/bin	$\boldsymbol{v}_g^G = \boldsymbol{x}_g^G + F \cdot (\boldsymbol{x}_{\mathrm{best}}^G - \boldsymbol{x}_{\mathrm{r1}}^G) + F \cdot (\boldsymbol{x}_{\mathrm{r2}}^G - x_{\mathrm{r3}}^G)$
DE/current-to-rand/2/bin	$\boldsymbol{v}_g^G = \boldsymbol{x}_g^G + F \cdot (\boldsymbol{x}_{\mathrm{r1}}^G - \boldsymbol{x}_g^G) + F \cdot (x_{\mathrm{r2}}^G - x_{\mathrm{r3}}^G)$
DE/current-to-best/2/bin	$\boldsymbol{v}_g^G = \boldsymbol{x}_g^G + F \cdot (\boldsymbol{x}_{\mathrm{best}}^G - \boldsymbol{x}_g^G) + F \cdot (x_{\mathrm{r2}}^G - x_{\mathrm{r3}}^G)$

For the selection process, the trial population $\boldsymbol{v}^G$ needs to compete with the current population $\boldsymbol{x}^G$. This trial population is generated by the cross-over of the current and mutation individuals following (3.32)

$$t_v^G = \begin{cases} v_v^G, & \mathrm{rand}(0,1) \leq CR \\ x_v^G, & \text{otherwise} \end{cases} \tag{3.32}$$

where $v \in [1, D]$ and the cross-over constant $CR \in [0, 1]$ determines the probability of the mutated variables being part of the trial population. After a numerical evaluation of the trial population, the selection process starts in which the trial and the current population has to compete against each other. The selection proceeds pairwise. The fittest (the individual with the best fitness value) of the two competing individuals becomes part of the population of the new generation.

3.2.2 Hybrid Differential Evolution

For the upper level optimization a hybrid DE algorithm similar to the approach proposed in [124] is deployed. Therewith, the general steps of a DE algorithm are combined with a Newton-Raphson (NR) based power flow. As the scope of this work includes AC systems with embedded HVDC systems, the power flow model needs to address both systems. The power flow module therefore first solves the power flow equations of the DC system with a solver based on [202]. The utilized power flow solver does not consider losses of the converter when converting from AC to DC or vice versa. A calculation of the losses would introduce additional equality constraints (cf. [83]) that would require, when using a hybrid solver, an iteration of AC and DC system power flows. Losses can also be assumed as a proportional share. The usage of a loss model is neglected as it yields no explicit benefit in regard to the questions addressed by this work. Subsequently, the AC system is solved using a conventional NR method. Please note that the solver of the DC system is a secant method and not an NR. Nonetheless, the term NR based power flow is used in the following to address the combined AC and DC system power flow model.

As a global optimizer, the DE finds the best combination of control variables and the NR minimizes the non-linear power flow. On the one hand, this simplifies the problem formulation as voltage magnitude and phase angle can be neglected as necessary degrees of freedom like in conventional OPF approaches. Otherwise, as the NR power flow is an iterative method that updates and evaluates

the full Jacobian at each step, the computational complexity is increased because the iterative DE now incorporates an iterative method in itself. Due to the nature of the NR algorithm to define a slack bus to balance inequalities (e.g. losses) in the system, the generator(s) connected to the slack bus are not available as usable degrees of freedom. The DE uses its population to explore the feasible search space, whereas each individual of the population is used as an initial guess for the NR power flow method. Since the power flow algorithm provides the solution of the nodal voltages for the given set-points, a converging power flow naturally complies with the equality constraints presented in Section 3.1.1.3. The procedure of the hybrid DE is visualized in Fig. 3.10.

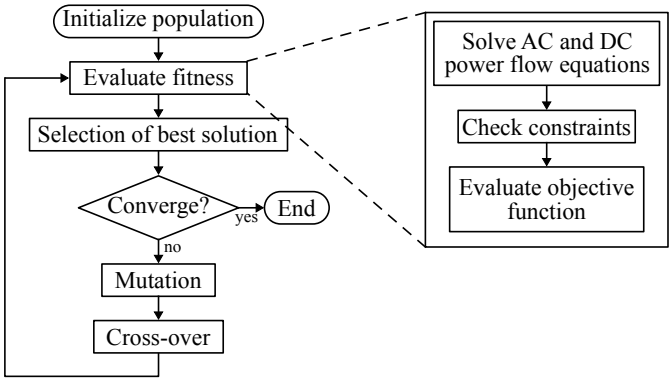

Figure 3.10: Sequence of a hybrid Differential Evolution algorithm, following [124]

As the lower level optimization is based on a linearized power flow model, the usage of an NR based power flow solver is not applicable. In its stead, a DC power flow solver (not to be confused with the solver of the HVDC power flow model) is implemented. Thereby, the simplification in regard to the reduced optimization variable, e.g., neglecting nodal voltage angles, is still valid. Additionally, the computational complexity compared to the upper level model is reduced, since the DC power flow is a direct solution method and does not need to iterate. Only the computation of the HVDC system power flow remains as iterative method.

3.2.3 Nesting of Upper and Lower Level Optimization

Compared to conventional methods, intelligent search algorithms bring the advantage to not be reliant on an exact mathematical description of the optimization problem. Instead, they use arbitrary functions to evaluate the optimality (cf. Section 2.2.2). This property is used to nest the CSCOPF problem into the PSCOPF, whereas for conventional methods, the lower level problem needs to be reformulated as additional constraints of the upper level problem. As such, due to the usage of DE as optimization solver, the proposed BLP-SCOPF is dependent on the structure of a population-based intelligent search algorithm and is therefore not valid for conventional algorithms.

3.2.3.1 Notation

For a better understanding of how the nesting of the upper and lower level optimization is realized, the notation in regard to the contingency sets is given in Fig. 3.11 using the exemplary test system introduced in Section 2.1.3. In the scope of the methodology, four contingency sets are defined:

- C as the total set of all possible contingencies
- C_{prev} is the set of all contingencies addressable by preventive measures
- C_{cur} comprises the contingencies that are solvable by curative actions[6]
- C_{viol} defines the remaining contingencies that cannot be resolved by any CMM

Given the design of the exemplary test system in Fig. 3.11a, Fig. 3.11b shows an arbitrary set definition of the given contingencies. In this case, the total set of all considered contingencies C comprises the single outages of each line, in the following denoted as L1, L2, L3 and L4.

$$C = \{\text{L1}, \text{L2}, \text{L3}, \text{L4}\} \tag{3.33}$$

Thereby, the set C can be further divided into sub-sets where each Lx is associated with one of those sub-set. Contingency L3 and L4 can be addressed by a preventive action, thus putting them in the set C_{prev}.

$$C_{\text{prev}} = \{\text{L3}, \text{L4}\} \tag{3.34}$$

Consequently, L1 and L2 still result in constraint violations after activating the preventive measure. A curative CMM exists to resolve the congestion of contingency L1. Thus, L1 is part of set C_{cur}.

$$C_{\text{cur}} = \{\text{L1}\} \tag{3.35}$$

Lastly, only contingency L2 remains unresolved as a critical contingency and is therefore an element of set C_{viol}.

$$\begin{aligned} C_{\text{viol}} &= C \setminus (C_{\text{prev}} \cup C_{\text{cur}}) \\ &= \{\text{L2}\} \end{aligned} \tag{3.36}$$

3.2.3.2 Fitness Evaluation of the BLP-SCOPF

To couple the two optimization problems, the fitness evaluation (see Fig. 3.10) of the upper level model is adapted. The fitness calculation is designed as shown in Fig. 3.12, and is performed for the population $\mathcal{X}$ of the DE. In each step of the evaluation process, the individuals $\boldsymbol{x} \in \mathcal{X}$

[6] Please note that "resolved" or "solved" contingencies are based on the contingency analysis, which examines the various outage variants and their effects on the system. The congestions caused by the outages are then resolved by preventive or curative CMM.

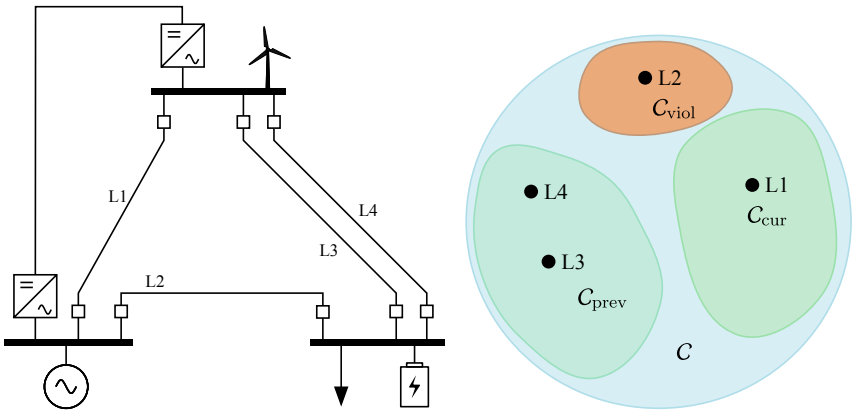

(a) Exemplary test system **(b)** Definition of contingency sets

Figure 3.11: Illustrative example of the set notation, showing the (a) exemplary test system and (b) contingency sets

are evaluated on their feasibility for the respective case. Each individual thereby represents one set of preventive actions according to (3.2). First, the base case feasibility is checked and the population $\mathcal{X}$ is further split in $\mathcal{X}_{\text{base}}$ and $\mathcal{X}_{\text{viol}}$ for the individuals complying to or violating the base case constraints respectively. This is needed due to the behavior of the DE algorithm. As the DE generates new set-points by using stochastic, those trial individuals (cf. (3.32)) can result in base case unfeasible regions especially in the early iterations. For the concurrent steps, an SSA of the preventive and curative cases is done. The mechanisms of each step are explained in the following.

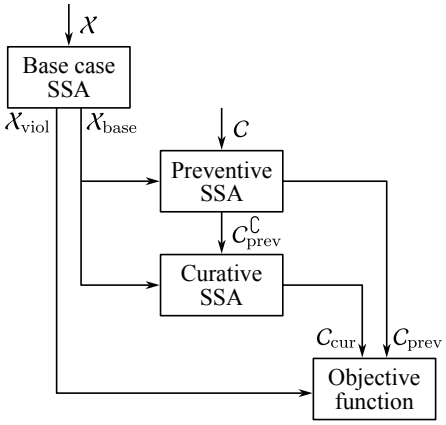

Figure 3.12: Fitness evaluation of the BLP-SCOPF showing the cascade of base case and contingency SSA

Base Case SSA

Fig. 3.13a depicts the process of the base case SSA. Each individual $\boldsymbol{x}$ is checked for their compliance with the constraints of the system base case. Based on the base case feasibility, the population $\mathcal{X}$ is divided into two subsets: $\mathcal{X}_{\text{base}}$, comprising the base case feasible individuals, and $\mathcal{X}_{\text{viol}}$. The latter one is the set of all individuals that cannot be activated in the base case and therefore would also not comply in any of the contingency scenarios. In the first step, the power flow for the current iteration of $\boldsymbol{x}$ and the base case topology is calculated. Subsequently, all constraints are checked on feasibility. If the individual is feasible, i.e., it complies with all constraints, it is added to the set $\mathcal{X}_{\text{base}}$. The set $\mathcal{X}_{\text{base}}$ is then used as input for the preventive and curative SSA calculation. When at least one constraint is violated, the individual is added to $\mathcal{X}_{\text{viol}}$. If all elements in $\mathcal{X}_{\text{viol}}$ are unfeasible in regard to acting as a preventive CMM, no further studies are considered for this set. Fig. 3.12 shows that the set $\mathcal{X}_{\text{viol}}$ is directly forwarded to the block of the objective function calculation.

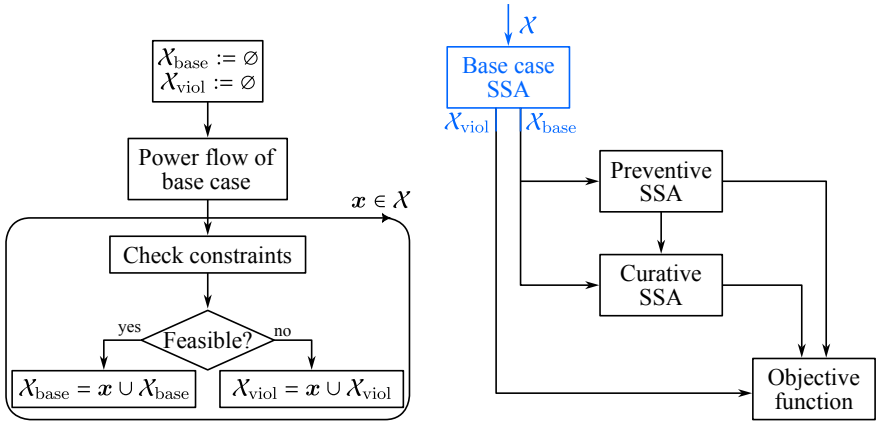

(a) Flow chart

(b) In- and outputs (marked in blue) of the base case SSA

Figure 3.13: Schematic of the base case SSA

Upper Level SSA

Subsequently, the population $\mathcal{X}_{\text{base}}$ is further processed in the upper level optimization, i.e., in the preventive SSA. At the beginning of the SSA, an empty set of preventive feasible contingencies C_{prev} is initialized. The procedure of Fig. 3.14a is analogous to the one of the base case SSA in Fig. 3.13a and extended to comprise the processing of multiple scenarios. This is realized by adding a looped process where subsequently each contingency case $c \in C$ is analyzed. For each scenario c the current $\boldsymbol{x} \in \mathcal{X}_{\text{base}}$ is checked on its respective constraint compliance. Same as with the base case SSA, if the feasibility is assured, the case c is included in the set of preventive feasible contingencies C_{prev}. The worst case result would be that $\boldsymbol{x}$ does not comply with the constraints of any contingency scenario, leaving the set of feasible contingencies in its initialized state as an

empty set $C_{\text{prev}} = \varnothing$. Otherwise, the best case is when the current set-point complies with all post-contingency constraints, leading to $C_{\text{prev}} = C$.

Fig. 3.14b shows the inputs and outputs of the preventive SSA module. On the input side, the two sets C and X_{base} are needed with C comprising all possible contingencies.

$$C = \{\text{L1}, \text{L2}, \text{L3}, \text{L4}\} \tag{3.37}$$

Two outputs are produced by the preventive SSA module: the set of preventive feasible contingencies C_{prev} as well as its absolute complement set $C_{\text{prev}}^{\complement}$, containing all preventive unfeasible cases. Based on the provided example, the effects of the outages of L3 and L4 are preventive feasible.

$$C_{\text{prev}} = \{\text{L3}, \text{L4}\} \tag{3.38}$$

Set $C_{\text{prev}}^{\complement}$ is defined as the complement set to C_{prev} and therefore comprises all contingencies in C that are not already elements of C_{prev}.

$$\begin{aligned} C_{\text{prev}}^{\complement} &= C \setminus C_{\text{prev}} \\ &= \{\text{L1}, \text{L2}\} \end{aligned} \tag{3.39}$$

As the contingencies in $C_{\text{prev}}^{\complement}$ remain as unresolved and critical contingencies, the set is further processed in the curative SSA.

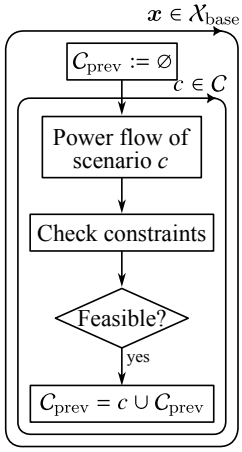

(a) Flow chart

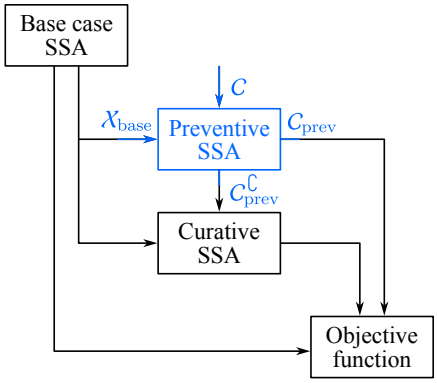

(b) In- and outputs (marked in blue) of the preventive SSA

Figure 3.14: SSA procedure within the upper level optimization

Lower Level SSA

The process of the curative SSA, as depicted in Fig. 3.15a, is mostly identical to the one described previously in terms of the involved steps. But, as the curative SSA belongs to the lower level optimization problem, the curative control variables $\boldsymbol{y}$ are used. Therefore, a third loop is added to accommodate for the optimization variable $\boldsymbol{y} \in \mathcal{Y}$ of the lower level DE where $\mathcal{Y}$ is the population of the CSCOPF.

In the beginning, for each $\boldsymbol{x} \in \mathcal{X}_{\text{base}}$ an empty set for the curative feasible contingencies C_{cur} is initialized. Same as for the upper level SSA, the set $C^{\complement}_{\text{prev}}$ is processed in a loop. For each $c \in C^{\complement}_{\text{prev}}$ the total transfer capacitys (TTCs) for the linearized power flow model (cf. Section 3.1.2) are calculated and used to update the model. Consequently, a CSCOPF optimization is performed for the current set of preventive actions $\boldsymbol{x}$. The result is an optimal set of curative set-points $\boldsymbol{y}$ for each contingency c. To evaluate the final feasibility of $\boldsymbol{y}$, a non-linear power flow for the respective case c is done. Based on the power flow results, the constraint compliance is analyzed. For the constraint satisfaction check, the original PATL values are used and not the ones calculated in the previous step. All contingencies that comply with the defined constraints are added successively to the set of curative feasible contingencies C_{cur}.

Looking at the inputs and outputs in Fig. 3.15b, the curative SSA is fed by the base case and preventive SSA with the upper level population $\mathcal{X}_{\text{base}}$ and the set of preventive unfeasible contingencies $C^{\complement}_{\text{prev}}$. In the exemplary test system shown in Fig. 3.11a, $C^{\complement}_{\text{prev}}$ is defined by (3.40).

$$C^{\complement}_{\text{prev}} = \{\text{L1}, \text{L2}\} \tag{3.40}$$

Only a single output is produced, namely the set of curative feasible contingencies C_{cur}, and used for the calculation of the objective function. For the used test system, the set comprises the outage of L1.

$$C_{\text{cur}} = \{\text{L1}\} \tag{3.41}$$

The set of unfeasible contingencies C_{viol} is not further processed as it can be derived from the sets C_{prev} and C_{cur}.

$$\begin{aligned} C_{\text{viol}} &= C^{\complement}_{\text{prev}} \setminus C_{\text{cur}} \\ &= C \setminus (C_{\text{prev}} \cup C_{\text{cur}}) \\ &= \{\text{L2}\} \end{aligned} \tag{3.42}$$

As mentioned previously, the curative SSA can be skipped if the input variables $C \setminus C_{\text{prev}}$ is an empty set. In those situations, the procedure stops after initializing the empty set for the next process in the overall SSA scheme.

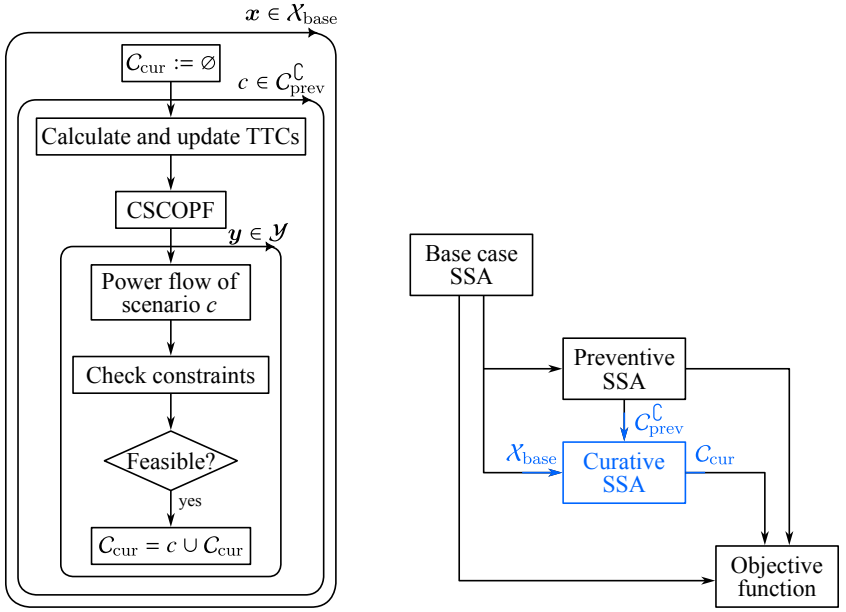

(a) Flow chart

(b) In- and outputs (marked in blue) of the curative SSA

Figure 3.15: SSA procedure within the lower level optimization

3.2.3.3 Mathematical Representation of the Nested Objective Function

As introduced in section 3.1.1, the objective function (see Fig. 3.16) of the BLP SCOPF is a many-objective function with its first sub-objective being described by (3.45) as the minimization of critical contingency scenarios.

It can be seen that the amount of critical contingencies, e.g., contingencies that violate at least one operational security constraint, is divided into the sets of preventive feasible C_{prev} and the curative feasible cases C_{cur}. As such, the calculation of those sets in the preceding fitness evaluation does not influence the optimality of the individuals $\boldsymbol{x} \in \mathcal{X}$ and $\boldsymbol{y} \in \mathcal{Y}$. To allow a numerical evaluation of the sets, $N_{feas,prev}$ and $N_{feas,cur}$ are introduced as the cardinality of the respective set.

$$N_{feas,prev}(\boldsymbol{x}, \boldsymbol{u}_c) = |C_{prev}| \tag{3.43}$$

$$N_{feas,cur}(\boldsymbol{x}, \boldsymbol{y}, \boldsymbol{u}_c) = |C_{cur}| \tag{3.44}$$

For the calculation of $N_{cc,opt}$, the weighted sums of the number of elements in the aforementioned sets is used. Note that w_{prev} and w_{cur} are the corresponding weighting factors.

$$N_{cc,opt}(\boldsymbol{x}, \boldsymbol{y}_c, \boldsymbol{u}_c) = |C| - (w_{prev} N_{feas,prev}(\boldsymbol{x}, \boldsymbol{u}_c) + w_{cur} N_{feas,cur}(\boldsymbol{x}, \boldsymbol{y}_c, \boldsymbol{u}_c)) \tag{3.45}$$

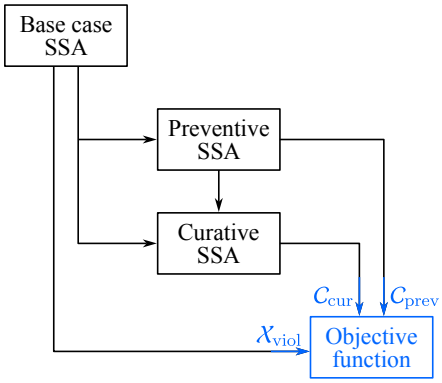

Figure 3.16: In- and outputs (marked in blue) of the objective function

3.3 Summary of the BLP-SCOPF Methodology

To allow a coordination of preventive and curative CMMs in the optimization, the problem formulation must allow the definition of multiple objective functions (cf. Section 2.2.1.2). This thesis proposes the use of a BLP-SCOPF as the optimization problem. Thereby, the determination of preventive and curative remedial actions can be, to a certain extent, modeled independent of each other. The PSCOPF defines the framework for the subsequent CSCOPF optimization by setting the preventive set-points that build the starting point of the curative optimization. The proposed approach of this thesis, for the combined determination of preventive and curative CMM, can be embedded in the today's operational planning landscape. Constraint violation in the CSCOPF can then be given as feedback to the PSCOPF so that the preventive landscape can get adjusted to allow the determination of feasible curative actions.

The proposed method encompasses the use of conventional thermal power plants, HVDC systems and grid boosters. Due to some constraints, a differentiation of the technologies and their field of application is needed. As thermal generators have long time constants, they are generally not suited for curative actions that must be activated as soon as possible. The use of BESS-based grid boosters on the other hand is constricted by the dimensioning of their energy storage and are therefore a viable degree of freedom strictly for the use as a curative CMM. HVDC systems are feasible for preventive and curative operation as they are based on power electronics allowing for quick set-point adaptations and not dependent on an external energy storage.

A hybrid solving algorithm is proposed to solve the formulated optimization problem. The solver is based on the DE method, a representative of the intelligent search algorithm, and the Newton Raphson method. Contrary to the conventional approach of OPF methods, the hybrid algorithm does not include the node voltages as a necessary degree of freedom. Instead, it exclusively uses

the operating points of the permissible technologies and calculates the voltage profile on the basis of a power flow calculation. This allows a drastic reduction of degrees of freedom for the OPF as the node voltages of the base case and all contingency scenarios are negligible. The modular design of the DE approach enables a nesting of the CSCOPF problem into the CSCOPF which would not be as easy as with a conventional approach.

4 Numerical Case Studies

In the following, the proposed method of the BLP-SCOPF in Section 3 is evaluated in different scenarios. For once, this serves to validate the general functionality of the proposed optimization method. Further, the focus is to study the differences between the current passive (N-1) security compared to the active (N-1) security as it is proposed in the scope of this thesis by incorporating curative actions in system operation. To outline the differences of passive and active (N-1) security, the results of the case studies investigate the overall security level of the proposed optimization model. Additionally, aspects such as arising redispatch costs and the utilization of AC lines are evaluated. Furthermore, the evaluation is meant to allow a statement about existing deficits and future research needs.

For testing purposes, an academic test system is used and described in detail in Section 4.1. The test system, first published in [211], is a 400 kV transmission system with a meshed HVDC overlay system. Followed by a general description of the initial test system, the applied modifications to the system are listed. To give a broader spectrum to the evaluation, different scenarios are composed and characterized in Section 4.1.3.

The results of the validation is presented in Section 4.2. Two different studies of the optimization model are studied. All cases are evaluated in regard to emerging costs, system security and utilization of the power system. In the first study, the determination of preventive and curative CMMs is done without any kind of consideration towards coordinating both measures. Thus, this subsequent optimization approach serves as a reference case for the following models. In the following studies, the BLP-SCOPF is investigated. As mentioned in Section 3.1.1, the optimization allows for a prioritization of either preventive or curative measures. To examine the effects of this flexibility, the optimization is performed using an equal priority on both kinds of measures and prioritizing one from each[7].

4.1 Test System

4.1.1 Description of the Grid Model

The validation is performed using a widely used HVDC benchmark system, first presented in [211] and shown in Fig. 4.1. It is designed especially for the study of SCOPF algorithms using HVDC systems and consists of a high-voltage AC transmission system with an isolated offshore wind farm (OWF) as well as a meshed HVDC overlay system.

The AC system is structured in three control areas comprising 67 busses, 104 transmission lines and 18 generating units. Its power flow situation is loosely oriented at the German power system with a significant power transfer from the north to south of the system. On top of the AC system, a

[7] Please note that no robustness analysis for the optimization model is done. As the robustness of the utilized DE algorithm is highly dependent on its parameterization (cf. Section 3.2.1). Thus, an optimization of the case-sensitive parameters is necessary which is out of the scope of this thesis. The presented studies are meant to serve as a proof of concept.

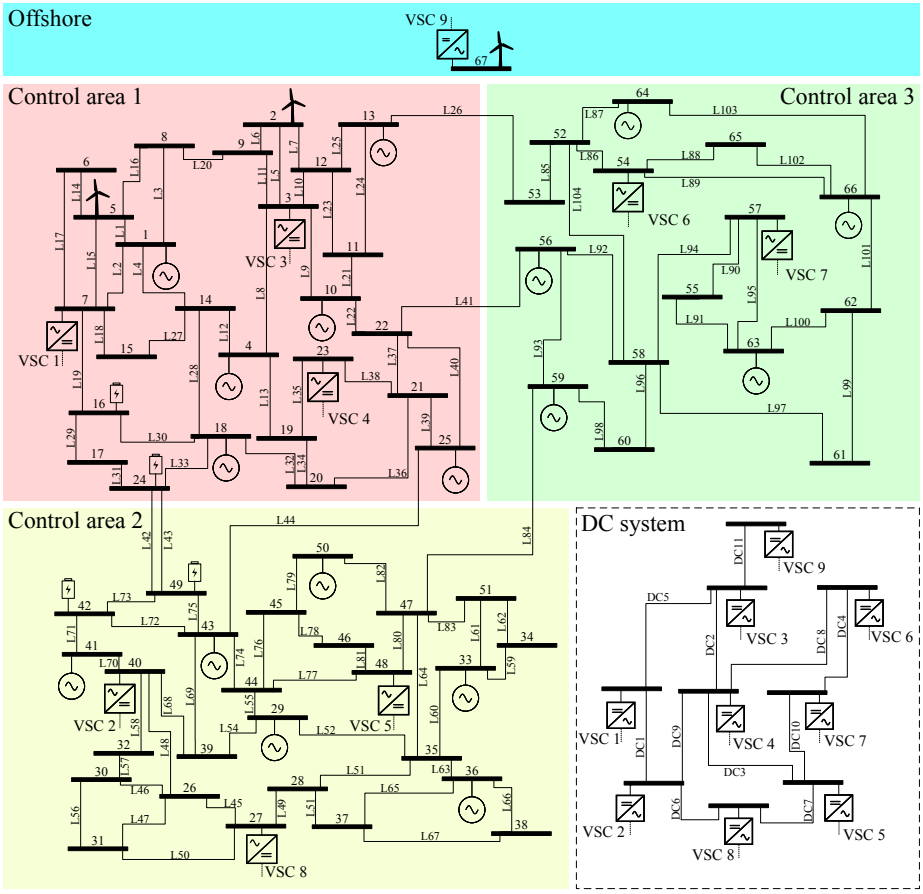

Figure 4.1: Modified test system, based on [211], showing the three control areas, the isolated OWF in the north and the layout of the HVDC overlay system in the bottom right corner

VSC-based meshed HVDC overlay system is installed. It consists of nine converter stations with three stations each located in control area 1 and 2, two stations in control area 3 and a single VSC used to connect the OWF in the north of the system.

Devices for Congestion Management

Some modifications are made compared to the original system to address some inherent problems as well as to integrate new degrees of freedom utilized by the proposed algorithm. The parameterization of the test system is given in Appendix A.3.2. For once, the parameters of the transmission lines are adjusted. [211] assumes a constant line length of 100 km for each line. All line lengths are adapted based on the approximate distance depicted by Fig. 4.1. Due to that, a second interconnetor in parallel to L42 is installed to compensate its short length. Additionally, line L104 is added in control

area 3 to circumvent a split of the control area in the event of an outage of L101. Furthermore, BESS based grid booster units are included to enable system operation concepts such as the systemic grid booster. In total, four units are installed with two units each in control area 1 and 2. Their positions are based on a congestion analysis on multiple grid utilization cases (cf. section 4.1.3). Over all contingency cases, the four busses with sensitivities on most congestions are chosen as grid booster connection busses.

Market Model

In regard to the synchronous generators, four machine types are introduced defining specific limit values, fuel types and associated costs. The changes of the limit values are of minor impact but lead to a change of the slack generator. Instead of a single generating unit, two natural gas power plants with synchronous generators are used as power source for the slack bus now. The redispatch costs of the conventional generators are assumed as marginal costs. Marginal costs are calculated by (4.1).

$$\text{marginal costs} = \frac{\text{fuel costs}}{\eta} + \text{carbon price} \cdot \frac{\text{carbon emission}}{\eta} + \text{variable costs} \tag{4.1}$$

Fuel costs are the sum of the actual fuel and transport cost and are based on [212], same as the variable costs. Efficiency rates η are based on [213] and the carbon emissions from [214]. The carbon price is assumed as 84.11 €/t [215]. The assumed data used for the calculation is summarized in Tab. 4.1.

Table 4.1: Determination of marginal costs by energy source

	Costs in €/MWh		Efficiency η	Carbon emissions	Marginal costs
Energy source	Fuel	Variable	in %	in t/MWh	in €/MWh
Lignite	3.10	1.70	46.5	0.53	99.15
Hard coal	15.81	1.30	47.5	0.40	79.19
Natural gas	54.56	1.50	61.0	0.25	69.05

Pumped storage cannot be priced like other energy sources because there are essentially no fuel costs. Therefore, shadow prices[8] are used to represent the lack of storage as well as represent energy losses during pumping and generation, maintenance and auxiliary power consumption. An offer at actual marginal cost would result in an immediate emptying of the storage in the first hours of operation. However, this does not lead to an optimal result either from a business point of view (maximizing contribution margins) nor from an economic point of view (additional power supply when demand is high). Dispatch optimization is therefore carried out with the aim of limiting the supply of electricity generated in storage power plants to the hours with the highest load and thus

[8] A shadow price defines a monetary value to an intangible good or commodity that cannot be traded in a marketplace.

the highest market prices [216]. Here, the marginal costs of pumped-hydro storage is assumed as the mean value of all installed generators, thus leading to costs of 79.10 €/MWh.

For generation scheduling, the marginal costs are used to implement a merit order model. Therefore, expensive generation units are deactivated first in case of a surplus of power infeed compared to the total demand.

Meshed HVDC Overlay System

The meshed HVDC overlay system presented in the initial design of the test system is a monopolar VSC-based system. In the scope of this work, a bipolar system with dedicated metallic return is used as shown in Fig. 4.2. Thereby, each VSC station now comprises two individual converters which are operated symmetrically in the base case. To comply with the initial power flow presented in [211], their active power set-points and their limit values are halved.

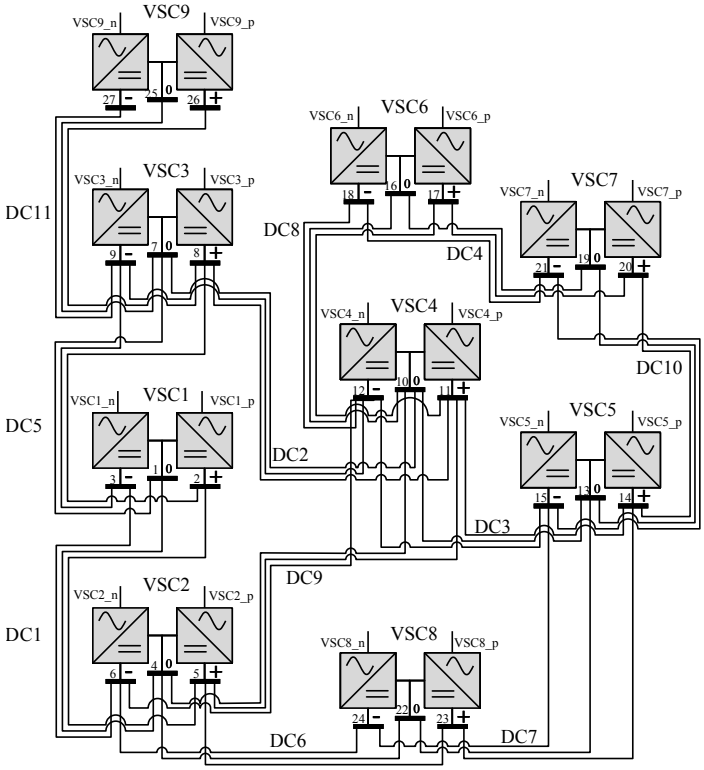

Figure 4.2: Detailed depiction of the meshed bipolar HVDC overlay system, as shown in [92]

For reasons of simplicity, the power flows of the HVDC system are identical as the ones in [211], but with a design as bipole with dedicated metallic return conductor. This can be done without restriction of generality, due to the objective of the thesis is about the demonstration of the

optimization procedure and not about the exact planning study of a real HVDC overlay system. To retain the initial transport capacities of the monopolar system, the rated voltage is set to ±250 kV and thereby creating a voltage drop of 500 kV between the positive and negative pole. Analogous to the AC transmission lines, the length of the DC lines is also adapted based on the distance of their AC grid connection point. The modeling of the VSCs is kept simple. Regarding the VSC station, only the converter itself is modelled, neglecting possible low pass filters and transformers. As the VSCs are modelled as MMC, a low pass filter is not necessary. Lastly, no loss model is considered for the power transfer from the DC to the AC system. This is mainly due to the implementation of such a model into a power flow based optimization method. The calculation of the conversion losses would require an iterative calculation of the power flows of the AC and DC system, resulting in a significant computational overhead that does not justify the added value to the calculation result.

Available Degrees of Freedom

Given the defined degrees of freedom, Tab. 4.2 lists the intervals[9] for each variable as well as their number of appearances in the test system. Based on this list, the number of available degrees of freedom for the preventive and curative operation can be calculated. The upper level model comprises all synchronous generators and the full capabilities of the VSCs, totaling at 64 degrees of freedom. For the lower level optimization, the generators and the droop parameter are neglected and in their stead, grid boosters are added as operational degree of freedom, totaling at 40 degrees of freedom.

Table 4.2: List of intervals and number of appearance per degree of freedom

Technology	Degree of freedom	Appearances	Interval
Lignite generator	P_{gen}	4	$[360, 850]$
Hard coal generator	P_{gen}	2	$[225, 630]$
Natural gas generator	P_{gen}	6	$[180, 560]$
Pumped storage generator	P_{gen}	4	$[270, 720]$
VSC	P_{VSC}	16	$[-1000, 1000]$
	Q_{VSC}	16	$[-1000, 1000]$
	k_{droop}	16	$[0, 2, 000]$
Grid booster	P_{GB}	4	$[-250, 250]$
	Q_{GB}	4	$[-250, 250]$

4.1.2 Contingency Modeling

One of the most likely contingency events in power systems is the loss of a transmission branch (overhead line, cable, transformer, etc.) in the AC system. The effects on the system are a change

[9] Please note that the intervals are given in the form of $[P_{\text{min}}, P_{\text{max}}]$.

on the power flow of the whole system due to the topological changes. In a steady-state power flow model, new line losses would lead to a slight adaptation of the active power set-point of the slack generator to balance the system as well as changes in the reactive power provision of the PU nodes in the proximity of the outage.

Similarly to AC line outage, line outages in the HVDC grid lead to changes in the topology and thereby to changes in the voltage profile. Depending on the design of the HVDC system, the post-contingency state can vary. The bipolar HVDC system offers new opportunities for system operation due to its inherent redundancy, as failures or faults in the HVDC system do not always result in a failure of the entire transmission corridor, as it would be the case in a monopole configuration. A brief overview of the possible failure modes for point-to-point and meshed HVDC systems is shown in Fig. 4.3.

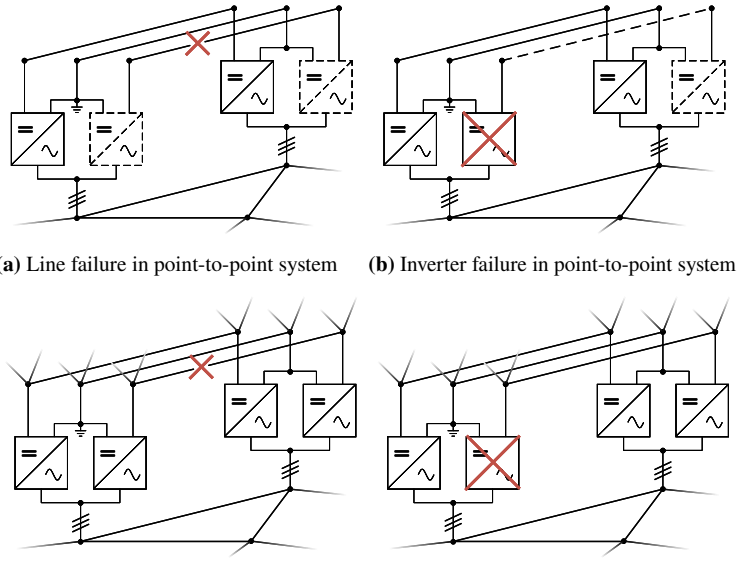

(a) Line failure in point-to-point system **(b)** Inverter failure in point-to-point system

(c) Line failure in meshed system **(d)** Inverter failure in meshed system

Figure 4.3: Overview of fault types in bipolar HVDC system with dedicated metallic return with outages indicated as red crosses

In general, two different types of faults can be distinguished: the failure of a transmission line (see Fig. 4.3a and Fig. 4.3c) or of an inverter (see Fig. 4.3b and Fig. 4.3d). In the event of a line failure in a point-to-point system, both converters are still operating and can provide reactive power. In addition, the active power provision of the grid connection point on the AC side is not lost because the healthy pole circuit and the dedicated metallic return are still in operation. This is also true for a meshed configuration, with the difference that the converters connected to the failed line can still be supplied by the other DC lines. In the meshed bipolar system, the transport capacity of the

corresponding transmission corridor is therefore halved, but not the energy transport between the AC and DC systems.

Regarding the failure of a single converter, most assumptions are consistent with the failure of the line. The faulty converter is taken out of service, but the corresponding converter at the connected station can continue to provide reactive power (see Fig. 4.3b) and, for meshed systems, active power (see Fig. 4.3d). The difference is that in the event of a converter failure in a meshed system, the total transmission capacity of the line is not affected.

Another impact on the post-contingency state is the control concept. In general, converter can be operated in three different control modes: constant power, constant voltage or voltage control where the power changes accordingly to voltage deviations. The utilized test system uses the DC voltage control mode for the VSCs except for VSC 9. That means, except for VSC 9 all VSCs participate in the balancing of occurring inequalities in the DC voltage profile. VSC 9 is used solely to connect the OWF to the system. Therefore, the infeed of VSC 9 is strictly dependent on the infeed of the OWF so that the converter are operated in a constant power mode. Due to that, the contingency modeling regarding VSC 9 is a particularity. When a single converter pole is affected by an outage or isolated due to a line outage, the remaining VSCs take over the lost power up to their capabilities. If the infeed of the OWF is higher than the power limits of a single VSC, the OWF is curtailed to the $P_{\max}$ of the VSC. For the remaining VSC, their set-point adaptation in the event of a DC contingency depends on the parameterization of their DC voltage control.

In the event of a monopolar contingency, the bipolar system is operated asymmetrically, i.e., the set-point adaptation of the VSCs participating in the DC voltage control is not identical for the positive and negative system as the voltage deviation is unequal in both systems.

As the focus of application lies on systems with a meshed HVDC overlay system, contingencies also include the DC system. In both systems, the loss of transmission branches and generating units is considered. The details in regard to each contingency type are summarized in Tab. 4.3.

Table 4.3: Summary of the effects of contingencies on the AC system

Outage	Effect
AC line	change in topology
	eventual islanding of busses
DC line	change in topology and loss covered by DC voltage control
	eventual operation of connected VSC in STATCOM mode
HVDC converter	halving of total P & Q provision at the AC terminal
	set-point adaptation of all converter participating in DC voltage control

For the presented test system, the contingencies list comprises the outages of all AC as well as DC transmission lines and all VSCs. Therefore, the contingency list consists of 144 elements. As already mentioned, contingencies in the bipolar HVDC system are symmetrical regarding their

post-contingency states, i.e., the congestions in the AC system are identical if the fault occurs either on the positive or negative pole while the congestions in the DC system simply occur on the other polarity. Therefore, only contingencies in the negative DC system are considered, reducing the total number by eleven. One AC line contingency is also omitted due to redundancy. As line L42 and L43 run parallel to each other, their post-fault effects are identical. Thus, only one of those contingencies needs to be considered. The total number of contingencies is thus reduced to 123 events.

4.1.3 Characterization of Test Scenarios

To showcase the functionality of the proposed optimization algorithm, it is tested on four different grid utilization cases. The scenarios are oriented on the typical scenarios used in grid planning studies, permuting the cases: high load (HL), high wind (HW), low load (LL) and low wind (LW), thereby leading to the scenarios:

1. HL/HW,
2. HL/LW,
3. LL/HW and
4. LL/LW.

Tab. 4.4 gives a short overview of the four scenarios. It presents their total load, infeed of conventional generation and wind infeed for their base cases. Appendix 4.1.3 gives a detailed description of the scenarios and the individual set-points of the equipment.

The data for the infeed of the wind farms is based on a generic wind turbine power curve (cf. Appendix A.3.2.2). High wind is assumed as a wind speed of 15 m/s, i.e., an infeed of 1 pu, while low wind is assumed as wind speeds of $6 - 7$ m/s and an infeed of 0.6 pu[10]. Load data is scaled according to the spread commonly seen on the German load profile [217]. When peak load is assumed as 1 pu, low load usually is around $0.2 - 0.3$ pu. Based on the characteristics of the test system, high and low load are defined as 1.0 pu and 0.4 pu respectively.

Lastly, the generation profile is adapted to serve the total demand under the new load and wind profile. Each generator infeed is raised or lowered in a manner that the set-point of the slack generators remained roughly the same as in the initial state of the adjusted system. For the LL scenarios, the minimum infeed from all generators is higher than the actual load. To match this, generators are deactivated according to their marginal costs from the most expensive ones to the cheapest, as mentioned in Section 4.1.1. For the scenario LL/HW this leads to only three active generators: the two connected to the slack bus and the generator at bus 64 in CA 3. As mentioned in Section 3.2.2, due to the nature of the hybrid optimization technique the slack generators cannot be used as degrees of freedom. Therefore, only a single generator is available for the redispatch optimization, basically impeding a redispatch for scenario LL/HW.

[10] Please note that the nominal power of the wind farms is increased to 1.1 pu compared to the values used in [211].

Table 4.4: Summary on generation and load data for each scenario

	HL/HW	HL/LW	LL/HW	LL/LW
$\sum p_{\text{load}}$	11, 820 MW	11, 820 MW	4, 728 MW	4, 728 MW
$\sum p_{\text{gen}}$	8, 439 MW	10, 088 MW	1, 272.5 MW	2, 823.6 MW
$\sum p_{\text{wind}}$	3, 850 MW	2, 100 MW	3, 850 MW	2, 100 MW

To evaluate the distribution of the AC line loadings, box plots are used. Box plots, as shown in Fig. 4.4, are a means of representing and summarizing statistics of a dataset. Its features are listed and explained in the following as well as their thematic classification into line loading and higher asset utilization respectively.

1. **Median** The median is shown by the vertical line, marking the midpoint of the dataset and separates it into two equal parts.
   It can be used as a single number indicator of the line loading. In the context of higher asset utilization, a higher median indicates an improvement.

2. **Box** The colored box shows the middle 50 % of the dataset from the 25th to the 75th percentile and are called the lower and upper quartiles or Q1 and Q3 respectively. Thereby, the lower quartile ranges from the lower end of the box to the median line and the upper quartile from the median line to the upper end of the box.
   A strictly numerical comparison of the interquartile range (IQR) is not purposeful to make statements regarding the higher line utilization as it depends on its upper and lower bounds. Therefore, the IQR lengths must be evaluated together with the median and whiskers.

3. **Whiskers** Whiskers give information regarding the spread and variability of the dataset. They provide information about the range of values within which most of the data points fall.
   In the context of higher line loading, the maximum value is interesting. Analogous to the median, a higher value shows a higher utilization.

4. **Outliers** Data points that fall outside the whiskers are considered outliers and are displayed as individual points. Outliers are defined as values that are more than 1.5 times the IQR away from the nearest quartile.
   In the context of congestion management, a classification as an outlier value has no significant meaning as a line loading above a certain threshold, e.g., the PATL, is critical for system operation and must therefore be addressed. Thus, in the following outliers are not respected in the evaluation.

The distribution of the loading over all AC lines for the (N-0) state is shown in Fig. 4.5. Only scenario HL/HW shows an even distribution of the upper and lower quartiles whereas for the other three scenarios, the density is higher in the range of the 25th to 50th percentile. The lower whiskers are all around a value of three to six percent while the differences in the maximum line loading are more significant. In scenario HL/LW, the highest line loading is seen with almost 95 %. Over

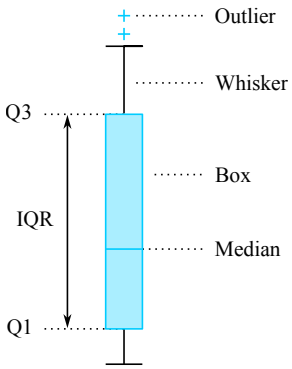

Figure 4.4: Illustrative example of a box plot to show its respective features

all scenarios, the maximum values are above 80 %, thus resulting in congestions in case of line outages. The summary of the statistical evaluation of Fig. 4.5 is presented in Appendix A.2.3.

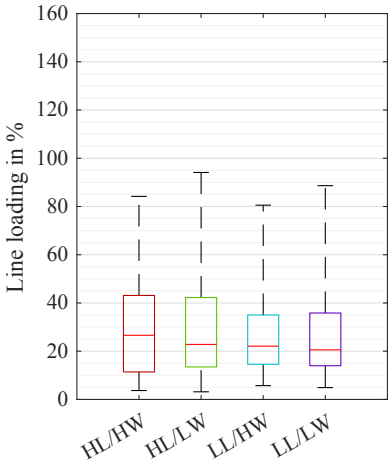

Figure 4.5: Distribution of the loading of all AC lines of the four scenarios in the base case for the (N-0) state

Tab. 4.5 presents the number of critical contingencies $N_{\text{cc,base}}$ for the four scenarios. Scenario LL/HW shows the highest amount of critical contingencies. Out of the total 123 possible outage cases, 104 result in any kind of constraint violation. All remaining scenarios have a reduced list of critical contingencies with HL/HW comprising nine cases, 20 for HL/LW and LL/LW having seven outages violating the (N-1) criterion.

Table 4.5: Overview of the number of critical contingencies for each scenario

	HL/HW	HL/LW	LL/HW	LL/LW
$N_{\text{cc,base}}$	9	20	106	7

For illustrative purposes, Fig. 4.6 shows the power flows of the HL/LW scenario in the AC system with congested lines highlighted in orange. In total, 16 congestions are present over all contingency cases. As can be seen, control area 3 is free of congestions with an exception to the interconnetor to control area 2. For control area 2, the congestions are centered around three hotspots. Two of those spots are the busses 40 and 43 where VSC2 and a generating unit are installed respectively. As this control area is characterized by a generation deficit, congestions from the top to the bottom of this area are typical. Furthermore, all interconnetors to other control areas are affected by congestions. Control area 1 is mostly free of congestions. The three existing ones are at the lines in the proximity to bus 24 where two interconnetors are installed.

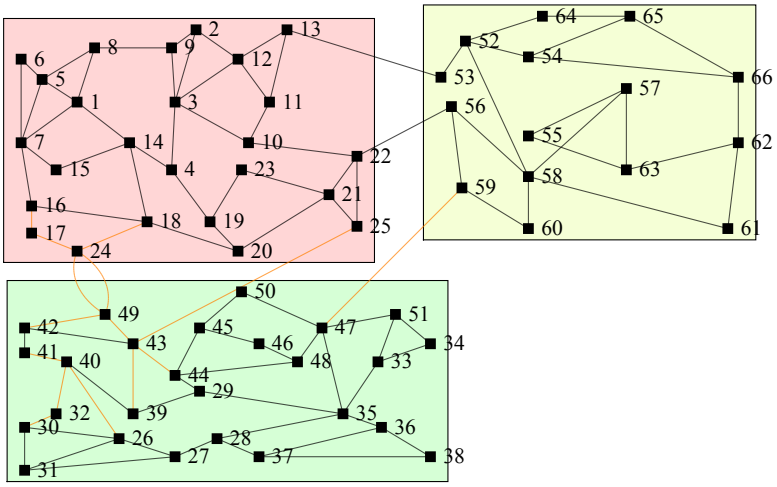

Figure 4.6: Highest power flows of the HL/LW scenario over all (N-1) situations with congested lines colored in orange

Scenario LL/HW is the case with the highest amount of critical contingencies. The reason for this is the lack of active generating units in the AC system and therefore the lack of reactive power. As a result, most contingencies result in violations of the defined voltage range. Fig. 4.7 shows the topology of the system with a color coded voltage profile in the background. It can be seen that in control area 3, the operating voltage is close to the upper limit around the busses 56 and 59 with 1.092 pu and 1.099 pu respectively. Other critical areas are the bottom and upper left corners in the system with tendencies to under voltage as they lack voltage controlling busses in their proximity.

4.2 Results

This section is meant to validate the proposed BLP-SCOPF method by applying it to the described test system. The validation comprises two study cases. Study case 1 serves to investigate the impact on CMM determination by coordinating the preventive and curative actions. Therefore, two optimization models are compared. First, in study case 1a, a reference model without any kind of coordination between preventive and curative system security is used. Thereby, the optimization

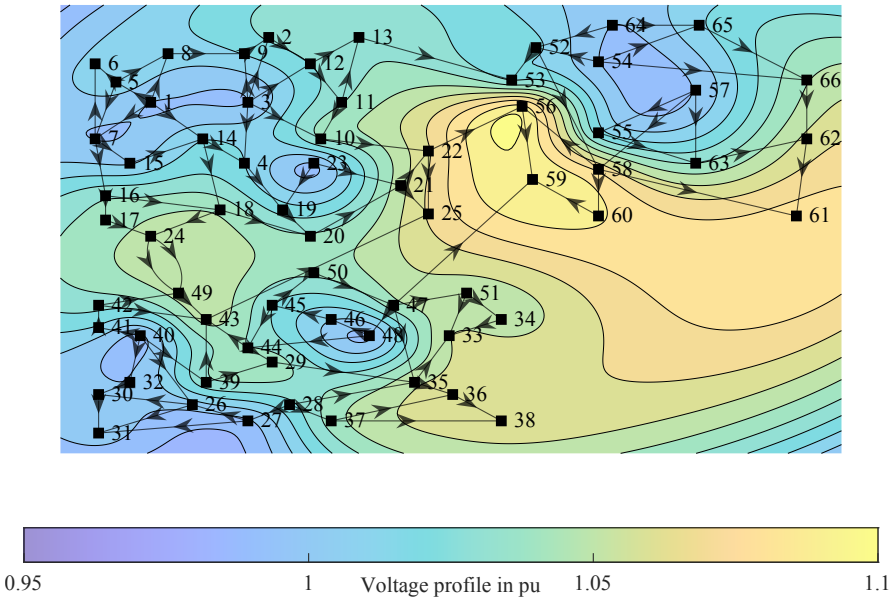

Figure 4.7: Voltage profile for the base case of the LL/HW scenario with power flows indicated by arrows

model proposed in Section 3 will not be used. Both, preventive and curative actions, are determined in a subsequent manner where, in the first run, all contingencies are optimized using a PSCOPF model and all remaining contingencies are solved by a CSCOPF. Then, in study case 1b, the proposed BLP-SCOPF is used to determine CMMs for the same scenarios in a coordinated manner. For study case 2, the investigation of the BLP-SCOPF is extended to examine the effects of varying the weighting of either preventive or curative actions. The study case is split into two subcases, where case 2a prioritizes the determination of preventive actions and case 2b the curative measures. The section closes with a discussion of the simulation results, highlighting possible advantages and disadvantages between the approaches. A summary of the utilized optimization models used in the study cases is given in Tab. 4.6.

Table 4.6: Overview of the utilized optimization per study case

Study case	Model	Coordination	Weighting
1a	PSCOPF + CSCOPF according to [188, 189]	–	–
1b	BLP-SCOPF	✓	equal
2a	BLP-SCOPF	✓	preventive > curative
2b	BLP-SCOPF	✓	curative > preventive

Please note that as mentioned in Section 3.1.1.2, the optimization model does not incorporate load shedding as a viable degree of freedom as a standard SCOPF model would. Therefore, the optimization is bound to end in an impermissible system state with non-addressed critical contingencies as this is not the aim of this investigation but to examine the benefits and deficits of the BLP-SCOPF. Additionally, an in-depth presentation and discussion of specific contingencies is omitted for the sake of simplicity. As the optimization solver is based on the DE algorithm, the performance is influenced by stochastic. Therefore, multiple simulation runs are performed, and the following sections present the best results for each study case.

4.2.1 Study Case 1 – Impact of Coordinated Determination

In the first study case, case 1a, a subsequent optimization model is used. The model is similar to the one shown in Fig. 3.1a but without the feedback loop and thereby removing the coordinating aspect of the model. Case 1b uses the proposed BLP-SCOPF shown in Fig. 3.1b.

4.2.1.1 Study Case 1a – Subsequent Optimization Approach

Study case 1a is used as base case for benchmarking the results of the proposed method and is therefore without any coordination of the preventive and curative actions. The modules for the PSCOPF and CSCOPF are state-of-the-art optimization models, as they are also described in Section 2.2.3.3. Thereby, the model of the PSCOPF complies with the upper level problem of the BLP-SCOPF (cf. Section 3.1.1) and the CSCOPF with the lower level formulation cf. Section 3.1.2. In detail this means that the approach starts with a preventive operation. After the PSCOPF, the remaining critical contingencies are identified and are successively addressed by a CSCOPF (see Fig. 4.8).

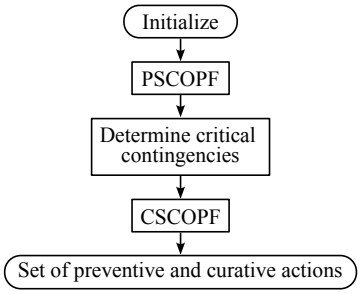

Figure 4.8: Schematic of the subsequent optimization approach

For scenario HL/HW, the highest redispatch costs $C_{\text{redispatch}}$ are incurred with around €40,000[11] and the lowest costs for LL/LW with €4,948 as seen in Tab. 4.7. The low cost of LL/HW lies in the small number of active generators that can contribute to the redispatch measures, whereas HL/HW

[11] Please note that . is used as decimal separator and , as thousands separator.

comprises the most AC line congestions in its base case so that extensive redispatch measures become necessary.

Table 4.7: Redispatch costs of the subsequent optimization of preventive and curative actions

	HL/HW	HL/LW	LL/HW	LL/LW
$C_{\text{redispatch}}$ in €	40,690	22,658	5,404	4,948

Tab. 4.8 gives an overview of the pre- and post-optimization state of the number of critical contingencies $N_{\text{cc,opt}}$ of the simulation results for study case 1a[12]. Besides the total number of remaining critical contingencies after the optimization, the table also shows the cardinality of the sets of preventive and curative feasible contingencies $|C_{\text{prev}}|$ and $|C_{\text{cur}}|$ respectively, i.e., the number of contingencies that can be resolved by either a preventive or curative measure[13].

Overall, a reduction of the total number of critical contingencies N_{cc} can be achieved in all scenarios. The best result is achieved for the scenario HL/LW with zero remaining critical contingencies whereas the worst result is produced for scenario LL/HW. Here, three curative action are identified which reduces the total amount of 16 critical contingencies after the PSCOPF down to 13. Scenario LL/LW has one feasible curative solution for two preventive unfeasible contingency, thus reducing the total amount of critical contingencies $N_{\text{cc,opt}}$ to one. For HL/HW and HL/LW, no curative actions are found to address the congestions remaining after the activation of the preventive measure. Thus, scenario HL/HW keeps one unresolved contingencies while HL/LW solves everything preventively.

Table 4.8: Representation of set of critical contingencies pre- ($N_{\text{cc,base}}$) and post-optimization ($N_{\text{cc,opt}}$) for the subsequent optimization approach

	HL/HW	HL/LW	LL/HW	LL/LW
$N_{\text{cc,base}}$	9	20	106	7
$N_{\text{cc,opt}}$	4	0	13	1
$N_{\text{feas,prev}}$	119	123	107	121
$N_{\text{feas,cur}}$	0	0	3	1

For a better understanding of the post-optimization state, Tab. 4.9 summarizes the constraint violations per scenario. In scenario HL/HW, the only constraint violation is a congestion in the AC system caused by the outage of L48. This line is directly connected to the terminal of VSC2 in control area 2. The outage overloads the parallel line L58 (cf. Fig. 4.1). For the LL/HW scenario, the same problems as for the base case of the scenario remain, as most constraint violations are

[12] A critical contingency is defined as a contingency that results in at least one constraint violation, e.g., a line loading of over 100 % or violation of the permissible voltage range.

[13] Please note that "resolved" or "solved" contingencies are based on the contingency analysis, which examines the various outage variants and their effects on the system. The congestions caused by the outages are then resolved by preventive or curative CMM.

violations of the AC voltage range. This concerns the outages of the VSCs as well as the AC lines that connect the converter stations to the system as the few remaining sources to provide and distribute reactive power are lost. Furthermore, three contingencies (L49, L94 and L100) result in various constraint violations as the power equilibrium is disturbed. Regarding the LL/LW scenario, the outage of a converter at VSC7 results in overvoltage, as not enough inductive power can be provided. A more detailed insight on the critical contingencies is given in Appendix A.2.2.

Table 4.9: Summary of constraint violations over all (N-1) cases per each scenario for the subsequent optimization approach

	HL/HW	HL/LW	LL/HW	LL/LW
AC line loading	4	0	3	0
DC line loading	0	0	0	0
AC voltage range	1	0	11	1
Generator limits	0	0	1	0

The evaluation of the AC line loading for the (N-0) after the activation of preventive, and curative CMMs if applicable, based on the subsequent optimization approach is presented in Fig. 4.9. To assess the influence of the optimization, Fig. 4.9a shows the line loading distribution of the study case and the base case for each scenario. As visual aid, Fig. 4.9b shows the differences between the study and the base case for:

- median value,
- maximum value (upper whisker) and
- interquartile range (IQR).

Those values are chosen as they allow a better analysis, if the optimization brought a change to the line utilization. While the median value give a single number statement, they are both dependent on the overall distribution of the dataset. Therefore, the whiskers and IQR are added. The whiskers show the total spread of the data and give details especially towards the highest loaded line while the IQR supplements this by adding information regarding the distribution density.

By the subsequent optimization, a reduced line utilization for all scenarios can be seen in the (N-0) state of the systems. Both the upper whisker length and the IQR are greatly reduced compared to the base case, with a maximum of almost 29 percentage points (pp) for the maximum value of scenario LL/LW. For scenario LL/HW, the maximum line loading is reduced by 2 pp and the IQR by 2.6 pp. The median values are all reduced due to the preventive optimization. Changes at most up to 1.3 pp. The statistical data of the (N-0) dataset is summarized in Appendix A.2.3.

The subsequent optimization approach shows an improvement regarding the minimization of the amount of critical contingencies in the post-optimization state. As the optimization approach starts with the determination of preventive measures, the AC lines could not be utilized higher than

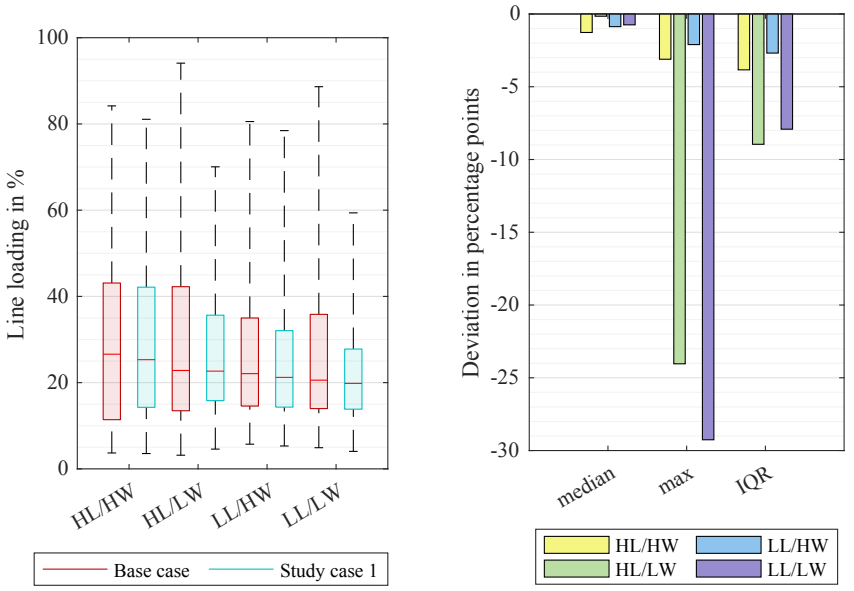

(a) Distribution

(b) Deviation of base case to study case

Figure 4.9: Evaluation of the loading of all AC lines with the subsequent optimization approach in the (N-0) situation showing (a) the distribution of the datasets and (b) deviations of key features in a bar diagram

in the base case, thus clearly showing the deficiency of the approach regarding the objective of implementing curative CMMs into system operation.

4.2.1.2 Study Case 1b – BLP-SCOPF

In the second study, the BLP-SCOPF described in Section 3.1 is investigated. The optimization uses the objective function shown in (4.2) with the weighting factors w_{prev} and w_{cur} parameterized equally. Thus, neither preventive nor curative CMMs are favored in the determination. As the optimization model uses a coordinated approach in the CMM determination, a reduction of the redispatch costs is to be expected as well as a higher line loading.

$$N_{\text{cc,opt}}(\boldsymbol{x}, \boldsymbol{y}_c, \boldsymbol{u}_c) = |C| - (w_{\text{prev}} N_{\text{feas,prev}}(\boldsymbol{x}, \boldsymbol{u}_c) + w_{\text{cur}} N_{\text{feas,cur}}(\boldsymbol{x}, \boldsymbol{y}_c, \boldsymbol{u}_c)) \tag{4.2}$$

When looking at the redispatch costs in Tab. 4.10, a reduction compared to the subsequent optimization can be observed for the HW scenarios while they are increased in the LW scenarios. The largest reduction is in scenario HL/HW with almost €20,000 savings while remaining at the same level of security. Whereas in LL/HW, the savings come at the expense of a slightly reduced level of security. Lastly, in scenario HL/LW and LL/LW the redispatch costs are increased by €255

and €1,180 respectively. Hereby, the difference for the HL/LW case one can be neglected while looking at the total costs.

Table 4.10: Redispatch costs of the BLP-SCOPF with equal priority on preventive and curative actions

	HL/HW	HL/LW	LL/HW	LL/LW
$C_{\text{redispatch}}$ in €	22,477	22,913	475	6,128

In Tab. 4.11, the results regarding the critical contingencies are presented. In all cases, an improvement compared to the base case can be seen. For both LL scenarios, HL/LW and LL/LW, the optimization resolves all critical contingencies. Explicitly in scenario HL/LW, the preventive action resolves all contingencies whereas in scenario LL/LW a combination of preventive and curative actions is needed. Scenario HL/HW has four remaining contingencies left, split into five remaining after the preventive optimization and one of those being resolved by a curative measure. Lastly, LL/HW is left with twelve critical contingencies.

Table 4.11: Representation of set of critical contingencies pre- ($N_{\text{cc,base}}$) and post-optimization ($N_{\text{cc,opt}}$) for the BLP-SCOPF with equal priority on preventive and curative actions

	HL/HW	HL/LW	LL/HW	LL/LW
$N_{\text{cc,base}}$	9	20	106	7
$N_{\text{cc,opt}}$	4	0	12	0
$N_{\text{feas,prev}}$	118	123	105	120
$N_{\text{feas,cur}}$	1	0	6	3

Tab. 4.12 summarizes the constraint violations associated with the unresolved critical contingencies listed in Appendix A.2.2. Scenario HL/HW comprises four violations of the maximum AC line loading. Two of those lines are L28 and L33 (cf. Fig. 4.1) in control area 1. They are highly loaded due to transporting the wind infeed to the load center in control area 2. If either one of those lines is taken out of service due to a fault, the remaining line gets overloaded. One congestion is triggered by an outage of a converter pole. The outage of either the positive or negative pole of VSC8 causes a congestion in the AC system due to the DC voltage control. The lost infeed in the AC system, primarily the infeed in control area 2, the converters in station VSC2 takes over a part the lost power leading to a congestion on L58. A similar occurrence happens with the outage of L58 that leads to a congestion on its parallel line L48. Additionally, the loss of L58 also leads to an undervoltage at the busses 30, 31 and 32 as not enough reactive power gets transported to those weakly connected busses. As with the base case and the subsequent optimization approach, scenario LL/HW mainly suffers from problems regarding the AC voltage range with ten different contingencies resulting in a violation of this constraint. From the four cases of AC line loading and generator limit violations, two are due to a disturbed power equilibrium and are therefore not

investigated any further. The remaining congestions are caused by the outages of either L5 or L11 which both lead to a reduced degree of meshing of VSC3. Thus, more power must be transported over L7, leading to a congestion on said line in both contingency cases.

Table 4.12: Summary of constraint violations over all (N-1) cases per each scenario for the BLP-SCOPF with equal weighing

	HL/HW	HL/LW	LL/HW	LL/LW
AC line loading	4	0	4	0
DC line loading	0	0	0	0
AC voltage range	1	0	10	0
Generator limits	0	0	2	0

The impact of the optimization on the line loadings is shown in Fig. 4.10 for all scenarios. Fig. 4.10a shows the line distribution for the (N-0) situation. Regarding the two HW scenarios, all changes are negligible as they at most reach up to 5 pp in absolute values (cf. Tab. A.8 in Appendix A.2.3). For the LW scenarios, the most significant changes are seen. Both optimizations have their overall line loading reduced as seen by the minimized maximum value as well as the IQR. In scenario LL/LW, a reduction of the median value is observed. Even though the IQR is shrunk by the optimization,

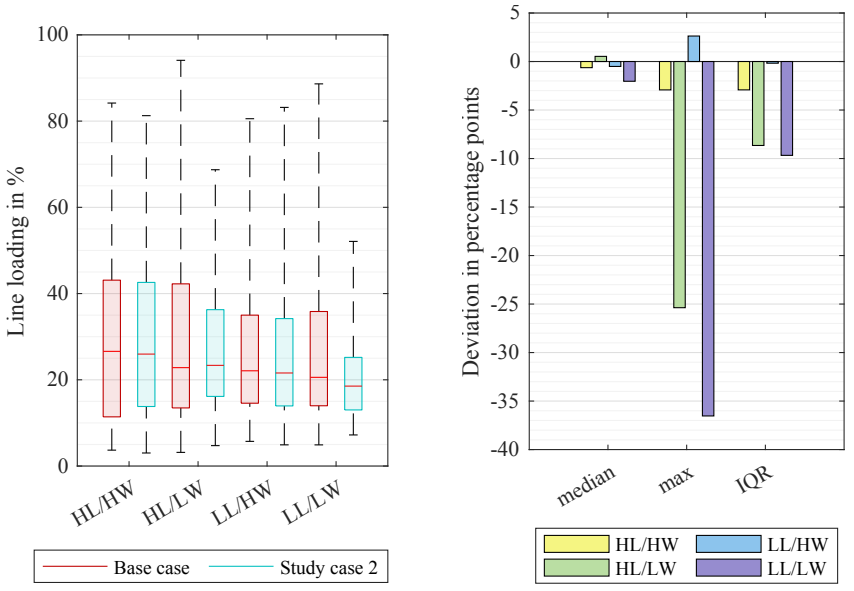

(a) Distribution **(b)** Deviation of base case to study case

Figure 4.10: Evaluation of the loading of all AC lines with the set-point optimized using the BLP-SCOPF with equal priority on preventive and curative actions in the (N-0) situation showing (a) the distribution of the datasets and (b) deviations of key features in a bar diagram

the proportion of Q1 and Q3 remain roughly the same with a slight reduction of Q1. For scenario LL/HW, an increase of the maximum line loading is observed, while the IQR and median are slightly reduced. Here, a higher line utilization is achieved by the optimization.

The coordinated determination of preventive and curative actions by the BLP-SCOPF shows a better performance than the subsequent optimization approach. This can be observed for once at the number of unresolved contingencies after the optimization as well as the total redispatch costs. Also, the BLP-SCOPF enables a higher utilization of the AC lines in the LL/HW scenario.

4.2.2 Study Case 2 – BLP-SCOPF with Prioritization

In study case 2, the same BLP-SCOPF is used as in 1b but not with an equal weighting on preventive and curative actions. Two separate simulations are run. Each case prioritizes either the preventive or curative CMMs. Study case 2a presents the results of the BLP-SCOPF with a focus on preventive measures, while study case 2b uses the same model with a focus on curative CMMs[14].

4.2.2.1 Study Case 2a – BLP-SCOPF with Priority on Preventive Actions

As already mentioned, study case 2a uses the BLP-SCOPF with a higher weighting factor on the determination of preventive CMMs. Therefore, the optimization is expected to perform worse than the BLP-SCOPF with equal weighting of case 1b, as the model favors preventive security. This should have an impact on both redispatch costs and line utilization.

Tab. 4.13 presents the redispatch costs. Compared to the optimization with the BLP-SCOPF with equal weighting in Section 4.2.1.2, an increase in the redispatch costs over all scenarios except LL/LW can be seen. The highest increase compared to the results of study case 1b is in scenario HL/HW with €15,000 and the lowest in scenario LL/HW with €3,000. Only in scenario LL/LW the redispatch costs are reduced compared to study case 1b by about €3,000.

Table 4.13: Redispatch costs of the BLP-SCOPF with the priority on preventive actions

	HL/HW	HL/LW	LL/HW	LL/LW
$C_{\text{redispatch}}$ in €	37,532	30,232	3,451	2,925

The results for all four scenarios are presented in Tab. 4.14 which shows the changes in N_{cc} for the pre- and post-optimization state as well as the allocation to the preventive and curative actions. As is shown by the results, no scenario is fully freed of critical contingencies. In general, a lack of curative actions can be observed. This is to be expected by giving curative CMMs a lower rating. At

[14] Please note that the results are of a representative nature as the choice of the exact weighting factors (see Appendix A.3.1) heavily affects the course of the optimization and therefore the quality of the actual solution. As the choice of the weighting factors needs additional tuning, the presented results are not representative for the performance of the BLP optimization model. The results are solely used to analyze the differences coming from giving priority to either preventive or curative actions.

most, a single viable curative action is found in each scenario. The best result is achieved for the LW scenarios. In HL/LW, one critical contingency remains, where the preventive action addresses 121 contingencies and leaves two to be resolved by a curative measure. For scenario LL/LW, the results are similar with a slightly different ratio of preventive and curative actions. Here, three critical contingencies remain, resulting in a total of two critical contingencies at the end of the optimization process. In case of the HW scenarios, the quality of the results is not as good as study case 1b, but still an improvement to the base case. Scenario HL/HW is the only scenario in which no viable curative actions are determined. The preventive measure leaves three critical contingencies that thereby are equal to the total number of remaining contingencies $N_{\text{cc,opt}}$. Lastly, scenario LL/HW has the highest number of remaining contingencies as in the previous simulations. The preventive optimization leaves 15 contingencies of which one could be addressed by a curative action.

Table 4.14: Representation of set of critical contingencies pre- ($N_{\text{cc,base}}$) and post-optimization ($N_{\text{cc,opt}}$) for the optimization with the priority on preventive security

	HL/HW	HL/LW	LL/HW	LL/LW
$N_{\text{cc,base}}$	9	20	106	7
$N_{\text{cc,opt}}$	3	1	14	2
$N_{\text{feas,prev}}$	120	121	108	120
$N_{\text{feas,cur}}$	0	1	1	1

For a better understanding of the critical contingencies, Tab. 4.15 gives an overview regarding the constraint violations occurring over all critical contingencies. A detailed list of all critical contingencies is given in Appendix A.2.2. The contingencies for the HL/HW scenario comprise three events in the AC system: the outages of the lines L29 and L33 that overload each other due to the high infeed of wind energy as well as the outage of L58 which causes voltage range violations at the busses 30, 31 and 32. Scenario HL/LW also suffers from the high demand of reactive power due to the high load situation. Here, the outage of L58 also results in over- and undervoltages in the lower left region of control area 2. Scenario LL/HW mostly has problems regarding the voltage range as it is in the previous studies which are therefore not discussed further. The only actual AC congestions are the outages of L35 and L81. L35 connects VSC4 to the lower part of control area 1 and contributes to the energy transfer from control area 1 to control area 2. After the outage of L35, L38 is the only remaining transmission line connecting the VSC station to the AC system. Due to the high preventive set-point of VSC4 (594 MW per pole), L38 is overloaded as it can not handle the provision of the converters. The same problem occurs with the outage of L81 at VSC5 in control area 2. Only L80 and L81 connect VSC5 to the AC system which feeds almost 1.2 GW into the system. This amount of energy cannot be transported by a single line, hence L80 is congested. In scenario LL/LW, two critical contingencies remain: the outages of L94 as well as either one of the converters stationed at VSC7. The former results in a disturbed power equilibrium. For the outage of the converter at VSC7, the voltage range does not comply to the limit values.

Table 4.15: Summary of constraint violations over all (N-1) cases per each scenario for the BLP-SCOPF with focus on preventive actions

	HL/HW	HL/LW	LL/HW	LL/LW
AC line loading	2	0	4	0
DC line loading	0	0	0	0
AC voltage range	1	1	13	2
Generator limits	0	0	2	1

To inspect the impact of the optimization on the line loading, Fig. 4.11 shows the distribution of the AC line loading for the (N-0) state as well as the deviation towards the base case for key features. Based on the changes of the maximum values depicted in Fig. 4.11b, the effects of a preventive security scheme become obvious. Both in regard to maximum line loading and the IQR a reduction to the base case is seen across all scenarios whereby which is to be expected when the optimization resolves contingencies by an intense use of preventive actions. The maximum line loading is reduced to a value of roughly 70 % for the remaining three scenarios which heightens the passive (N-1) security of the system. The data of the statistical evaluation is summarized in Appendix A.2.3.

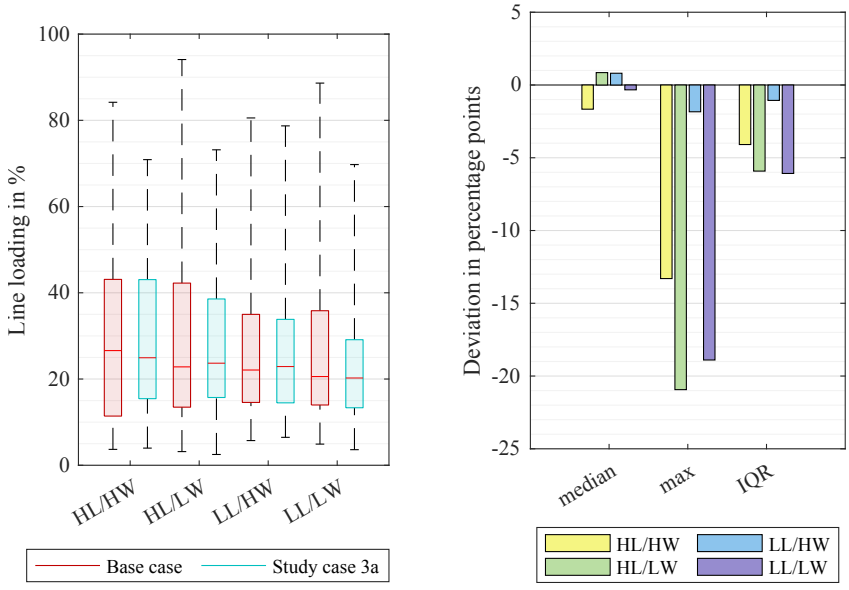

(a) Distribution

(b) Deviation of base case to study case

Figure 4.11: Distribution of the loading of all AC lines with the set-point optimized using the BLP-SCOPF with priority on preventive security in the (N-0) situation showing (a) the distribution of the datasets and (b) deviations of key features in a bar diagram

By raising the weighting factor on the preventive measures for the BLP-SCOPF, the determination of feasible curative actions is extremely limited. Over all four scenarios, only three curative actions are determined which results almost in a passive (N-1) security scheme. Compared to the model with an equal weighting in study case 1b, the redispatch costs are increased. This is an expected behavior, as the optimization has a more intense focus on preventive redispatch measures to achieve (N-1) security. Accordingly, the utilization of the AC lines is not increased compared to model 1b.

4.2.2.2 Study Case 2b – BLP-SCOPF with Priority on Curative Actions

For the last evaluation of the BLP optimization model, an optimization of the four scenario is done with the priority lying on curative CMMs. The expected result is therefore that, as there are less extensive preventive actions such as cost-expensive redispatch, the optimization is more cost-optimal compared to the previous one. Furthermore, as the curtailment of AC transport capacities should go down by the lack of preventive actions, a higher utilization of the capacity of the AC system should be seen.

In comparison to the optimization in study case 1b, the redispatch costs (see Tab. 4.16) are increased for all scenarios. While the risen costs in scenario LL/HW can be argued with the increased level of security, the opposite happens for HL/LW. The costs are increased by almost €8,000 while leaving four contingencies unattended.

Table 4.16: Redispatch costs of the BLP-SCOPF with the priority on curative actions

	HL/HW	HL/LW	LL/HW	LL/LW
$C_{\text{redispatch}}$ in €	27,094	30,714	4,509	8,133

The overview of critical contingencies are shown in Tab. 4.17. They reflect the expected behavior, i.e., the number of critical contingencies remaining after the preventive optimization $N_{\text{feas,prev}}$ being lower than in any of the previous models. Compared to the results of the first study case in Section 4.2.1, it can be seen that the number of critical contingencies $N_{\text{cc,opt}}$ is higher for the HL/LW scenario while an improvement is seen for the LL scenarios. For HL/HW, the level of security is identical compared to the BLP-SCOPF with focus on preventive actions. Five contingencies are unresolved after the preventive measures. Of those, two can be addressed by additional curative actions. In case of the HL/LW scenario, four unaddressed contingencies remain. The preventive optimization leaves 13 cases and the curative optimization resolves nine of those. An improvement to all previous study cases is seen especially for scenario LL/HW with the overall best result. In this case, more contingencies are addressed by the curative CMMs than by the preventive action. Preventively, 53 contingencies are resolved. From the leftover cases, 60 can be cured by an appropriate curative set-point, totaling at ten critical contingencies overall. For the LL/LW scenario, a similar performance as in study case 1b is seen with a total elimination of all critical contingency cases while the ratio of preventive and curative actions differs slightly.

Table 4.17: Representation of set of critical contingencies pre- ($N_{cc,base}$) and post-optimization ($N_{cc,opt}$) for the optimization with the priority on curative security

	HL/HW	HL/LW	LL/HW	LL/LW
$N_{cc,base}$	9	20	106	7
$N_{cc,opt}$	3	4	10	0
$N_{feas,prev}$	118	110	53	119
$N_{feas,cur}$	2	9	60	4

Analogous to the previous evaluations, Tab. 4.18 gives an overview regarding the corresponding constraint violations. Scenario HL/HW comprises three contingencies for which three AC congestions and one voltage range occur. Regarding the congestions, the outages of L29 and L58 are identical to the events described for the optimization prioritizing the preventive actions. The other congestion comes from the outage of a converter pole at VSC8. Here, a part of the lost infeed in control area 2 is taken up on VSC2 (80 MW at the unaffected converter and 260 MW at the affected one) and ultimately leads to a congestion on L58 as it is a rather short line with low resistance compared to, e.g., L48. In the HL/LW scenario, the outages of L58 and VSC8 are identical to scenario HL/HW. Additionally, the outages of L48 and a line of DC6 are added. The outages of L48 and L58 mutually define each other as they run parallel to each other. DC6 is the transmission branch connecting VSC2 and VSC8 on the DC side. A loss of one line reduces the power transfer to VSC8. As a result, VSC2 feeds more power into the AC system (150 MW on the affected pole and 50 MW on the healthy pole) which overloads L58. Out of the ten critical contingencies in scenario LL/HW, two of those result in a disturbed power equilibrium. The only actual AC congestion happens with the outages of L5 and L6. This reduced connectivity leads to a higher utilization especially of L11 and L7 where the latter is overloaded. All other contingencies lead to violations of the AC voltage range. Again, the events are either converter outages which reduce the actual amount of provided reactive power in the system or the loss of AC lines connecting the converters to the system.

Table 4.18: Summary of constraint violations over all (N-1) cases per each scenario for the BLP-SCOPF with focus on curative actions

	HL/HW	HL/LW	LL/HW	LL/LW
AC line loading	3	4	4	0
DC line loading	0	0	0	0
AC voltage range	1	1	8	0
Generator limits	0	0	1	0

Fig. 4.12a shows the distribution of the line loadings in the AC system for the (N-0) state of the system. Looking at the scale of Fig. 4.12b it can be seen that all changes are in a much lower range than for the previous study cases. While the maximum line loadings get reduced, the line utilization is increased compared to other operating schemes. Only in scenario LL/HW, an increase of the maximum line loading is observed. This is an unexpected behavior, as the study case resolves the highest amount of critical contingencies while still increasing the line utilization. The changes in the median values are all positively, i.e., an increase. While the medians for HL/HW and LL/LW remain almost constant, the deviation in the other two cases amount up a difference of around 2 pp. In scenario HL/HW, the total distribution of the line loadings remains widely unchanged.

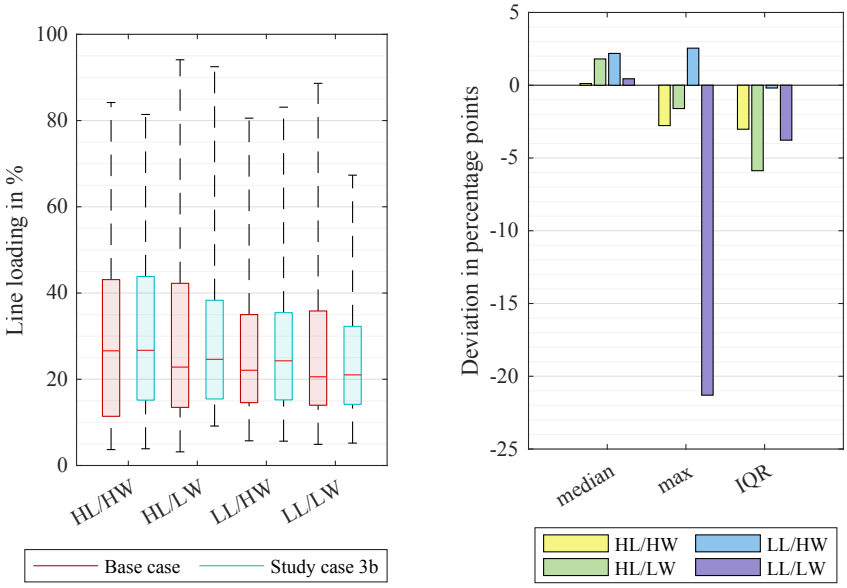

(a) Distribution

(b) Deviation of base case to study case

Figure 4.12: Distribution of the loading of all AC lines with the set-point optimized using the BLP-SCOPF with priority on curative security in the (N-0) situation showing (a) the distribution of the datasets and (b) deviations of key features in a bar diagram

The higher weighting on curative CMMs shows the results as initially assumed. While the general performance in regard to the total number of critical contingencies is slightly worse than the BLP-SCOPF with equal weighting, the determination of curative actions is more unrestricted. This becomes especially obvious in scenario LL/HW where the model of case 2b leaves the least number of critical contingencies for the three modifications of the BLP-SCOPF. In regard to the redispatch costs, a slight improvement towards the model with focus on preventive measures is seen while the costs are increased compared to the equally weighted BLP-SCOPF. The more intense use of curative actions has an effect on the line utilization. Over all study cases, case 2b has shown the highest line loadings in all scenarios.

4.2.3 Discussion

In the following, the results of the different optimization approaches are discussed. First, the level of achieved (N-1) security, the arising redispatch costs as well as the line loadings are compared side by side as they are only compared against the base case in the previous sections. By comparing the results, the impact on the line utilization in the pre-contingency state is to be inspected, i.e., if the line utilization changes with the number of contingencies addressed corrective instead of preventively. Based on this, the effect on (N-1-1) security is studied. The more contingencies that can be managed through curative measures, the closer the system can be operated securely to the boundary to unsafe operation. To evaluate this hypothesis, the (N-1-1) security is inspected briefly as it is not directly in the scope of the work. Furthermore, the computational performance is investigated. Pure computation time is an inaccurate measure as background tasks, different computation systems and other external factors can affect the performance in a non-deterministic manner. Therefore, the computational performance is compared by the number of power flow calculations needed for each simulation as this is the computational most intensive calculation in the design of the solver.

For each aspect, the discussion of the results is made while comparing the subsequent optimization approach with the BLP-SCOPF (study case 1a and 1b) and then again for comparing the variants of the BLP-SCOPF varying the priority of either preventive or curative actions (study case 2a and 2b). As the weighted optimization in study case 2 changes the behavior of the optimization model distinctively, a comparison with the subsequent optimization approach is not appropriate.

4.2.3.1 (N-1) Security

In Fig. 4.13, bar plots are shown to allow the comparison of the number of critical contingencies. The data is additionally summarized in Appendix A.2.1. First, in regard to the results of study 1 shown in Fig. 4.13a, when looking at the performance of case 1a and 1b, no distinct differences are seen. In the HL scenarios, both models perform equally whereas the BLP-SCOPF yields better results in the LL cases.

For study 2, shown in Fig. 4.13b, the results are very similar. When increasing the weighting on the determination of preventive measures, the level of security is better in regard to the HL scenarios. The simulations of case 2b show better results for the LL scenarios. Especially for LL/HW, the highest amount of curative feasible contingencies is found with 60 (cf. Tab. A.1). The scenario LL/LW is conspicuous as the best results are seen for Study 1b and 2b. With both optimization models, a higher amount of curative solutions are procured. Here, there is reason to believe that greater weighting in the determination of curative measures will benefit solution quality, as the landscape generated by the preventive actions will be appropriately adjusted to accommodate them.

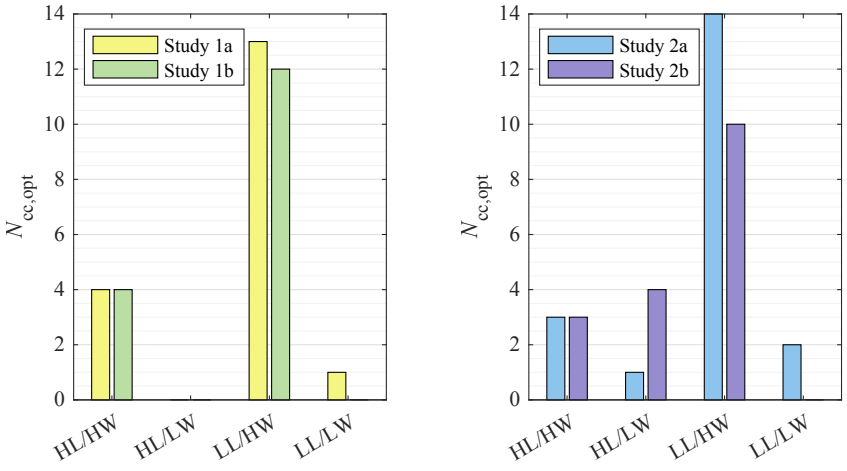

(a) Study 1 **(b)** Study 2

Figure 4.13: Comparison of the number of critical contingencies $N_{cc,opt}$ over all studies

4.2.3.2 Comparison of Redispatch Costs

Fig. 4.14 depicts a direct comparison of the redispatch costs for the subsequent optimization approach and the BLP-SCOPF with equal weighting. The aim of the comparison is to validate the hypothesis formulated at the outset that the coordinated use of preventive and curative measures reduces redispatch costs.

Looking strictly at the costs, a clear advantage of the BLP-SCOPF over the subsequent optimization approach can be seen. Especially for the HW scenarios, the redispatch costs of the subsequent

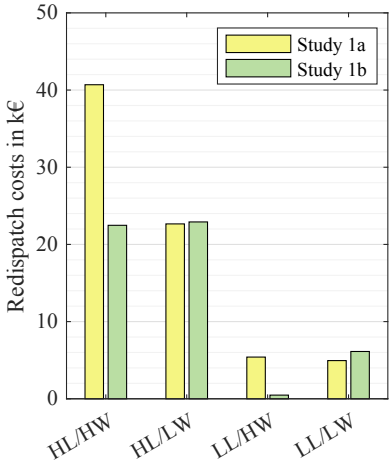

	1a	1b
HL/HW	40,690	22,477
HL/LW	22,658	22,913
LL/HW	5,404	475
LL/LW	4,948	6,128
$\sum$	73,700	51,994

Figure 4.14: Comparison of total redispatch costs for study case 1

optimization are higher than for the bilevel approach. In case of HL/HW, the costs based on the results of the subsequent optimization approach are €18,000 higher. On a relative scale, the highest savings are achieved in scenario LL/HW with up to 1,000 %. For the other two scenarios, the differences are smaller. With the subsequent model, a redispatch saving of €255 over the BLP-SCOPF in HL/LW €1,180 for the LL/LW case.

Fig. 4.15 compares the redispatch costs of the BLP-SCOPF with prioritization of either preventive or curative actions Regarding the plain redispatch costs for each scenario, an advantage of the optimization with a focus on preventive security is seen as the preventive focussed model is cheaper in three out of four scenarios. Only in scenario HL/HW, the use of generator redispatch leads to an increase in costs of €10,437 with the preventively focused model. The same model of study case 2a achieves a cost saving for all other cases with the biggest difference in scenario LL/LW. Here, the optimization of 2a saves €5,207 compared to the one focussing curative measures.

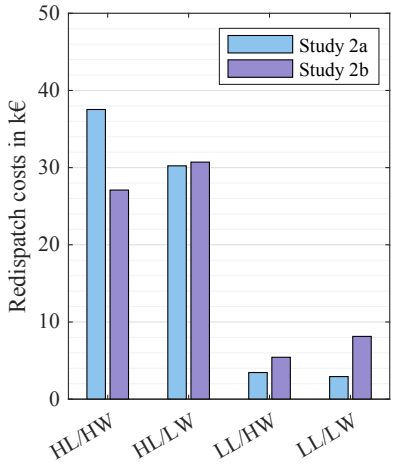

	2a	2b
HL/HW	37,532	27,094
HL/LW	30,232	30,714
LL/HW	3,451	5,428
LL/LW	2,925	8,133
$\sum$	74,140	71,369

Figure 4.15: Comparison of total redispatch costs for study case 2

Overall, the lowest redispatch costs are produced by the BLP-SCOPF with equal weighting factors. Compared to the subsequent optimization model of study case 1a, the BLP-SCOPF of study case 1b is cheaper by €21,700. This supports the hypothesis that the coordinated use of preventive and curative measures reduces redispatch costs. In regard to the models of study case 2, no distinct differences can be made out. The costs of study case 1a and 2a are around the same level which is to be expected as they both focus heavily on a preventive security scheme. By the use of curative actions in study case 2b, the total costs can be lowered slightly but due to the imperfect tuning of the weighting factors and the higher security level, the final costs are not significantly lowered compared to the results of model 2a.

4.2.3.3 Comparison of Line Loadings

Another evaluation aspect is the line loading. As stated in Section 1.1, a preventive operation scheme curtails transport capacities and leads to (cost-expensive) redispatch measures whereas the implementation of curative actions should raise the overall asset utilization. To give an overview, Fig. 4.16 shows the AC line distributions for each scenario and study case. It can be seen that all optimization models reduced the maximum line loading for each scenario, thus reducing the number of critical contingencies.

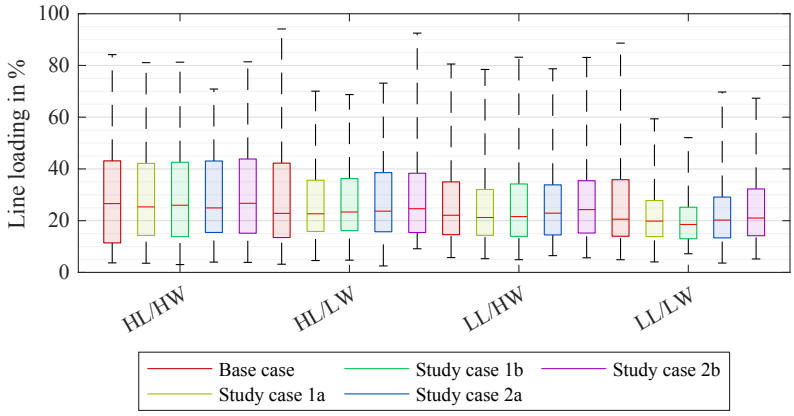

Figure 4.16: Distribution of AC line loadings for all (N-0) cases, clustered by grid scenarios

To compare the line loadings of all AC lines for the (N-0) state visually, they are represented as violin plots. The violin plot is a statistical graphic, combining features of box plots and kernel density plots to summarize statistics and show the distribution of numerical data. As the name implies, a violin plot represents its data in the form of a "violin" or as a half-violin. The width of the violin at any point represents the density of data points at this value. A wider body correlates with a higher density while the body narrows for lower densities. Here, a depiction of the half-violin plot is chosen to directly compare to density distributions side by side. On the left side of the violin, the line loading distribution of the unoptimized base case is shown, and the right side shows the distribution after the respective optimization model.

First, a comparison of study case 1a and 1b is conducted as shown in Fig. 4.17. When looking at the comparison of the base case and the subsequent optimization in Fig. 4.17a, no distinct differences can be made out. The median value is increased only in LL/HW. This can also be seen at the belly of the right-hand side half-violin (the widest part of the violin body, i.e., the part with the highest density regarding a specific line loading, as it is not as distinct at one level. Minimum line loadings are mostly unchanged, especially in LL/LW, and only slightly increased in all other scenarios with 1.2 pp at most. Regarding the upper line loadings, a degradation is observed for the HL/LW scenario where the upper limits only reach up to a level of 70 %. This can be traced back to the behavior of the optimization approach as it focuses solely on preventive security in the beginning. Due to the limitation of the maximum loading, the density of the distribution changes

significantly for scenario HL/LW. Instead of a distinct belly at around 15 % like in the initial state, the density declines slowly until the 38 % mark and then decreases steadily. Same with scenario LL/HW. In case of the LL scenarios, the maximum loading reach up to around 80 %. For LL/HW, a slight raise in the line loading is seen and a slight reduction in LL/LW.

Fig. 4.17b shows the violin plots based on the results of the BLP-SCOPF. As for the previous comparison, no distinct difference are observable between the base and optimized case. An increase of the median loading is only seen for HL/LW and is also visible by the clear upward shift of the violin belly. Regarding the HW scenarios, the median values are higher than for study case 1a but still lowered compared to the unoptimized cases and in LL/LW at the lowest across the three variants. For the most part, the changes in the upper line loading are better compared to study case 1a and the base case. The behavior for HL/LW and LL/HW is similar for both models. LL/LW is drastically changed with the maximum line loading is capped at 52 %. However, the minimum line loading is raised by 2.3 pp and 1.6 pp for HL/LW. The changes in the HW scenarios are negligible with 0.8 pp at most.

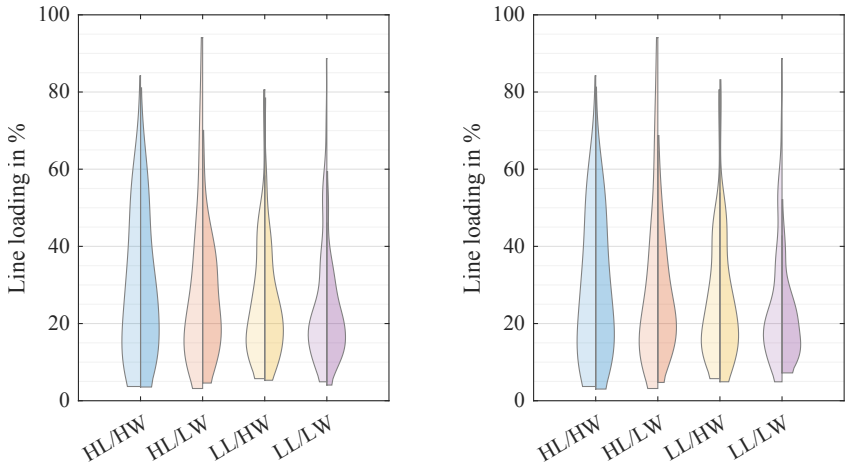

(a) Base case (left) vs. study case 1a (right)

(b) Base case (left) vs. study case 1b (right)

Figure 4.17: Comparison of the AC line loading of the systems in the (N-0) state for their initial (left side) and optimized set-points (right side) with the (a) subsequent optimization and (b) BLP-SCOPF

The comparison of Study 2a and Study 2b produces similar results. Fig. 4.18 shows the violin plots for both studies on the right side, and contrasts them with the distribution of the base case on the left side. Beginning with an analysis of the BLP-SCOPF with the priority and the determination of preventive actions in Fig. 4.18a, a similar trend as in Fig. 4.17a is seen. The maximum line loadings for the HL scenarios are capped at around 72 % which is due to the high preventive safety level. Analogous to the limitation of the maximum value, the distribution of the load in scenario HL/LW is adjusted by spreading it more in the middle area of the violin body (in the range of 20 to 40 %). Scenario LL/LW also has a limitation of the maximum line loading at around 70 % and

only in scenario LL/HW the limit is near the initial level at 79 % (a difference of −1.6 pp). For the minimum line loadings, only slight changes are seen with no significant differences.

With the BLP-SCOPF focussing on curative CMMs (see Fig. 4.18b), the effects of a higher line utilization are observed. For all scenarios, the median value of the AC line loading is increased, with the biggest improvement in scenario HL/LW by 1.8 pp. Along with the higher median value, the minimum line loading is significantly raised for this case. The initial state of HL/LW shows a minimum line loading of 3.2 % which is increased to 9.1 % by the optimization. Correspondingly, no capping of the maximum line loading is seen for this and also the two HW scenario. Only in case LL/LW a reduction of the maximum loading is seen with a difference of −13.3 pp.

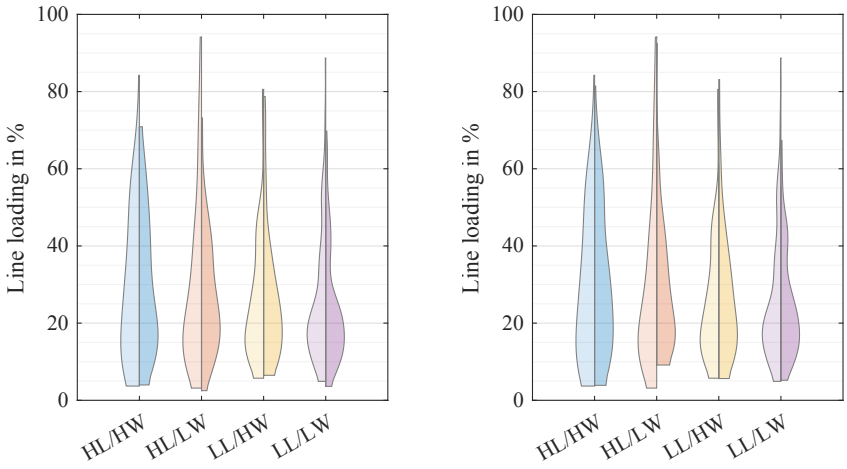

(a) Base case (left) vs. study case 2a (right)

(b) Base case (left) vs. study case 2b (right)

Figure 4.18: Comparison of the AC line loading of the systems in the (N-0) state for their initial (left side) and optimized set-points (right side) for the BLP-SCOPF with (a) preventive and (b) curative focus

Based on the median values, as depicted in Fig. 4.19, the BLP-SCOPF (study case 1b) performs better than the subsequent approach (study case 1a) for all scenarios except LL/LW, as it raises the line utilization. This is clear evidence of the effective use of curative actions and the coordinated CMM determination. The investigations of study case 2a and 2b further support this statement as the results of study case 2b show a clear advantage over case 2a, especially in scenario HL/LW where an increase in the minimum, median and maximum line loading is observed. Overall, the BLP-SCOPF with higher weighting on curative actions yields the best results in regard to increasing the line utilization and confirms the assumption that the usage of an active (N-1) security definition in system operation raises the efficiency of the existing system by reducing the curtailment of transport capacities.

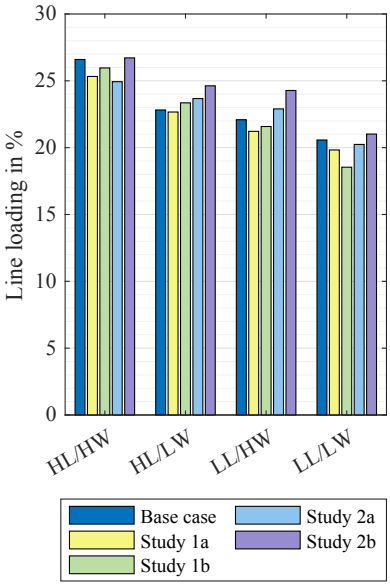

	Median line loading in %			
	HL/HW	HL/LW	LL/HW	LL/LW
Base case	26.60	22.82	22.09	20.57
Study case 1a	25.33	22.67	21.22	19.83
Study case 1b	25.96	23.35	21.58	18.54
Study case 2a	24.94	23.67	22.90	20.24
Study case 2b	26.72	24.63	24.28	21.02

Figure 4.19: Comparison of median AC line loadings for the base case and all study cases

4.2.3.4 (N-1-1) Security

The higher asset utilization by the use of curative actions in system operation brings power systems closer to their security limit, so the risk of critical (N-1-1) errors[15] increases. Therefore, an (N-1-1) SSA is conducted for all simulations.

In total, each scenario comprises 15,129 possible (N-1-1) contingency cases. Looking at the number of critical contingencies of the base case models shown in Fig. 4.20, a correlation to the number of critical (N-1) contingencies (cf. Tab. 4.5) is seen. In scenario LL/HW, 87 % of the possible (N-1-1) scenarios result in any kind of constraint violation which is a slight increase compared to the (N-1) security (85 % critical contingencies). The other scenarios show a similar correlation. The best results regarding the number of critical (N-1-1) situations, as indicated by the green coloring in Fig. 4.20, are produced by the BLP-SCOPF for the LL scenarios. For the HL scenarios, it varies between the subsequent optimization approach in HL/LW and the curative focused BLP-SCOPF in HL/HW. In regard to scenario HL/HW and LL/LW, the performance of all study cases is around the same level with a difference of 1.5 pp and 1.4 pp respectively. The biggest deviation of the critical (N-1-1) contingencies is seen for HL/LW where the delta between best and worst results is about 6.5 pp.

[15] Please note that (N-1-1) faults are defined as cascaded outages, i.e., a contingency happening after an initial outage scenario.

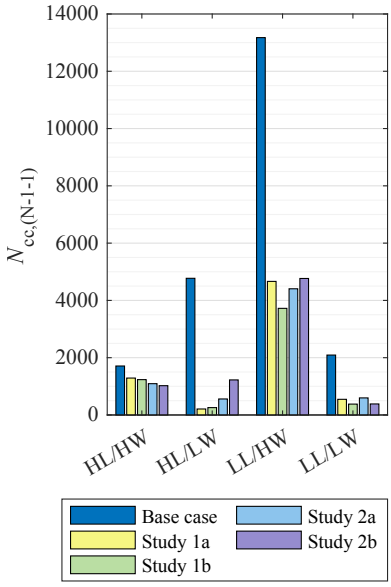

	HL/HW	HL/LW	LL/HW	LL/LW
Base case	1,710	4,772	13,175	2,092
Study case 1a	1,289	209	4,664	547
Study case 1b	1,234	257	3,723	380
Study case 2a	1,093	559	4,406	596
Study case 2b	1,023	1,224	4,766	385

Figure 4.20: Summary of (N-1-1) violations over all scenarios and optimization models, showing the best and worst result in the table per scenario in green and red respectively

4.2.3.5 Performance of the Optimization Models

Lastly, the performance of the presented optimization approaches is evaluated. Typically, performance of computation problems is analyzed by measuring the time to finish the computation. This procedure can get inaccurate for time extensive computations for multiple reasons. For once, as the optimization does not run exclusively on the machine. Therefore, background tasks that need to be scheduled by the CPU affect the time needed for an optimization in a non-deterministic way. Furthermore, the way of implementation influences the computational performance greatly as well as the hardware the code is running on. Within the framework of this thesis, the algorithms are implemented using MATLAB [218] and run on multiple servers, making a direct comparison unfeasible due to the varying hardware. To accommodate this, the performance is evaluated based on the number of completed power flow computations. Thus, a measure independent of the CPU load is used. The results can still be projected on a timescale by assuming a time needed for a power flow calculation to finish, e.g., 10 ms. This is not possible for the present model, since power flow calculations are parallelized based on the size of the DE population (cf. Appendix A.3.1)).

Fig. 4.21 shows the number of conducted power flow calculations for each optimization model and scenario in a bar plot. At first glance it becomes obvious that due to the scale, the bar of the subsequent optimization is barely visible. Based on the figure, it is seen that the subsequent optimization approach is by far the one with the best performance. Across all scenarios, each optimization needs at most one million power flow calculations until reaching convergence while the other models reached in the tens and hundreds of millions or even billions (cf. HL/LW for

Study 1b and HL/HW for Study 2a). The reason for this huge jump is the complexity of the BLP optimization problem. As described in Section 2.2.1.2, BLP formulations are $\mathcal{NP}$-hard even for linear–linear problems. The proposed BLP SCOPF is a non-linear–linear problem which further raises the complexity.

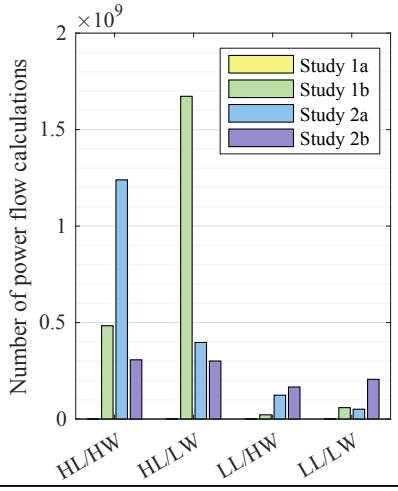

	HL/HW	HL/LW	LL/HW	LL/LW
Study 1a	397,149	1,142,269	376,715	902,300
Study 1b	483,586,459	1,672,696,233	21,961,052	59,078,228
Study 2a	1,239,519,232	396,856,595	123,730,905	51,074,750
Study 2b	306,971,319	300,743,142	166,010,267	205,734,244

Figure 4.21: Comparison of performed power flow calculations per study and scenario

Using the aforementioned illustrative example of 10 ms for each power flow calculation, a parallelization of 100 calculations simultaneously and neglecting the possible over-head of the parallelization as well as the burden of all other computational steps, the worst case result of 1.6 billion calculations results in a computation time of over 46 hours. The practicability of the proposed method is therefore not given for a mission-critical application as the determination of CMMs where only 15 minutes are available for the calculation (cf. Section 2.1.6).

To give a further comparison, the computational performance is evaluated against a brute force approach. For this, the listing of all degrees of freedom and their intervals is taken from Tab. 4.2. Based on the intervals and a set step-size $\lambda = 0.01$, according to (4.3) the number of possible combinations of available degrees of freedom $N_{\text{dof,PSCOPF}}$ for the base case total to 10,285,064 different combinations. This is also the number of variations of the degrees of freedom available for the preventive actions.

$$
\begin{aligned}
N_{\text{dof,PSCOPF}} &= 16 \cdot \left|\{P_{\text{gen,min}} + \lambda P_{\text{gen}} \mid P_{\text{gen}} \in \left[P_{\text{gen,min}}, P_{\text{gen,max}}\right]\}\right| + \\
&\quad 16 \cdot \left|\{P_{\text{VSC,min}} + \lambda P_{\text{VSC}} \mid P_{\text{VSC}} \in \left[P_{\text{VSC,min}}, P_{\text{VSC,max}}\right]\}\right| + \\
&\quad 16 \cdot \left|\{Q_{\text{VSC,min}} + \lambda Q_{\text{VSC}} \mid Q_{\text{VSC}} \in \left[Q_{\text{VSC,min}}, Q_{\text{VSC,max}}\right]\}\right| + \\
&\quad 16 \cdot \left|\{k_{\text{droop,min}} + \lambda k_{\text{droop}} \mid k_{\text{droop}} \in \left[k_{\text{droop,min}}, k_{\text{droop,max}}\right]\}\right| \\
&= 10{,}285{,}064
\end{aligned}
\tag{4.3}
$$

The amount of combinations for the curative actions $N_{\text{dof,PSCOPF}}$ can be determined by (4.4) and total to 3,400,020 different possibilities.

$$
\begin{aligned}
N_{\text{dof,CSCOPF}} &= 4 \cdot \left|\{P_{\text{GB,min}} + \lambda P_{\text{GB}} \mid P_{\text{GB}} \in \left[P_{\text{GB,min}}, P_{\text{GB,max}}\right]\}\right| + \\
&\quad 16 \cdot \left|\{P_{\text{VSC,min}} + \lambda P_{\text{VSC}} \mid P_{\text{VSC}} \in \left[P_{\text{VSC,min}}, P_{\text{VSC,max}}\right]\}\right| + \\
&= 3{,}400{,}020
\end{aligned}
\tag{4.4}
$$

As the optimization is applied to an SCOPF, those numbers must then be multiplied by the number of contingency cases plus the base case, resulting in 1,275,347,936 combinations for the base case and the PSCOPF cases. Additionally, 418,202,460 variations are added for the curative degrees of freedom. As shown in (4.5), a total number of 1,693,550,396 power flow calculations are needed to approach this optimization problem via brute force. Compared to the computational most expensive calculation (scenario HL/LW in study 1b), the brute force solution needs 20,854,163 additional power flow calculations, i.e., an increase of 1.2 %. Given the assumptions of parallelization and a computation time of 10 ms, the brute force approach needs 47 hours to complete.

$$
\begin{aligned}
N_{\text{dof,total}} &= (123 + 1) \cdot N_{\text{dof,PSCOPF}} + 123 \cdot N_{\text{dof,CSCOPF}} \\
&= 1{,}275{,}347{,}936 + 418{,}202{,}460 \\
&= 1{,}693{,}550{,}396
\end{aligned}
\tag{4.5}
$$

4.3 Summary of the Case Study Evaluation

For validation purposes, an academic test system is used to study the feasibility of the proposed optimization approach. The test system is designed for studies on SCOPF algorithms. It depicts an AC system comprising three control areas, integration of renewable energies (on- and offshore wind farms) and incorporates a meshed HVDC overlay system. Based on the initial description of the test system in [211], some modifications are made. Accordingly, the line length of the AC and DC system are modified to correspond to the apparent length shown in Fig. 4.1. Furthermore, the generation landscape is adapted. First, the conventional generator units are mapped to different fuel types, thereby standardizing the machine types. A new degree of freedom for congestion management is added by integrating BESS-based grid booster units. To diversify the evaluation,

four scenarios are designed. The scenarios are based on principles of grid planning studies and comprise the cases high and low load as well as high and low wind.

As benchmark for the proposed coordinated optimization approach, a *subsequent optimization model* is introduced as study case 1a which starts with a preventive optimization and subsequently tries to address the remaining contingencies via a CSCOPF. Thereafter, three variations of the BLP-SCOPF model presented in Section 3 are investigated, differentiating the measure by weighting of preventive and curative CMMs. The first, study case 1b, corresponds to an equal weighting of both kinds of actions and following this, study case 2 examines the optimization with a higher priority on preventive (study case 2a) and curative (study case 2b) measures to further look into the possibilities of a preventive or curative operated power system.

Due to the limitation of the operational degrees of freedom, not all contingencies are addressed for all scenarios, leaving some of them still remaining. This is due to the limited number of available flexibility for congestion management in the system and the omission of load shedding as viable degree of freedom. The key findings are summarized in Tab. 4.19.

Table 4.19: Summary of simulation results

Hypothesis	Finding
Overall security level	Similar performance for subsequent optimization model and BLP-SCOPF with a slight advantage for BLP-SCOPF
Redispatch savings	Significant savings potential by the use of an active (N-1) security definition
Higher asset utilization	Best results are shown by the BLP-SCOPF with priority on curative operation due to the reduced curtailment by the preventive actions
(N-1-1) security	Correlation to the (N-1) security level and therefore no direct differences in the uncoordinated and coordinated model

The general performance of the subsequent optimization approach and BLP-SCOPF is largely at the same level with an advantage for the BLP-SCOPF. This roughly translates to the arising redispatch costs. Here, the BLP-SCOPF performs significantly better fur the high load/high wind scenario. A general tendency in regard to the weighted study cases can be seen. Especially for the objective of higher line utilization, the stronger prioritization of curative actions shows the expected results and enables a more efficient asset utilization. As the ratio of the weighting factors in this work is chosen rather extreme (100:1, cf. Appendix A.3.1), a clear statement on the influence of the weighting factors is not possible. Lastly, the investigation of the computational performance underlines the complexity of the BLP optimization problem. Thus, it cannot compare to the one of the subsequent approach. An application in a mission-critical environment is therefore not recommended. To reduce the computational costs of the optimization problem, the overall complexity of the optimization model must be reduced. Here, multiple ways are possible for this:

- switching to a more performance oriented solving algorithm (e.g. Interior Point or other conventional methods),

- application of convex relaxation techniques,
- applying a contingency filtering approach [219–221],
- the use of decomposition techniques (e.g. Benders Decomposition [222]) or
- discarding the NLP formulation of the upper level problem.

5 Conclusion and Outlook

Due to the energy transition, there are two significant developments in the transmission system in Europe and worldwide. On the one hand, the transmission system must be extended. For the new construction of long-distance transmission, high voltage direct current (HVDC) is the best choice. On the other hand, the existing assets must be utilized to a higher degree in order to reduce the network expansion to the minimum. In addition to a change in the operating concept of the interconnected power system, this will require the installation of new control elements in the network. These include, e.g., storage units with which a so-called grid booster can be set up or some regulating transformers for active flow control.

The multiple new control options in the transmission grid must be optimally managed in the system management process. Network security can be established passively by purely preventive means, i.e., a *passive (N-1)* security, or actively by preventive-curative means as *active (N-1)* security. Curative measures are actions by control elements in the network (e.g. HVDC) in order to convert an impermissible network state automatically and within a short time after the occurrence of an event into a permissible state. This means that, according to today's standards, an (N-0) safe state plus suitable curative measures results in an *active (N-1)* secure state.

5.1 Thesis Summary

This thesis takes the upcoming assets and their operational degrees of freedom as well as the approaches of active and passive (N-1) security into account, while designing a model for a coordinated determination of preventive and curative actions for congestion management in power systems. Therefore, three research questions Q1-Q3 are formulated at the beginning (see Section 1.3), which will be answered in summary in the following.

Q1 What are the specifics of operational planning in terms of a coordinated determination of preventive and curative measures?

The system operation guideline [28], which defines the legal framework for the Central European Transmission System, is open to technology in regard to the way (N-1) security is established. Looking at the regulations of the predecessor organization UCTE, the use of curative or rather corrective actions is already well-defined [223]. Therefore, no constraints in respect of viable technologies are made for curative actions. Since the determination of curative measures within ENTSO-E is permitted by regulations but not yet practiced uniformly, there are no clear processes for coordinating them. Coordination is relevant in various aspects:

- Enhanced coordination processes between transmission system operators (TSOs) and regional security operators in operational planning
- Updated and standardized data exchange formats to include curative actions, trigger information and replacement measures

- Determination of curative actions with inclusion of variable preventive systems

Q2 By using a coordinated congenstion management measure determination, what must be taken into account in the modeling?

The determination of congestion management measures (CMMs) is fundamentally done in the planning step of the day-ahead congestion forecast (DACF). Only starting in this step, a consideration of the actual power system takes place by means of an Optimal Power Flow. An optimization method for coordinating preventive and curative CMMs must therefore be based on the standard Security Constrained Optimal Power Flow (SCOPF) model and include characteristics of pre- and post-fault clearing as well as take the dependency of curative actions on the preventive set-points into account.

To combine the aspects of determining preventive and curative actions, the bilevel programming (BLP) method is used, formulating a *BLP-SCOPF*. Besides the functionality of mixing different objectives in one model, the BLP formulation also allows the application of separate problem classes and optimization variables. Therefore, the preventive optimization can be formulated using a non-linear formulation of a power system while using a linearized model to compute the curative measures. Using embedded HVDC systems as example, the availabe degrees of freedom can be customized as needed. In the pre-fault scope, the power infeed into the AC system is availabe as well as the parameterization of the DC voltage control. For the curative optimization, the control parameter cannot be adapted due to the time constraints and is therefore omitted.

Bilevel optimization problems are based on nesting an optimization problem into another. In this application, the determination of the preventive set-point is used as the upper level problem, i.e., the leader problem. Accordingly, the curative CMM is determined in the lower level optimization, i.e., the follower. For the lower level problem, the current iteration is used as the initial state and any kind of infeasibility (e.g. constraint violations) are forwarded to the upper level problem. Based on those inputs, the determination of preventive actions is influenced to allow better curative actions.

Q3 To what extent must a prioritization of preventive or curative system management be enabled?

Based on the investigation on an uncoordinated and coordinated optimization model, similar levels of security are achieved. For the evaluation, the following criteria are used:

- Overall security level
- Arising redispatch costs
- Impact on asset utilization
- (N-1-1) security

When examining the results in detail, it stands out that the subsequent optimization approach fails to resolve the remaining contingencies by means of curative adaptation, and it remains for the most part a *passive (N-1)* security. As for the (N-1-1) security level, no clear differences are made out. Here, a direct correlation to the (N-1) security level is seen. This has a direct impact on the redispatch costs: through the intense use of preventive actions, the subsequent approach produces significantly higher costs than the BLP-SCOPF. Regarding the higher utilization of transmission lines, a tendency is shown that the intense use of curative actions in system operation allows a higher utilization of the existing asset.

The BLP-SCOPF allows a prioritization of either preventive or curative actions. Accordingly, further investigations are carried out to show to what extent a prioritization of preventive or curative actions has an influence on the results. The framework of investigation here is identical to the previous one and considers the same scenarios. A preference for a certain type of prioritization is clearly reflected in the results regarding the ratio of preventive or curative CMMs. Similar to the subsequent approach, the BLP-SCOPF with weighting on the provision of preventive actions places emphasis on the same, so that only an insignificant number of curative actions is recorded. With focus on curative measures, their number increases and the level of preventive security decreases. With regard to the security level after optimization, a similar behavior can be seen as in the comparison of the subsequent optimization approach and the BLP-SCOPF. Both variants of the BLP-SCOPF achieve largely the same level of system security, while isolated differences can be discovered in the scenarios. The redispatch costs for the BLP-SCOPF with equal weighting are lower than the costs of the subsequent optimization approach. Regarding the line utilization, there is a clear effect of the curative actions. If these are the focus of the investigation, all line utilization rates are improved and the existing network is thus operated more efficiently.

5.2 Further Research Topics

The approach presented in this thesis addresses aspects of the current challenges, TSOs are faced in their operation. Still, not all aspects are covered and the work can be further improved. Some of the most important research aspects are listed in the following and explained thereafter.

1. Increasing the computational performance and robustness
2. Optimization based on time-series
3. Inclusion of forecast errors
4. Implementation of further degrees of freedom
5. In-depth consideration of various technologies (e.g. grid boosters)

One of the biggest downsides of the presented optimization model is its computational performance as well as its robustness due to the stochastic nature of the solving technique. Enhancements for

the approach are, e.g., switching to a conventional algorithm to solve the optimization problem or the application of relaxation and decomposition techniques.

In the presented methodology and case study, the investigation focused on single scenarios leaving the aspect of considering time series in the optimization which is an important topic for applying the approach in practice. For once, the actual environment such an optimization model is used in is operational planning where not single, time-independent scenarios are investigated but, depending on the actual process, e.g., one to two days in quarter-hour resolution for the DACF. Thus, longer forecase windows are possible and an application for the week ahead planning process, where a consideration of curative actions in the scheduling stage is promising in regard to leverage further potentials in redispatch cost-savings.

Another aspect arising with the thought of implementing time series optimization is the handling of forecast errors. An extension of the proposed model into a probabilistic method is a topic of interest not only in regard of uncertainties in the infeed of renewable energy sources (RESs), which is necessary with the rising share of RES on the net electricity production, but also in terms of outage probabilities. Thereby, the quality of the SCOPF results is enhanced as the effect of unlikely scenarios is dampened.

Currently, the proposed optimization model comprises degrees of freedom that are node-based in their influence on power flows. An extension of the model to include further technologies, e.g., dispatch from underlying systems or branch-based actions such as phase-shifting transformers (PSTs), is promising in regard to further address unresolved contingencies as well as reduced redispatch costs.

The consideration of time series also allows a much more detailed modeling of certain technologies. The application of grid boosters gets more complicated as the restoration of activated units needs consideration. Additionally, thermal-based generator units are affected by constraints such as ramping rates, limiting the effect of preventive redispatch. When looking at a longer time span, the determination of preventive generator set-points becomes a more significant topic regarding the determination of curative actions.

6 Bibliography

[1] *Communication from the Commission of the European Parliament, the Council, the European Economic and Social Committee and the Committee of the Regions - Energy Roadmap 2050*.

[2] European Union, "Long-term low greenhouse gas emission development strategy of the European Union and its Member States", 2020. [Online]. Available: https://unfccc.int/sites/default/files/resource/HR-03-06-2020%20EU%20Submission%20on%20Long%20term%20strategy.pdf (visited on 2023-07-19).

[3] Bundesministerium für Wirtschaft und Klimaschutz, "Natinales Reformprogramm 2023", 2023. [Online]. Available: https://www.bmwk.de/Redaktion/DE/Publikationen/Europa/nationales-reformprogramm-2023.pdf?__blob=publicationFile&v=20 (visited on 2023-07-19).

[4] Bundesministerium für Wirtschaft und Klimaschutz, "Klimaschutzplan 2050", 2016. [Online]. Available: https://www.bmwk.de/Redaktion/DE/Publikationen/Industrie/klimaschutzplan-2050.pdf?__blob=publicationFile&v=1 (visited on 2023-07-19).

[5] *Gesetz Zur Grundlegenden Reform Des Erneuerbare-Energien-Gesetzes Und Zur Änderung Weiterer Bestimmungen Des Energiewirtschaftsrechts Vom 21. Juli 2014 (BGBl. I Nr. 33)*.

[6] *Energiewirtschaftsgesetz Vom 7. Juli 2005 (BGBl. I S. 1970, 3621), Das Zuletzt Durch Artikel 84 Des Gesetzes Vom 10. August 2021 (BGBl. I S. 3436) Geändert Worden Ist: EnWG*.

[7] Umweltbundesamt, "Erneuerbare Energien in Deutschland - Daten zur Entwicklung im Jahr 2022", 2023. [Online]. Available: https://www.umweltbundesamt.de/sites/default/files/medien/1410/publikationen/2023-03-16_uba_hg_erneuerbareenergien_dt_bf.pdf.

[8] REN21, "Renewables 2019 Global Status Report", 2019. [Online]. Available: https://wedocs.unep.org/20.500.11822/28496.

[9] European Environment Agency and European Topic Centre for Air Pollution and Climate Change Mitigation, *Renewable Energy in Europe 2020: Recent Growth and Knock on Effects*. LU: Publications Office, 2020, 113 pp. [Online]. Available: https://www.eionet.europa.eu/etcs/etc-cme/products/etc-cme-reports/etc-cme-report-7-2020-renewable-energy-in-europe-2020-recent-growth-and-knock-on-effects.

[10] Bundesministerium für Wirtschaft und Technologie, "Energiekonzept für eine umweltschonende, zuverlässige und bezahlbare Energieversorgung", 2010. [Online]. Available: https://www.bmwk.de/Redaktion/DE/Downloads/E/energiekonzept-2010.pdf?__blob=publicationFile&v=1.

[11] Federal Ministry for Economic Affairs and Climate Action and AGEE Stat, "Time series for the development of renewable energy sources in Germany". [Online]. Available: https://www.erneuerbare-energien.de/EE/Redaktion/DE/Downloads/zeitreihen-zur-entwicklung-der-erneuerbaren-energien-in-deutschland-1990-2022-en.pdf?__blob=publicationFile&v=3 (visited on 2023-07-19).

[12] BDEW Bundesverband der Energie- und Wasserwirtschaft e.V. "Bruttostromverbrauch in Deutschland in den Jahren 1990 bis 2022 (in Terawattstunden) [Graph]", Statista. (2022), [Online]. Available: https://de.statista.com/statistik/daten/studie/256942/umfrage/bruttostromverbrauch-in-deutschland/ (visited on 2023-07-20).

[13] Fraunhofer-Institut für Solare Energiesysteme ISE. "Installierte Netto-Leistung zur Stromerzeugung in Deutschland in 2022". (2023), [Online]. Available: https://www.energy-charts.info/charts/installed_power/chart.htm?l=de&c=DE&chartColumnSorting=default&legendItems=1000111111111&year=2022 (visited on 2023-07-20).

[14] Deutsche Energie-Agentur GmbH (dena), "Dena-Netzstudie II: Integration erneuerbarer Energien in die deutsche Stromversorgung im Zeitraum 2015 – 2020 mit Ausblick auf 2025", Berlin, 2010. [Online]. Available: https://www.dena.de/fileadmin/user_upload/Download/Dokumente/Studien___Umfragen/Endbericht_dena-Netzstudie_II.PDF (visited on 2023-07-10).

[15] *Bundesbedarfsplangesetz Vom 23. Juli 2013 (BGBl. I S. 2543; 2014 I S. 148, 271), Das Zuletzt Durch Artikel 5 Des Gesetzes Vom 22. Mai 2023 (BGBl. 2023 I Nr. 133) Geändert Worden Ist*.

[16] 50Hertz Transmission GmbH, Amprion GmbH, TenneT TSO GmbH, and TransnetBW GmbH, "Netzentwicklungsplan Strom 2037/2045: Version 2023", 2023. [Online]. Available: https://www.netzentwicklungsplan.de/sites/default/files/2023-06/NEP_2037_2045_V2023_2_Entwurf_Teil1_2.pdf.

[17] *Energieleitungsausbaugesetz Vom 21. August 2009 (BGBl. I S. 2870), Das Zuletzt Durch Artikel 3 Des Gesetzes Vom 2. Juni 2021 (BGBl. 2024 I S. 1295, 1296) Geändert Worden Ist*.

[18] *Netzausbaubeschleunigungsgesetz Übertragungsnetz Vom 28. Juli 2011 (BGBl. I S. 1690), Das Zuletzt Durch Artikel 4 Des Gesetzes Vom 8. Oktober 2022 (BGBl. I S. 1726, 1734) Geändert Worden Ist*.

[19] ENTSO-E, "TYNDP 2022: High-Level Report", 2023. [Online]. Available: https://eepublicdownloads.blob.core.windows.net/public-cdn-container/tyndp-documents/TYNDP2022/public/high-level-report.pdf (visited on 2023-07-20).

[20] netztransparenz.de. "Redispatch-Maßnahmen". (), [Online]. Available: https://www.netztransparenz.de/EnWG/Redispatch (visited on 2023-07-21).

[21] ENTSO-E Subgroup System Protection and Dynamics, “Report on Special Protection Schemes”, Brussel, 2012. [Online]. Available: https://eepublicdownloads.entsoe.eu/clean-documents/pre2015/publications/entsoe/RG_SOC_CE/120425_RG_CE_TOP_06.5_D.2_SPS_report_1_.pdf.

[22] “InnoSys 2030 – Innovationen in der Systemführung bis 2030”. (), [Online]. Available: https://www.innosys2030.de/ (visited on 2022-11-28).

[23] A. Lukaschik, A. Waserrab, I. Sacar, M. Abel, S. Horn, and H. Askan, “Innovationen in der Systemführung bis 2030 : InnoSys 2030 : Abschlussbericht”, [Bayreuth], 2021.

[24] D. Westermann, S. Schlegel, F. Sass, R. Schwerdfeger, *et al.*, “Curative actions in the power system operation to 2030”, in *International ETG-Congress 2019; ETG Symposium*, 2019, pp. 1–6.

[25] A. Raab, T. Sennewald, P. Wiest, S. Schlegel, *et al.*, “Implementation of closed-loop Adaptive Power Control for VSC-HVDC in a Power System Control Center Demonstrator”, in *CIGRÉ 2022 Kyoto Symposium*, Kyoto, 2022.

[26] F. Sass, “Beitrag zur Systemsicherheit durch kurative Maßnahmen von HGÜ-Systemen”, 2018, ISBN: 978-3-86360-195-9.

[27] A. Raab, G. Mehlmann, M. Luther, T. Sennewald, S. Schlegel, and D. Westermann, “Steady-State and Dynamic Security Assessment for System Operation”, in *2021 International Conference on Smart Energy Systems and Technologies (SEST)*, 2021, pp. 1–6. DOI: 10.1109/SEST50973.2021.9543423.

[28] *Commission Regulation (EU) 2017/1485 of 2 August 2017 Establishing a Guideline on Electricity Transmission System Operation (Text with EEA Relevance.)*

[29] T. E. DyLiacco, “Control of Power Systems via the Multi-Level Concept”, Case Western Reserve University, Division of Engineering, 1968.

[30] A. Debs, “Security constrained optimization for power systems”, in *1975 IEEE Conference on Decision and Control Including the 14th Symposium on Adaptive Processes*, Houston, TX, USA: IEEE, 1975, pp. 303–308. DOI: 10.1109/CDC.1975.270697.

[31] *Commission Regulation (EU) 2015/1222 of 24 July 2015 Establishing a Guideline on Capacity Allocation and Congestion Management (Text with EEA Relevance).*

[32] *Regulation (EC) No 714/2009 of the European Parliament and of the Council of 13 July 2009 on Conditions for Access to the Network for Cross-Border Exchanges in Electricity and Repealing Regulation (EC) No 1228/2003 (Text with EEA Relevance).*

[33] VDE Verband der Elektrotechnik, Elektronik und Informationstechnik, *VDE-AR-N 4140: Kaskadierung von Maßnahmen für die Systemsicherheit von elektrischen Energieversorgungsnetzen*, VDE Verlag GmbH, Berlin, 2017. [Online]. Available: https://www.vde-verlag.de/normen/0100363/vde-ar-n-4140-anwendungsregel-2017-02.html.

[34] VDE Verband der Elektrotechnik, Elektronik und Informationstechnik, *VDE-AR-N 4142: Automatische Letztmaßnahmen zur Vermeidung von Systemzusammenbrüchen*, VDE Verlag GmbH, Berlin, 2020. [Online]. Available: https://www.vde-verlag.de/normen/0100567/vde-ar-n-4142-anwendungsregel-2020-04.html.

[35] UCTE, "Continental Operation Handbook: A3: Operational Security", 2009. [Online]. Available: https://www.ucte.org/_library/ohb/appendix1_v19.pdf (visited on 2022-02-14).

[36] D. Mende, "Modellierung von Maßnahmen der Leistungsflusssteuerung in einer nichtlinearen mathematischen Optimierung zur Anwendung im operativen Engpassmanagement elektrischer Energieversorgungssysteme", Ph.D. dissertation, Gottfried Wilhelm Leibniz Universität Hannover, Stuttgart, 2022, 248 pp. [Online]. Available: https://publica.fraunhofer.de/entities/publication/275b9c51-4487-41c4-ade2-f4d0d136b397 (visited on 2022-09-21).

[37] T. Dy-Liacco, "Enhancing power system security control", *IEEE Computer Applications in Power*, vol. 10, no. 3, pp. 38–41, 1997, ISSN: 1558-4151. DOI: 10.1109/67.595291.

[38] T. van Leeuwen, A.-K. Meinerzhagen, S. Rats, and A. Roedher, "Integration kurativer Maßnahmen in das Engpassmanagement im deutschen Übertragungsnetz", presented at the 16. Symposium Energieinnovation, Graz/Austria, 2020.

[39] T. Sennewald, F. Linke, F. Sass, and D. Westermann, "Curative Actions by embedded bipolar HVDC-interconnections", in *International ETG-Congress 2019; ETG Symposium*, 2019, pp. 1–6, ISBN: 978-3-8007-4954-6. [Online]. Available: https://ieeexplore.ieee.org/document/8836019.

[40] F. Sass, T. Sennewald, and D. Westermann, "Automated Corrective Actions by VSC-HVDC-Systems: A Novel Remedial Action Scheme", *IEEE Transactions on Power Systems*, vol. 35, no. 1, pp. 385–394, 2020, ISSN: 1558-0679. DOI: 10.1109/TPWRS.2019.2928887.

[41] K. Kollenda, A. Schrief, C. Biele, M. Lindner, *et al.*, "Curative measures identification in congestion management exploiting temporary admissible thermal loading of overhead lines", *IET Generation, Transmission & Distribution*, vol. 16, no. 16, pp. 3171–3183, 2022, ISSN: 1751-8695. DOI: 10.1049/gtd2.12512.

[42] 50Hertz Transmission GmbH, Amprion GmbH, TenneT TSO GmbH, and TransnetBW GmbH, "Deutsches Grenzwertkonzept - Regeln zur Ermittlung und Überwachung von Grenzwerten für die Systemführung des deutschen Übertragungsnetzes", 2021. [Online]. Available: https://www.netztransparenz.de/portals/1/%c3%9cNB-DeutschesGrenzwertkonzept_202111.pdf (visited on 2022-10-25).

[43] K. F. Schäfer, *Systemführung: Betrieb elektrischer Energieübertragungsnetze*. Wiesbaden [Heidelberg]: Springer Vieweg, 2022, 308 pp., ISBN: 978-3-658-36198-3.

[44] 50Hertz Transmission GmbH, Amprion GmbH, TenneT TSO GmbH, and TransnetBW GmbH, "Grundsätze für die Ausbauplanung des deutschen Übertragungsnetzes". [Online]. Available: https://www.50hertz.com/de/Netz/Netzausbau/LeitlinienderPlanung/Netzplanungsgrundsaetzedervierdeutschen Uebertragungsnetzbetreiber (visited on 2022-10-27).

[45] "iTesla: Innovative Tools for Electrical System Security within Large Areas". (), [Online]. Available: https://cordis.europa.eu/project/id/283012 (visited on 2022-10-28).

[46] S. Boeck, D. Van Hertem, K. Das, P. Sorensen, *et al.*, "Review of defence plans in europe: Current status, strengths and opportunities", *Cigré Science & Engineering Journal*, vol. 5, pp. 6–16, 2016.

[47] J. McCalley and W. Fu, "Reliability of special protection systems", *IEEE Transactions on Power Systems*, vol. 14, no. 4, pp. 1400–1406, 1999, ISSN: 1558-0679. DOI: 10.1109/59.801903.

[48] K. Kamps, F. Möhrke, K. F. Schäfer, M. Zdrallek, *et al.*, "Modelling and Risk Assessment of Special Protection Schemes in Transmission Systems", in *2020 International Conference on Probabilistic Methods Applied to Power Systems (PMAPS)*, 2020, pp. 1–6. DOI: 10.1109/PMAPS47429.2020.9183639.

[49] J. Mccalley, O. Olatujoye, V. Krishnan, R. Dai, C. Singh, and K. Jiang, *System Protection Schemes: Limitations, Risks, and Management*. 2010. DOI: 10.13140/RG.2.1.1946.3842.

[50] F. Ebe, "Kurative Ausführungsinstanz - vom Forschungsprojekt zur Implementierung", presented at the Symposium Netzleittechnik 2023 (Hamburg), 2023.

[51] M. Shahidehpour, F. Tinney, and Y. Fu, "Impact of Security on Power Systems Operation", *Proceedings of the IEEE*, vol. 93, no. 11, pp. 2013–2025, 2005, ISSN: 1558-2256. DOI: 10.1109/JPROC.2005.857490.

[52] M. Knittel, "Betriebliche Spannungshaltung im Übertragungsnetz unter Berücksichtigung von Unsicherheit", RWTH Aachen University, 2021, pages 1 Online–Ressource : Illustrationen, Diagramme, Karten. DOI: 10.18154/RWTH-2021-04688.

[53] R. Schwerdfeger, "Vertikaler Netzbetrieb: ein Ansatz zur Koordination von Netzbetriebsinstanzen verschiedener Netzebenen", Technische Universität Ilmenau, Ilmenau, 2017, 161 pp.

[54] C. Brosinsky, "On power system automation: A Digital Twin-centric framework for the next generation of Energy Management Systems", Ph.D. dissertation, Technische Universität Ilmenau, 2022. [Online]. Available: https://www.db-thueringen.de/receive/dbt_mods_00054812.

[55] 50Hertz Transmission GmbH, Amprion GmbH, TenneT TSO GmbH, TransnetBW GmbH, *et al.*, "Der InnoSys-Systemführungsprozess", 2022. [Online]. Available: https://www.innosys2030.de/wp-content/uploads/InnoSys_Systemfuehrungsprozess.pdf (visited on 2023-06-20).

[56] BDEW Bundesverband der Energie- und Wasserwirtschaft e.V., "Durchführung und Abrechnung von Redispatch-Maßnahmen", 2019, p. 22. [Online]. Available: https://www.bdew.de/media/documents/Stn_20190521_RD-Prozessdokument.pdf (visited on 2023-06-21).

[57] F. Reinke, "Status und Ausblick Engpassmanagement: Anmerkungen zur Novelle der §§13ff EnWG: "Redispatch mit Erneuerbaren Energien"", presented at the Strommarkttreffen, 2019. [Online]. Available: https://www.strommarkttreffen.org/2019-03-15_Reinke_Aktuelle_Entwicklungen_bei_RD_Einsman.pdf (visited on 2022-09-21).

[58] "TSCNET: Services", TSCNET. (), [Online]. Available: https://www.tscnet.eu/services/ (visited on 2023-10-22).

[59] ENTSO-E, "ENTSO-E SOC StG ReC – Working Group Monitoring and Reporting: Regional Coordination Assessment Annual Reporting (SOGL ART. 17)", 2022. [Online]. Available: https://eepublicdownloads.entsoe.eu/clean-documents/nc-tasks/220926_RCA_Annual_Reporting.pdf (visited on 2023-10-22).

[60] M. Wolfram, "Netzbetriebsverfahren zur Koordinierung von Phasenschiebertransformatoren und HGÜ-Verbindungen im Verbundnetz", Universitätsverlag Ilmenau, Ilmenau, 2019, 150 pp.

[61] UCTE, "Continental Operation Handbook: Policy 4:Coordinated Operational Planning", 2009. [Online]. Available: https://eepublicdownloads.entsoe.eu/clean-documents/Publications/SOC/Continental_Europe/oh/160302_TOP_6_Policy%204-Draft_V4_2.pdf (visited on 2023-10-20).

[62] Agency for the Cooperation of Energy Regulators, "ACER Decision on CSAM: Annex I: Methodology for coordinating operational security analysis", 2019. [Online]. Available: https://acer.europa.eu/Individual%20Decisions_annex/Annex%20I%20-%20ACER%20Decision%20on%20CSAM.pdf (visited on 2023-10-22).

[63] O. Scheufeld, M. Wolters, S. Krahl, D. Fraß, *et al.*, "Der Redispatch-Ermittlungs-Server (RES): Ein innovatives Werkzeug für die Betriebsplanung", in *International ETG-Congress 2019; ETG Symposium*, 2019.

[64] K. Schlarb. "Leuchtturmprojekt der deutschen Übertragungsnetzbetreiber", Soptim. (2018), [Online]. Available: https://www.soptim.de/leuchtturmprojekt-der-deutschen-uebertragungsnetzbetreiber/ (visited on 2022-11-04).

[65] Bundesnetzagentur für Elektrizität, Gas, Telekommunikation, Post und Eisenbahnen, "Gemeinsame Methode der Core-ÜNB für die regionale Koordination der Betriebssicherheit in Übereinstimmung mit Artikel 76 der Verordnung (EU) 2017/1485 der Kommission vom 2. August 2017". [Online]. Available: https://www.bundesnetzagentur.de/DE/Beschlusskammern/1_GZ/BK6-GZ/2019/BK6-19-585/BK6-19-585_Antrag_20200131.pdf?__blob=publicationFile&v=1 (visited on 2023-06-20).

[66] "Coordinating Remedial Actions In Core Region", TenneT. (), [Online]. Available: https://www.tennet.eu/news/coordinating-remedial-actions-core-region (visited on 2023-06-20).

[67] K. Van den Bergh, D. Couckuyt, E. Delarue, and W. D'haeseleer, "Redispatching in an interconnected electricity system with high renewables penetration", *Electric Power Systems Research*, vol. 127, pp. 64–72, 2015, ISSN: 03787796. DOI: 10.1016/j.epsr.2015.05.022.

[68] Bundesnetzagentur für Elektrizität, Gas, Telekommunikation, Post und Eisenbahnen, "Netzengpassmanagement Gesamtjahr 2022", 2023. [Online]. Available: https://www.bundesnetzagentur.de/SharedDocs/Downloads/DE/Sachgebiete/Energie/Unternehmen_Institutionen/Versorgungssicherheit/Engpassmanagement/Ganzjahreszahlen2022.pdf?__blob=publicationFile&v=3.

[69] H. Rissik, *Mercury-Arc Current Convertors: An Introduction to the Theory and Practice of Vapour-Arc Discharge Devices and to the Study of Rectification Phenomena*. Sir I. Pitman & sons, Limited, 1941.

[70] IEEE Global History Network. "Milestones:Nelson River HVDC Transmission System, 1972", ETHW. (2015), [Online]. Available: https://ethw.org/Milestones:Nelson_River_HVDC_Transmission_System,_1972 (visited on 2023-02-06).

[71] G. Asplund, "DC transmission based on voltage source converter", in *CIGRE SC14 Colloquium in South Africa, 1997*, 1997.

[72] A. Lesnicar and R. Marquardt, "An innovative modular multilevel converter topology suitable for a wide power range", in *2003 IEEE Bologna Power Tech Conference Proceedings,*, vol. 3, 2003, pp. 1–6. DOI: 10.1109/PTC.2003.1304403.

[73] N. R. Chaudhuri, B. Chaudhuri, R. Majumder, and A. Yazdani, *Multi-Terminal Direct-Current Grids: Modeling, Analysis, and Control*. Hoboken, New Jersey: IEEE / Wiley & Sons, Inc, 2014, 1 p., ISBN: 978-1-118-96053-0 978-1-118-72934-2.

[74] F. Schettler, B. Whitehouse, D. Westermann, *et al.*, "CENELEC workinggroup TC8x/WG06-system aspects of HVDC grids", *Ongoing*,

[75] Cigré Working Group 14.04, "Compendium of HVDC schemes throughout the world", Technical Brochures 003, 1987, pp. 100–103.

[76] C. Zhao, Q. Wang, and R. Yang, "Research on Demonstration Project of Zhangbei Flexible DC Grid", in *2020 10th International Conference on Power and Energy Systems (ICPES)*, 2020, pp. 77–82. DOI: 10.1109/ICPES51309.2020.9349696.

[77] A. Pizano-Martinez, C. R. Fuerte-Esquivel, H. Ambriz-Pérez, and E. Acha, "Modeling of VSC-Based HVDC Systems for a Newton-Raphson OPF Algorithm", *IEEE Transactions on Power Systems*, vol. 22, no. 4, pp. 1794–1803, 2007, ISSN: 0885-8950. DOI: 10.1109/TPWRS.2007.907535.

[78] R. Wiget and G. Andersson, "Optimal power flow for combined AC and multi-terminal HVDC grids based on VSC converters", in *IEEE Power and Energy Society General Meeting, 2012: 22 - 26 July 2012, San Diego, CA, USA*, Piscataway, NJ: IEEE, 2012, pp. 1–8, ISBN: 978-1-4673-2729-9. DOI: 10.1109/PESGM.2012.6345448.

[79] R. Wiget, "Combined AC and Multi-Terminal HVDC Grids – Optimal Power Flow Formulations and Dynamic Control", Zürich, ETH-Zürich, 2015. DOI: 10.3929/ethz-a-010546428.

[80] S. Chatzivasileiadis and G. Andersson, "Security constrained OPF incorporating corrective control of HVDC", in *Power Systems Computation Conference (PSCC), 2014: 18 - 22 Aug. 2014, Wrocław, Poland*, Piscataway, NJ: IEEE, 2014, pp. 1–8, ISBN: 978-83-935801-3-2. DOI: 10.1109/PSCC.2014.7038443.

[81] R. Wiget, E. Iggland, and G. Andersson, "Security constrained optimal power flow for HVAC and HVDC grids", in *Power Systems Computation Conference (PSCC), 2014: 18 - 22 Aug. 2014, Wrocław, Poland*, Piscataway, NJ: IEEE, 2014, pp. 1–7, ISBN: 978-83-935801-3-2. DOI: 10.1109/PSCC.2014.7038444.

[82] W. Huang, Z. Wei, G. Sun, Q. Li, and J. Liu, "A novel hybrid MTDC model for optimal power flow using interior-point method", in *2015 5th International Conference on Electric Utility Deregulation and Restructuring and Power Technologies (DRPT)*, pp. 2389–2394. DOI: 10.1109/DRPT.2015.7432646.

[83] H. Ergun, J. Dave, D. Van Hertem, and F. Geth, "Optimal Power Flow for AC–DC Grids: Formulation, Convex Relaxation, Linear Approximation, and Implementation", *IEEE Transactions on Power Systems*, vol. 34, no. 4, pp. 2980–2990, 2019, ISSN: 1558-0679. DOI: 10.1109/TPWRS.2019.2897835.

[84] F. Linke, F. Sass, and D. Westermann, "Preventive Parameterization of DC Voltage Control for N-1 Security of AC-HVDC-systems", in *2018 Power Systems Computation Conference (PSCC)*, IEEE, 2018, pp. 1–7, ISBN: 978-1-910963-10-4. DOI: 10.23919/PSCC.2018.8442868.

[85] J. Cao, W. Du, and H. F. Wang, "An Improved Corrective Security Constrained OPF for Meshed AC/DC Grids With Multi-Terminal VSC-HVDC", *IEEE Transactions on Power Systems*, vol. 31, no. 1, pp. 485–495, 2016, ISSN: 0885-8950. DOI: 10.1109/TPWRS.2015.2396523.

[86] N. Huebner, N. Schween, M. Suriyah, V. Heuveline, and T. Leibfried, "Multi-area Coordination of Security-Constrained Dynamic Optimal Power Flow in AC-DC Grids with Energy Storage", in *Advances in Energy System Optimization*, V. Bertsch, A. Ardone, M. Suriyah, W. Fichtner, T. Leibfried, and V. Heuveline, Eds., ser. Trends in Mathematics, Cham: Springer International Publishing, 2020, pp. 27–40, ISBN: 978-3-030-32157-4. DOI: 10.1007/978-3-030-32157-4_3.

[87] F. Linke, E. Glende, D. Westermann, and M. Wolter, "Multikriterielle Optimierung für Wirkleistungseinsatzkonzepte von vermaschten AC-HGÜ-Systemen", *at - Automatisierungstechnik*, vol. 67, no. 11, pp. 912–921, 2019, ISSN: 0178-2312. DOI: 10.1515/auto-2019-0074.

[88] A.-K. Marten and D. Westermann, "Local HVDC grid operation with multiple TSO coordination at a global optimum", in *IEEE International Energy Conference (ENERGYCON), 2014: 13 - 16 May 2014, Dubrovnik, Croatia*, I. Kuzle, Ed., Piscataway, NJ: IEEE, 2014, pp. 1549–1553, ISBN: 978-1-4799-2449-3. DOI: 10.1109/ENERGYCON.2014.6850629.

[89] A.-K. Marten, F. Sass, and D. Westermann, "Mixed AC/DC OPF using differential evolution for global minima identification", in *2015 IEEE Eindhoven PowerTech*, 2015, pp. 1–6. DOI: 10.1109/PTC.2015.7232830.

[90] N. Meyer-Huebner, M. Suriyah, and T. Leibfried, "Distributed Optimal Power Flow in Hybrid AC–DC Grids", *IEEE Transactions on Power Systems*, vol. 34, no. 4, pp. 2937–2946, 2019, ISSN: 1558-0679. DOI: 10.1109/TPWRS.2019.2892240.

[91] S.-S. Lee, Y. T. Yoon, S.-I. Moon, and J.-K. Park, "VSC-HVDC model-based power system optimal power flow algorithm and analysis", in *2013 IEEE Power & Energy Society General Meeting*, pp. 1–5. DOI: 10.1109/PESMG.2013.6672413.

[92] T. Sennewald, F. Sass, F. Linke, and D. Westermann, "Preventive coordination of active power set-points and DC voltage control for enhanced N-1 security in mixed AC-HVDC-systems", in *15th IET International Conference on AC and DC Power Transmission (ACDC 2019)*, 2019, pp. 1–7. DOI: 10.1049/cp.2019.0041.

[93] T. Sennewald, F. Linke, F. Sass, and D. Westermann, "Preventive and Corrective System Operation of Hybrid AC-HVDC-Systems", in *Cigré Symposium Aalborg, Denmark*, Cigré, Ed., 2019, pp. 1–10.

[94] R. Wiget, M. Vrakopoulou, and G. Andersson, "Probabilistic security constrained optimal power flow for a mixed HVAC and HVDC grid with stochastic infeed", in *Power Systems Computation Conference (PSCC), 2014: 18 - 22 Aug. 2014, Wrocław, Poland*, Piscataway, NJ: IEEE, 2014, pp. 1–7, ISBN: 978-83-935801-3-2. DOI: 10.1109/PSCC.2014.7038408.

[95] U. Kilic and K. Ayan, "Transient stability constrained optimal power flow solution of ac-dc systems using genetic algorithm", in *2013 3rd International Conference on Electric Power and Energy Conversion Systems (EPECS): 2-4 Oct. 2013, Yildiz Technical University,*

Davutpase Campus, Istanbul, Turkey, Piscataway, NJ: IEEE, 2013, pp. 1–6, ISBN: 978-1-4799-0688-8. DOI: 10.1109/EPECS.2013.6712996.

[96] R. F. Mochamad and R. Preece, "Impact of HVDC integration on the dynamic security of power systems", in *Mediterranean Conference on Power Generation, Transmission, Distribution and Energy Conversion (MedPower 2016)*, Institution of Engineering and Technology, 2016, pp. 977–977, ISBN: 978-1-78561-406-4. DOI: 10.1049/cp.2016.1086.

[97] E. Rakhshani, H. Mehrjerdi, N. A. Al-Emadi, and K. Rouzbehi, "On sizing the required energy of HVDC based inertia emulation for frequency control", in *2017 IEEE Power & Energy Society General Meeting*, Chicago, IL: IEEE, 2017, pp. 1–5, ISBN: 978-1-5386-2212-4. DOI: 10.1109/PESGM.2017.8274379.

[98] M. Aragüés-Peñalba, A. Egea-Àlvarez, O. Gomis-Bellmunt, and A. Sumper, "Optimum voltage control for loss minimization in HVDC multi-terminal transmission systems for large offshore wind farms", *Electric Power Systems Research*, vol. 89, pp. 54–63, 2012, ISSN: 0378-7796. DOI: 10.1016/j.epsr.2012.02.006.

[99] C. Barker and R. Whitehouse, "Autonomous converter control in a multi-terminal HVDC system", in *9th IET International Conference on AC and DC Power Transmission (ACDC 2010)*, London, UK: IET, 2010, O61–O61, ISBN: 978-1-84919-308-5. DOI: 10.1049/cp.2010.0988.

[100] T. M. Haileselassie and K. Uhlen, "Impact of DC Line Voltage Drops on Power Flow of MTDC Using Droop Control", *IEEE Transactions on Power Systems*, vol. 27, no. 3, pp. 1441–1449, 2012, ISSN: 1558-0679. DOI: 10.1109/TPWRS.2012.2186988.

[101] J. Beerten, D. Van Hertem, and R. Belmans, "VSC MTDC systems with a distributed DC voltage control - A power flow approach", in *2011 IEEE Trondheim PowerTech*, 2011, pp. 1–6. DOI: 10.1109/PTC.2011.6019434.

[102] Lie Xu, Liangzhong Yao, and M. Bazargan, "DC grid management of a multi-terminal HVDC transmission system for large offshore wind farms", in *2009 International Conference on Sustainable Power Generation and Supply*, Nanjing: IEEE, 2009, pp. 1–7, ISBN: 978-1-4244-4934-7. DOI: 10.1109/SUPERGEN.2009.5348101.

[103] T. K. Vrana, J. Beerten, R. Belmans, and O. B. Fosso, "A classification of DC node voltage control methods for HVDC grids", *Electric Power Systems Research*, vol. 103, pp. 137–144, 2013, ISSN: 0378-7796. DOI: 10.1016/j.epsr.2013.05.001.

[104] A.-K. Marten, F. Sass, and D. Westermann, "Continuous p-v-characteristic parameterization for multi-terminal HVDC systems", *IEEE Transactions on Power Delivery*, pp. 1–1, 2016, ISSN: 0885-8977. DOI: 10.1109/TPWRD.2016.2599821.

[105] B. Johnson, R. Lasseter, F. Alvarado, and R. Adapa, "Expandable multiterminal DC systems based on voltage droop", *IEEE Transactions on Power Delivery*, vol. 8, no. 4, pp. 1926–1932, 1993, ISSN: 1937-4208. DOI: 10.1109/61.248304.

[106] A. D. Del Rosso and S. W. Eckroad, "Energy Storage for Relief of Transmission Congestion", *IEEE Transactions on Smart Grid*, vol. 5, no. 2, pp. 1138–1146, 2014, ISSN: 1949-3061. DOI: 10.1109/TSG.2013.2277411.

[107] Consentec GmbH, "Netzstresstest", 2016. [Online]. Available: https://www.tennet.eu/fileadmin/user_upload/Our_Grid/Stakeholders_DE/netzstresstest/nst/Consentec_TenneT_Netzstresstest_Bericht_Langfassung_20161125.pdf.

[108] M. Lindner, D. Mende, A. Wasserrab, I. Saçar, *et al.*, "Corrective Congestion Management in Transmission Grids Using Fast-Responding Generation, Load and Storage", in *2021 IEEE Electrical Power and Energy Conference (EPEC)*, 2021, pp. 1–6. DOI: 10.1109/EPEC52095.2021.9621491.

[109] J. Porst, J. Richter, G. Mehlmann, and M. Luther, "Operation of Grid Boosters in Highly Loaded Transmission Grids", in *2022 IEEE International Conference on Power Systems Technology (POWERCON)*, 2022, pp. 1–6. DOI: 10.1109/POWERCON53406.2022.9929764.

[110] Bundesnetzagentur für Elektrizität, Gas, Telekommunikation, Post und Eisenbahnen, *Festlegungsverfahren zum bilanziellen Ausgleich von Redispatch-Maßnahmen: BK6-20-059*, 2020.

[111] Bundesnetzagentur für Elektrizität, Gas, Telekommunikation, Post und Eisenbahnen, *Festlegung zur Informationsbereitstellung für Redispatch-Maßnahmen: BK6-20-061*, 2021.

[112] Bundesnetzagentur für Elektrizität, Gas, Telekommunikation, Post und Eisenbahnen, *Mindestfaktor-Festlegung: Beschluss az. PGMF-8116-EnWG*, 2020.

[113] R. Fourer, D. M. Gay, and B. W. Kernighan, *AMPL: A Modeling Language for Mathematical Programming*, 2nd ed. Pacific Grove, CA: Thomson/Brooks/Cole, 2003, 517 pp., ISBN: 978-0-534-38809-6.

[114] F. Jarre and J. Stoer, *Optimierung: Einführung in mathematische Theorie und Methoden* (Masterclass), 2. Auflage. Berlin [Heidelberg]: Springer Spektrum, 2019, 519 pp., ISBN: 978-3-662-58854-3. DOI: 10.1007/978-3-662-58855-0.

[115] T. Van Acker and D. Van Hertem, "Modeling Preventive and Corrective Actions Using Linear Formulation", in *Dynamic Vulnerability Assessment and Intelligent Control for Sustainable Power Systems*. Chichester, UK: John Wiley & Sons, Ltd, 2018, pp. 177–192, ISBN: 978-1-119-21498-4 978-1-119-21495-3. DOI: 10.1002/9781119214984.ch8.

[116] J. Zhu, *Optimization of Power System Operation*. Wiley-Interscience, 2015, 664 pp., ISBN: 978-1-118-85415-0.

[117] G. B. Dantzig, "Linear Programming", *Operations Research*, vol. 50, no. 1, pp. 42–47, 2002, ISSN: 0030-364X. DOI: 10.1287/opre.50.1.42.17798.

[118] J. M. Ortega and W. C. Rheinboldt, *Iterative Solution of Nonlinear Equations in Several Variables* (Classics in Applied Mathematics 30). Philadelphia: Society for Industrial and Applied Mathematics, 2000, 572 pp., ISBN: 978-0-89871-461-6.

[119] J. L. W. V. Jensen, “Sur les fonctions convexes et les inégalités entre les valeurs moyennes”, *Acta Mathematica*, vol. 30, no. 0, pp. 175–193, 1906, ISSN: 0001-5962. DOI: 10.1007/BF02418571.

[120] O. Stein, *Grundzüge der nichtlinearen Optimierung* (Lehrbuch). Berlin [Heidelberg]: Springer Spektrum, 2018, 218 pp., ISBN: 978-3-662-55593-4 978-3-662-55592-7. DOI: 10.1007/978-3-662-55593-4.

[121] B. Lesieutre and I. Hiskens, “Convexity of the set of feasible injections and revenue adequacy in FTR markets”, *IEEE Transactions on Power Systems*, vol. 20, no. 4, pp. 1790–1798, 2005, ISSN: 1558-0679. DOI: 10.1109/TPWRS.2005.857268.

[122] J. Lavaei and S. H. Low, “Zero Duality Gap in Optimal Power Flow Problem”, *IEEE Transactions on Power Systems*, vol. 27, no. 1, pp. 92–107, 2012, ISSN: 1558-0679. DOI: 10.1109/TPWRS.2011.2160974.

[123] H. Hijazi, C. Coffrin, and P. V. Hentenryck, “Convex quadratic relaxations for mixed-integer nonlinear programs in power systems”, *Mathematical Programming Computation*, vol. 9, no. 3, pp. 321–367, 2017, ISSN: 1867-2949, 1867-2957. DOI: 10.1007/s12532-016-0112-z.

[124] M. R. AlRashidi and M. E. El-Hawary, “Hybrid Particle Swarm Optimization Approach for Solving the Discrete OPF Problem Considering the Valve Loading Effects”, *IEEE Transactions on Power Systems*, vol. 22, no. 4, pp. 2030–2038, 2007, ISSN: 1558-0679. DOI: 10.1109/TPWRS.2007.907375.

[125] M. Avriel and B. Golany, Eds., *Mathematical Programming for Industrial Engineers* (Industrial Engineering 20). New York: Marcel Dekker, 1996, 637 pp., ISBN: 978-0-8247-9620-4.

[126] H. Wei, H. Sasaki, J. Kubokawa, and R. Yokoyama, “An interior point nonlinear programming for optimal power flow problems with a novel data structure”, in *Proceedings of the 20th International Conference on Power Industry Computer Applications*, 1997, pp. 134–141. DOI: 10.1109/PICA.1997.599388.

[127] C. Coffrin and L. Roald. “Convex Relaxations in Power System Optimization: A Brief Introduction”. version 1. arXiv: 1807.07227 [math]. (2018), preprint.

[128] X. Bai, H. Wei, K. Fujisawa, and Y. Wang, “Semidefinite programming for optimal power flow problems”, *International Journal of Electrical Power & Energy Systems*, vol. 30, no. 6, pp. 383–392, 2008, ISSN: 0142-0615. DOI: 10.1016/j.ijepes.2007.12.003.

[129] R. Jabr, “Radial distribution load flow using conic programming”, *IEEE Transactions on Power Systems*, vol. 21, no. 3, pp. 1458–1459, 2006, ISSN: 1558-0679. DOI: 10.1109/TPWRS.2006.879234.

[130] M. Farivar, C. R. Clarke, S. H. Low, and K. M. Chandy, “Inverter VAR control for distribution systems with renewables”, in *2011 IEEE International Conference on Smart Grid Communications (SmartGridComm)*, 2011, pp. 457–462. DOI: 10.1109/SmartGridComm.2011.6102366.

[131] D. K. Molzahn and I. A. Hiskens, "Moment-based relaxation of the optimal power flow problem", in *2014 Power Systems Computation Conference*, 2014, pp. 1–7. DOI: 10.1109/PSCC.2014.7038397.

[132] D. K. Molzahn and I. A. Hiskens, "Sparsity-Exploiting Moment-Based Relaxations of the Optimal Power Flow Problem", *IEEE Transactions on Power Systems*, vol. 30, no. 6, pp. 3168–3180, 2015, ISSN: 1558-0679. DOI: 10.1109/TPWRS.2014.2372478.

[133] K. Miettinen, "Concepts", in *Nonlinear Multiobjective Optimization*, F. S. Hillier, red. Boston, MA: Springer US, 1998, vol. 12, pp. 5–36, ISBN: 978-1-4613-7544-9 978-1-4615-5563-6. DOI: 10.1007/978-1-4615-5563-6_1.

[134] T. Tušar and B. Filipič, "Visualization of Pareto Front Approximations in Evolutionary Multiobjective Optimization: A Critical Review and the Prosection Method", *IEEE Transactions on Evolutionary Computation*, vol. 19, no. 2, pp. 225–245, 2015, ISSN: 1941-0026. DOI: 10.1109/TEVC.2014.2313407.

[135] S. Kukkonen and J. Lampinen, "Ranking-Dominance and Many-Objective Optimization", in *2007 IEEE Congress on Evolutionary Computation*, 2007, pp. 3983–3990. DOI: 10.1109/CEC.2007.4424990.

[136] H. Ishibuchi, N. Tsukamoto, and Y. Nojima, "Evolutionary many-objective optimization: A short review", in *2008 IEEE Congress on Evolutionary Computation (IEEE World Congress on Computational Intelligence)*, 2008, pp. 2419–2426. DOI: 10.1109/CEC.2008.4631121.

[137] S. Yang, M. Li, X. Liu, and J. Zheng, "A Grid-Based Evolutionary Algorithm for Many-Objective Optimization", *IEEE Transactions on Evolutionary Computation*, vol. 17, no. 5, pp. 721–736, 2013, ISSN: 1941-0026. DOI: 10.1109/TEVC.2012.2227145.

[138] H. Von Stackelberg, *Marktform Und Gleichgewicht*. Springer, 1934.

[139] J. Bracken and J. T. McGill, "Mathematical Programs with Optimization Problems in the Constraints", *Operations Research*, vol. 21, no. 1, pp. 37–44, 1973, ISSN: 0030-364X. JSTOR: 169087. [Online]. Available: https://www.jstor.org/stable/169087 (visited on 2022-11-24).

[140] J. Bracken and J. T. McGill, "Defense applications of mathematical programs with optimization problems in the constraints", *Operations Research*, vol. 22, pp. 1086–1096, 1974.

[141] B. Colson, P. Marcotte, and G. Savard, "An overview of bilevel optimization", *Annals of Operations Research*, vol. 153, no. 1, pp. 235–256, 2007, ISSN: 0254-5330, 1572-9338. DOI: 10.1007/s10479-007-0176-2.

[142] C. D. Kolstad, "A review of the literature on bi-level mathematical programming", *Technical Report LA-10284-MS*, 1985.

[143] R. G. Jeroslow, "The polynomial hierarchy and a simple model for competitive analysis", *Mathematical Programming*, vol. 32, no. 2, pp. 146–164, 1985, ISSN: 1436-4646. DOI: 10.1007/BF01586088.

[144] X. Deng, “Complexity Issues in Bilevel Linear Programming”, in *Multilevel Optimization: Algorithms and Applications*, ser. Nonconvex Optimization and Its Applications, A. Migdalas, P. M. Pardalos, and P. Värbrand, Eds., Boston, MA: Springer US, 1998, pp. 149–164, ISBN: 978-1-4613-0307-7. DOI: 10.1007/978-1-4613-0307-7_6.

[145] A. Sinha, P. Malo, and K. Deb, “A Review on Bilevel Optimization: From Classical to Evolutionary Approaches and Applications”, *IEEE Transactions on Evolutionary Computation*, vol. 22, no. 2, pp. 276–295, 2018, ISSN: 1941-0026. DOI: 10.1109/TEVC.2017.2712906.

[146] R. Mathieu, L. Pittard, and G. Anandalingam, “Genetic algorithm based approach to bi-level linear programming”, *RAIRO - Operations Research*, vol. 28, no. 1, pp. 1–21, 1 1994, ISSN: 0399-0559, 1290-3868. DOI: 10.1051/ro/1994280100011.

[147] I. I. Dikin, “Iterative solution of problems of linear and quadratic programming”, *Soviet Mathematics. Doklady*, vol. 8, pp. 674–675, 1967, ISSN: 0197-6788.

[148] N. Karmarkar, “A new polynomial-time algorithm for linear programming”, in *Proceedings of the Sixteenth Annual ACM Symposium on Theory of Computing*, ser. STOC ’84, New York, NY, USA: Association for Computing Machinery, 1984, pp. 302–311, ISBN: 978-0-89791-133-7. DOI: 10.1145/800057.808695.

[149] K. G. Murty, *Linear Programming*. New York: Wiley, 1983, 482 pp., ISBN: 978-0-471-09725-9.

[150] D. C. Sorensen, “Newton’s Method with a Model Trust Region Modification”, *SIAM Journal on Numerical Analysis*, vol. 19, no. 2, pp. 409–426, 1982, ISSN: 0036-1429. DOI: 10.1137/0719026.

[151] A.-K. Marten, “Operation of meshed high voltage direct current (HVDC) overlay grids: From operational planning to real time operation”, Ilmenau, 2015.

[152] R. Mallipeddi and P. N. Suganthan, “Ensemble of Constraint Handling Techniques”, *IEEE Transactions on Evolutionary Computation*, vol. 14, no. 4, pp. 561–579, 2010, ISSN: 1941-0026. DOI: 10.1109/TEVC.2009.2033582.

[153] G. Coath and S. Halgamuge, “A comparison of constraint-handling methods for the application of particle swarm optimization to constrained nonlinear optimization problems”, in *The 2003 Congress on Evolutionary Computation, 2003. CEC ’03.*, vol. 4, 2003, 2419–2425 Vol.4. DOI: 10.1109/CEC.2003.1299391.

[154] T. Bäck, F. Hoffmeister, and H.-P. Schwefel, “A Survey of Evolution Strategies”, in *Proceedings of the Fourth International Conference on Genetic Algorithms*, Morgan Kaufmann, 1991, pp. 2–9.

[155] A. Homaifar, C. X. Qi, and S. H. Lai, “Constrained Optimization Via Genetic Algorithms”, *SIMULATION*, vol. 62, no. 4, pp. 242–253, 1994, ISSN: 0037-5497. DOI: 10.1177/003754979406200405.

[156] B. Tessema and G. Yen, "A Self Adaptive Penalty Function Based Algorithm for Constrained Optimization", in *2006 IEEE International Conference on Evolutionary Computation*, 2006, pp. 246–253. DOI: 10.1109/CEC.2006.1688315.

[157] Y. Xu, Z. Y. Dong, R. Zhang, K. P. Wong, and M. Lai, "Solving Preventive-Corrective SCOPF by a Hybrid Computational Strategy", *IEEE Transactions on Power Systems*, vol. 29, no. 3, pp. 1345–1355, 2014, ISSN: 0885-8950. DOI: 10.1109/TPWRS.2013.2293150.

[158] C.-H. Huang, Y.-M. Tsao, C.-C. Huang, J.-F. Lin, K.-C. Lin, and B.-L. Wu, "A preventive security-constrained optimal power flow with hybrid genetic-ant colony optimization", in *2010 International Symposium on Computer, Communication, Control and Automation (3CA)*, pp. 349–352. DOI: 10.1109/3CA.2010.5533460.

[159] A. Bhattacharya and P. K. Chattopadhyay, "Hybrid Differential Evolution With Biogeography-Based Optimization for Solution of Economic Load Dispatch", *IEEE Transactions on Power Systems*, vol. 25, no. 4, pp. 1955–1964, 2010, ISSN: 0885-8950. DOI: 10.1109/TPWRS.2010.2043270.

[160] T. O. Ting, M. Rao, and C. K. Loo, "A Novel Approach for Unit Commitment Problem via an Effective Hybrid Particle Swarm Optimization", *IEEE Transactions on Power Systems*, vol. 21, no. 1, pp. 411–418, 2006, ISSN: 0885-8950. DOI: 10.1109/TPWRS.2005.860907.

[161] D. Wolpert and W. Macready, "No free lunch theorems for optimization", *IEEE Transactions on Evolutionary Computation*, vol. 1, no. 1, pp. 67–82, 1997, ISSN: 1941-0026. DOI: 10.1109/4235.585893.

[162] K. T. Chaturvedi, M. Pandit, and L. Srivastava, "Self-Organizing Hierarchical Particle Swarm Optimization for Nonconvex Economic Dispatch", *IEEE Transactions on Power Systems*, vol. 23, no. 3, pp. 1079–1087, 2008, ISSN: 0885-8950. DOI: 10.1109/TPWRS.2008.926455.

[163] A. Glotic, A. Glotic, P. Kitak, J. Pihler, and I. Ticar, "Parallel Self-Adaptive Differential Evolution Algorithm for Solving Short-Term Hydro Scheduling Problem", *IEEE Transactions on Power Systems*, vol. 29, no. 5, pp. 2347–2358, 2014, ISSN: 0885-8950. DOI: 10.1109/TPWRS.2014.2302033.

[164] T. M. Haileselassie and K. Uhlen, "Primary frequency control of remote grids connected by multi-terminal HVDC", in *IEEE PES General Meeting*, 2010, pp. 1–6. DOI: 10.1109/PES.2010.5589327.

[165] A. K. Qin, K. Tang, H. Pan, and S. Xia, "Self-adaptive differential evolution with local search chains for real-parameter single-objective optimization", in *IEEE Congress on Evolutionary Computation (CEC), 2014: 6 - 11 July 2014, Beijing, China ; [Part of the 2014 IEEE World Congress on Computational Intelligence (IEEE WCCI 2014)]*, Piscataway, NJ: IEEE, 2014, pp. 467–474, ISBN: 978-1-4799-1488-3. DOI: 10.1109/CEC.2014.6900636.

[166] D. E. C. Vargas, A. C. C. Lemonge, H. J. C. Barbosa, and H. S. Bernardino, "Differential evolution with the adaptive penalty method for structural multi-objective optimization", *Optimization and Engineering*, vol. 20, no. 1, pp. 65–88, 2019, ISSN: 1573-2924. DOI: 10.1007/s11081-018-9395-4.

[167] R. H. Kerr, J. L. Scheidt, A. J. Fontanna, and J. K. Wiley, "Unit Commitment", *IEEE Transactions on Power Apparatus and Systems*, vol. PAS-85, no. 5, pp. 417–421, 1966, ISSN: 0018-9510. DOI: 10.1109/TPAS.1966.291678.

[168] A. Bhardwaj, V. K. Kamboj, V. K. Shukla, B. Singh, and P. Khurana, "Unit commitment in electrical power system-a literature review", in *2012 IEEE International Power Engineering and Optimization Conference Melaka, Malaysia*, 2012, pp. 275–280. DOI: 10.1109/PEOCO.2012.6230874.

[169] J. A. Muckstadt and S. A. Koenig, "An Application of Lagrangian Relaxation to Scheduling in Power-Generation Systems", *Operations Research*, vol. 25, no. 3, pp. 387–403, 1977, ISSN: 0030-364X, 1526-5463. DOI: 10.1287/opre.25.3.387.

[170] S. Takriti, J. Birge, and E. Long, "A stochastic model for the unit commitment problem", *IEEE Transactions on Power Systems*, vol. 11, no. 3, pp. 1497–1508, 1996, ISSN: 1558-0679. DOI: 10.1109/59.535691.

[171] N. Padhy, "Unit commitment-a bibliographical survey", *IEEE Transactions on Power Systems*, vol. 19, no. 2, pp. 1196–1205, 2004, ISSN: 1558-0679. DOI: 10.1109/TPWRS.2003.821611.

[172] C. Richter and G. Sheble, "A profit-based unit commitment GA for the competitive environment", *IEEE Transactions on Power Systems*, vol. 15, no. 2, pp. 715–721, 2000, ISSN: 1558-0679. DOI: 10.1109/59.867164.

[173] A. J. Wood, B. F. Wollenberg, and G. B. Sheblé, *Power Generation, Operation, and Control*, Third edition. Hoboken, New Jersey: Wiley-IEEE, 2013, 1 p., ISBN: 978-1-118-73391-2 978-1-118-73384-4 978-1-118-73386-8.

[174] B. Chowdhury and S. Rahman, "A review of recent advances in economic dispatch", *IEEE Transactions on Power Systems*, vol. 5, no. 4, pp. 1248–1259, 1990, ISSN: 1558-0679. DOI: 10.1109/59.99376.

[175] H. Happ, "Optimal power dispatch - A comprehensive survey", *IEEE Transactions on Power Apparatus and Systems*, vol. 96, no. 3, pp. 841–854, 1977, ISSN: 0018-9510. DOI: 10.1109/T-PAS.1977.32397.

[176] G. R. Davison, "Dividing load between units", *Electrical World*, vol. 80, no. 26, pp. 1385–1387, 1922.

[177] A. Wilston, "Dividing Load Economically among Power Plant", *A.I.E.E. Journal*, 1928.

[178] H. Happ, J. Aldrich, P. Chan, M. El-Hawary, *et al.*, "Description and Bibliography of Major Economy-Security Functions Part II-Bibliography (1959 - 1972)", *IEEE Transactions on Power Apparatus and Systems*, vol. PAS-100, no. 1, pp. 215–223, 1981, ISSN: 0018-9510. DOI: 10.1109/TPAS.1981.316791.

[179] "Description and Bibliography of Major Economy-Security Functions Part III-Bibliography (1973 - 1979)", *IEEE Transactions on Power Apparatus and Systems*, vol. PAS-100, no. 1, pp. 224–235, 1981, ISSN: 0018-9510. DOI: 10.1109/TPAS.1981.316792.

[180] L. S. Vargas, V. H. Quintana, and A. Vannelli, "A tutorial description of an interior point method and its applications to security-constrained economic dispatch", *IEEE Transactions on Power Systems*, vol. 8, no. 3, pp. 1315–1324, 1993, ISSN: 0885-8950. DOI: 10.1109/59.260862.

[181] X. Yan and V. H. Quintana, "An efficient predictor-corrector interior point algorithm for security-constrained economic dispatch", *IEEE Transactions on Power Systems*, vol. 12, no. 2, pp. 803–810, 1997, ISSN: 0885-8950. DOI: 10.1109/59.589693.

[182] J. Carpentier, "Contribution a l'etude du dispatching economique", *Bulletin de la Societe Francaise des Electriciens*, vol. 3, no. 1, pp. 431–447, 1962.

[183] H. Dommel and W. Tinney, "Optimal Power Flow Solutions", *IEEE Transactions on Power Apparatus and Systems*, vol. PAS-87, no. 10, pp. 1866–1876, 1968, ISSN: 0018-9510. DOI: 10.1109/TPAS.1968.292150.

[184] S. Frank, I. Steponavice, and S. Rebennack, "Optimal power flow: A bibliographic survey I", *Energy Systems*, vol. 3, no. 3, pp. 221–258, 2012, ISSN: 1868-3967. DOI: 10.1007/s12667-012-0056-y.

[185] M. B. Cain, R. P. O' Neill, and A. Castillo, "History of optimal power flow and Models", 2012, pp. 1–36. [Online]. Available: https://www.ferc.gov/sites/default/files/2020-04/acopf-1-history-formulation-testing.pdf.

[186] J. Momoh, M. El-Hawary, and R. Adapa, "A review of selected optimal power flow literature to 1993. II. Newton, linear programming and interior point methods", *IEEE Transactions on Power Systems*, vol. 14, no. 1, pp. 105–111, 1999, ISSN: 1558-0679. DOI: 10.1109/59.744495.

[187] J. Momoh, R. Adapa, and M. El-Hawary, "A review of selected optimal power flow literature to 1993. I. Nonlinear and quadratic programming approaches", *IEEE Transactions on Power Systems*, vol. 14, no. 1, pp. 96–104, 1999, ISSN: 1558-0679. DOI: 10.1109/59.744492.

[188] B. Stott, O. Alsac, and A. J. Monticelli, "Security analysis and optimization", *Proceedings of the IEEE*, vol. 75, no. 12, pp. 1623–1644, 1987, ISSN: 00189219. DOI: 10.1109/PROC.1987.13931.

[189] A. Monticelli, M. V. F. Pereira, and S. Granville, "Security-Constrained Optimal Power Flow with Post-Contingency Corrective Rescheduling", *IEEE Transactions on Power Systems*, vol. 2, no. 1, pp. 175–180, 1987, ISSN: 0885-8950. DOI: 10.1109/TPWRS.1987.4335095.

[190] F. Capitanescu, J. L. Martinez Ramos, P. Panciatici, D. Kirschen, *et al.*, "State-of-the-art, challenges, and future trends in security constrained optimal power flow", *Electric Power Systems Research*, vol. 81, no. 8, pp. 1731–1741, 2011, ISSN: 0378-7796. DOI: 10.1016/j.epsr.2011.04.003.

[191] O. Alsac and B. Stott, "Optimal Load Flow with Steady-State Security", *IEEE Transactions on Power Apparatus and Systems*, vol. PAS-93, no. 3, pp. 745–751, 1974, ISSN: 0018-9510. DOI: 10.1109/TPAS.1974.293972.

[192] A. Hoffrichter, K. Kollenda, M. Schneider, and R. Puffer, "Simulation of Curative Congestion Management in Large-Scale Transmission Grids", in *2019 54th International Universities Power Engineering Conference (UPEC)*, 2019, pp. 1–6. DOI: 10.1109/UPEC.2019.8893627.

[193] M. Lindner, J. Peper, N. Offermann, C. Biele, *et al.*, "Operation strategies of battery energy storage systems for preventive and curative congestion management in transmission grids", *IET Generation, Transmission & Distribution*, vol. n/a, no. n/a, 2022, ISSN: 1751-8695. DOI: 10.1049/gtd2.12739.

[194] T. J. Kolster, "Reliable Flexibility Provision from Distribution Systems to Enable Higher Grid Utilization by Curative Operation", Ph.D. dissertation, Technische Universität Darmstadt, Darmstadt, 2022, 218 pp. [Online]. Available: http://tuprints.ulb.tu-darmstadt.de/21887.

[195] *Commission Regulation (EU) 2016/1447 of 26 August 2016 Establishing a Network Code on Requirements for Grid Connection of High Voltage Direct Current Systems and Direct Current-Connected Power Park Modules*.

[196] *Directive (EU) 2019/944 of the European Parliament and of the Council of 5 June 2019 on Common Rules for the Internal Market for Electricity and Amending Directive 2012/27/EU (Recast) (Text with EEA Relevance.)*

[197] R. D. Zimmerman, C. E. Murillo-Sanchez, and R. J. Thomas, "MATPOWER: Steady-State Operations, Planning, and Analysis Tools for Power Systems Research and Education", *IEEE Transactions on Power Systems*, vol. 26, no. 1, pp. 12–19, 2011, ISSN: 0885-8950. DOI: 10.1109/TPWRS.2010.2051168.

[198] M. Aragues-Penalba, J. Beerten, J. Rimez, D. Van Hertem, and O. Gomis-Bellmunt, "Optimal power flow tool for hybrid AC/DC systems", in *11th IET International Conference on AC and DC Power Transmission*, 2015, pp. 1–7. DOI: 10.1049/cp.2015.0077.

[199] A.-K. Marten and D. Westermann, "Schedule for converters of a meshed HVDC grid and a contingency schedule for adaption to unscheduled power flow changes", in *2013 IEEE Power Energy Society General Meeting*, 2013, pp. 1–5. DOI: 10.1109/PESMG.2013.6672303.

[200] J. Rimez and R. Belmans, "A combined AC/DC optimal power flow algorithm for meshed AC and DC networks linked by VSC converters", *International Transactions on Electrical Energy Systems*, vol. 25, no. 10, pp. 2024–2035, 2015, ISSN: 2050-7038. DOI: 10.1002/etep.1943.

[201] N. Hübner, "Cost-Optimal Operational Security in Transmission Grids with Embedded HVDC Systems and Energy Storage", Ph.D. dissertation, Karlsruher Institut für Technologie (KIT), 2019. DOI: 10.5445/IR/1000098845.

[202] F. Linke, T. Sennewald, and D. Westermann, "Derivation-free Steady State Power Flow Calculation Approach for HVDC Systems with Distributed DC Voltage Control and Arbitrary p-v-Characteristics", in *2020 IEEE Power Energy Society General Meeting (PESGM)*, 2020, pp. 1–5. DOI: 10.1109/PESGM41954.2020.9281821.

[203] B. Stott, J. Jardim, and O. Alsac, "DC Power Flow Revisited", *IEEE Transactions on Power Systems*, vol. 24, no. 3, pp. 1290–1300, 2009, ISSN: 1558-0679. DOI: 10.1109/TPWRS.2009.2021235.

[204] A. Kaushal, H. Ergun, and D. V. Hertem, "Frequency restoration reserves procurement with HVDC systems", in *The 17th International Conference on AC and DC Power Transmission (ACDC 2021)*, vol. 2021, 2021, pp. 155–160. DOI: 10.1049/icp.2021.2461.

[205] TenneT TSO GmbH, "SuedOstLink: Sichere Stromversorgung für Bayern". [Online]. Available: https://www.tennet.eu/fileadmin/user_upload/Our_Grid/Onshore_Germany/SuedOstLink/TenneT_im_Dialog/Mediathek/SuedOstLink_Brosch%C3%BCre_Projekt_01.pdf (visited on 2022-06-22).

[206] VDE Verband der Elektrotechnik, Elektronik und Informationstechnik, *VDE-AR-N 4131: Technical requirements for grid connection of high voltage direct current systems and direct current-connected power park modules (TAR HVDC)*, VDE Verlag GmbH, Berlin, 2019.

[207] S. Schlegel, "Wahrung der Netzsicherheit durch Nutzung flexibler Lasten am Beispiel des gesteuerten Ladens von Elektrofahrzeugen", Universitätsverlag Ilmenau; Universitätsbibliothek, Ilmenau, 2016, 135 pp., ISBN: 9783863601287. [Online]. Available: http://www.db-thueringen.de/servlets/DocumentServlet?id=26954.

[208] R. Storn and K. Price, "Differential evolution–a simple and efficient heuristic for global optimization over continuous spaces", *Journal of global optimization*, vol. 11, no. 4, pp. 341–359, 1997, ISSN: 0925-5001.

[209] K. Weicker, *Evolutionäre Algorithmen* (Leitfäden Der Informatik), 1. Aufl. Stuttgart: Teubner, 2002, 260 pp., ISBN: 3-519-00362-7.

[210] A. K. Qin, V. L. Huang, and P. N. Suganthan, "Differential Evolution Algorithm With Strategy Adaptation for Global Numerical Optimization", *IEEE Transactions on Evolutionary Computation*, vol. 13, no. 2, pp. 398–417, 2009, ISSN: 1941-0026. DOI: 10.1109/TEVC.2008.927706.

[211] F. Sass, T. Sennewald, A.-K. Marten, and D. Westermann, "Mixed AC high-voltage direct current benchmark test system for security constrained optimal power flow calculation", *IET Generation, Transmission & Distribution*, vol. 11, no. 2, pp. 447–455, 2017, ISSN: 1751-8695. DOI: 10.1049/iet-gtd.2016.0993.

[212] EWI, "Merit Order Tool - Dokumentation", Energiewirtschaftliches Institut an der Universität zu Köln gGmbH (EWI), 2022. [Online]. Available: https://www.ewi.uni-koeln.de/cms/wp-content/uploads/2022/01/Dokumentation_EWI_Merit_Order_Tool_v2022.pdf (visited on 2023-02-09).

[213] C. Kost, S. Shammugam, V. Fluri, D. Peper, A. D. Memar, and T. Schlegl, "Studie: Stromgestehungskosten Erneuerbare Energien", Fraunhofer-Institut für Solare Energiesysteme ISE, 2021. [Online]. Available: https://www.ise.fraunhofer.de/content/dam/ise/de/documents/publications/studies/DE2021_ISE_Studie_Stromgestehungskosten_Erneuerbare_Energien.pdf (visited on 2023-02-09).

[214] P. Icha, T. Lauf, and G. Kuhs, "Entwicklung der spezifischen Treibhausgas-Emissionen des deutschen Strommix in den Jahren 1990 - 2021", Umweltbundesamt. [Online]. Available: https://www.umweltbundesamt.de/sites/default/files/medien/1410/publikationen/2022-04-13_cc_15-2022_strommix_2022_fin_bf.pdf (visited on 2023-02-09).

[215] "EU Carbon Price Tracker", Ember. (), [Online]. Available: https://ember-climate.org/data/data-tools/carbon-price-viewer/ (visited on 2023-02-10).

[216] Bundeskartelamt, "Sektoruntersuchung Stromerzeugung und -großhandel", 2011. [Online]. Available: https://www.bundeskartellamt.de/SharedDocs/Publikation/DE/Sektoruntersuchungen/Sektoruntersuchung%20Stromerzeugung%20Stromgrosshandel%20-%20Abschlussbericht.pdf?__blob=publicationFile&v=3.

[217] BDEW Bundesverband der Energie- und Wasserwirtschaft e.V. "Standardlastprofile Strom". (), [Online]. Available: https://www.bdew.de/energie/standardlastprofile-strom/ (visited on 2023-08-01).

[218] The MathWorks Inc., *MATLAB version: 9.13.0 (R2022b)*, Natick, Massachusetts, United States: The MathWorks Inc., 2022. [Online]. Available: https://www.mathworks.com.

[219] F. Capitanescu, M. Glavic, D. Ernst, and L. Wehenkel, "Contingency Filtering Techniques for Preventive Security-Constrained Optimal Power Flow", *IEEE Transactions on Power Systems*, vol. 22, no. 4, pp. 1690–1697, 2007, ISSN: 0885-8950. DOI: 10.1109/TPWRS.2007.907528.

[220] G. C. Ejebe, H. P. van Meeteren, and B. F. Wollenberg, "Fast contingency screening and evaluation for voltage security analysis", *IEEE Transactions on Power Systems*, vol. 3, no. 4, pp. 1582–1590, 1988, ISSN: 0885-8950. DOI: 10.1109/59.192968.

[221] T. Runarsson and X. Yao, "Stochastic ranking for constrained evolutionary optimization", *IEEE Transactions on Evolutionary Computation*, vol. 4, no. 3, pp. 284–294, 2000, ISSN: 1941-0026. DOI: 10.1109/4235.873238.

[222] J. F. Benders, "Partitioning procedures for solving mixed-variables programming problems", *Numerische Mathematik*, vol. 4, no. 1, pp. 238–252, 1962, ISSN: 0029-599X. DOI: 10.1007/BF01386316.

[223] UCTE, "Continental Operation Handbook: Policy 3: Operational Security", 2009. [Online]. Available: https://www.ucte.org/_library/ohb/Policy3_v13.pdf (visited on 2022-02-14).

[224] F. Kiessling, *Overhead Power Lines: Planning, Design, Construction*. Berlin: Springer, 2010, ISBN: 978-3-642-05556-0.

[225] Cigré Working Group B4.57, Ed., *Guide for the Development of Models for HVDC Converters in a HVDC Grid* (604 Technical Brochures). Paris: CIGRÉ, 2014, 222 pp., ISBN: 978-2-85873-305-7.

A Appendix

A.1 Publications by the Author

Parts of the scientific results of this work, which are presented coherently in this thesis, have been published previously in international publications. For reasons of transparency and scientific integrity, these are listed below in cronological order.

A.2 Simulation Results

A.2.1 Comparison of Unresovled Contingencies

Tab. A.1 summarizes the number of critical contingencies after the optimization $N_{\text{cc,opt}}$ for all study cases and scenarios. Additionally, the number of preventive feasible contingencies cases $N_{\text{cc,prev}}$ as well as the curative feasible ones $N_{\text{cc,cur}}$ are given.

Table A.1: Results of optimization with the priority on preventive actions

	Case	HL/HW	HL/LW	LL/HW	LL/LW
$N_{\text{cc,opt}}$	Study case 1a	4	0	13	1
	Study case 1b	4	0	12	0
	Study case 2a	3	1	14	2
	Study case 2b	3	4	10	0
$N_{\text{feas,prev}}$	Study case 1a	119	123	107	121
	Study case 1b	118	123	105	120
	Study case 2a	120	121	108	120
	Study case 2b	118	111	55	119
$N_{\text{feas,cur}}$	Study case 1a	0	0	3	1
	Study case 1b	1	0	6	3
	Study case 2a	0	1	1	1
	Study case 2b	2	8	58	4

A.2.2 Critical Contingencies per Study Case

Bases on the presentation of the constraint violations and critical contingencies in Section 4.2, the following tables detail the critical contingencies for each study case. Thereby, a checkmark (✓) indicates the outage for each scenario that results in any kind of constraint violation.

Table A.2: Critical contingencies for study case 1a - subsequent approach

	HL/HW	HL/LW	LL/HW	LL/LW		HL/HW	HL/LW	LL/HW	LL/LW
AC line 8	–	–	✓	–	VSC 6	–	–	✓	–
AC line 48	✓	–	–	–	VSC 10	–	–	✓	–
AC line 49	–	–	✓	–	VSC 12	–	–	✓	–
AC line 94	–	–	✓	–	VSC 14	–	–	✓	✓
AC line 100	–	–	✓	–	VSC 16	–	–	✓	–
VSC 4	–	–	✓	–					

Table A.3: Critical contingencies for study case 1b - BLP-SCOPF with equal weigthing

	HL/HW	HL/LW	LL/HW	LL/LW		HL/HW	HL/LW	LL/HW	LL/LW
AC line 5	–	–	✓	–	AC line 95	–	–	✓	–
AC line 6	–	–	✓	–	AC line 100	–	–	✓	–
AC line 29	✓	–	–	–	DC line 3	–	–	✓	–
AC line 44	–	–	✓	–	VSC 4	–	–	✓	–
AC line 48	✓	–	–	–	VSC 6	–	–	✓	–
AC line 49	–	–	✓	–	VSC 10	–	–	✓	–
AC line 58	✓	–	–	–	VSC 14	–	–	✓	✓
AC line 80	–	–	✓	–	VSC 16	✓	–	✓	–

Table A.4: Critical contingencies for study case 2a - BLP-SCOPF with focus on preventive actions

	HL/HW	HL/LW	LL/HW	LL/LW		HL/HW	HL/LW	LL/HW	LL/LW
AC line 29	✓	–	–	–	AC line 86	–	–	✓	✓
AC line 33	✓	–	–	–	AC line 94	–	–	✓	✓
AC line 35	–	–	✓	–	AC line 95	–	–	✓	–
AC line 38	–	–	✓	–	AC line 100	–	–	✓	–
AC line 49	–	–	✓	–	VSC 4	–	–	✓	–
AC line 58	✓	✓	–	–	VSC 8	–	–	✓	–
AC line 80	–	–	✓	–	VSC 10	–	–	✓	–
AC line 81	–	–	✓	–	VSC 14	–	–	✓	–
AC line 84	–	–	✓	–					

Table A.5: Critical contingencies for study case 2a - BLP-SCOPF with focus on curative actions

	HL/HW	HL/LW	LL/HW	LL/LW		HL/HW	HL/LW	LL/HW	LL/LW
AC line 5	–	–	✓	–	AC line 84	–	–	✓	–
AC line 6	–	–	✓	–	AC line 86	–	–	✓	–
AC line 29	✓	–	–	–	AC line 94	–	–	✓	–
AC line 41	–	–	✓	–	AC line 100	–	–	✓	–
AC line 48	–	✓	–	–	DC line 18	–	✓	–	–
AC line 49	–	–	✓	–	VSC 14	–	–	✓	–
AC line 58	✓	✓	–	–	VSC 16	✓	✓	–	–
AC line 80	–	–	✓	–					

A.2.3 Summary of AC Line Loadings

For the comparison of the effect of the optimized preventive and curative set-points on the distribution of the loading of AC transmission lines, the data of the box plots shown in Section 4.2 are summarized in the following. Thereby, each table shows the data of the mean and median values as well as the intervall of the interquartile range and whiskers for each scenario, both for the (N-0) and (N-1) state of the respective system. Both the quartile and whisker intervals are given in the form of [lower value, upper value].

Table A.6: Statistical summary of the AC line loading data for the base case of the scenarios

	Median	Quartiles	Whiskers
HL/HW	26.60	[11.41, 43.11]	[3.69, 84.19]
HL/LW	22.82	[13.48, 42.25]	[3.17, 94.10]
LL/HW	22.09	[14.58, 35.00]	[5.72, 80.55]
LL/LW	20.57	[13.98, 35.84]	[4.91, 88.63]

Table A.7: Statistical summary of the AC line loading data for study case 1a

	Median	Quartiles	Whiskers
HL/HW	25.33	[14.28, 42.14]	[3.55, 81.08]
HL/LW	22.67	[15.83, 35.64]	[4.58, 70.06]
LL/HW	21.22	[14.32, 32.06]	[5.31, 78.45]
LL/LW	19.83	[13.85, 27.79]	[4.06, 59.37]

Table A.8: Statistical summary of the AC line loading data for study case 1b

	Median	Quartiles	Whiskers
HL/HW	25.96	[13.81, 42.59]	[3.03, 81.26]
HL/LW	23.35	[16.15, 36.27]	[4.73, 68.72]
LL/HW	21.58	[13.94, 34.19]	[4.91, 83.18]
LL/LW	18.54	[13.01, 25.20]	[7.21, 52.10]

Table A.9: Statistical summary of the AC line loading data for study case 2a

	Median	Quartiles	Whiskers
HL/HW	24.94	[15.45, 43.06]	[3.98, 70.88]
HL/LW	23.67	[15.72, 38.57]	[2.50, 73.16]
LL/HW	22.90	[14.48, 33.84]	[6.48, 78.71]
LL/LW	20.24	[13.34, 29.12]	[3.61, 69.74]

Table A.10: Statistical summary of the AC line loading data for study case 2b

	Median	Quartiles	Whiskers
HL/HW	26.72	[15.16, 43.84]	[3.88, 81.41]
HL/LW	24.63	[15.43, 38.33]	[9.15, 92.49]
LL/HW	24.28	[15.22, 35.45]	[5.64, 83.10]
LL/LW	21.02	[14.19, 32.27]	[5.20, 67.34]

A.3 Parameters

A.3.1 Differential Evolution Algorithm

In the following, the parameterization of the differential evolution (DE) algorithm is detailed. The presentation is split in two tables. First, Tab. A.11 shows the general parameters needed for the DE algorithm (cf. Appendix 3.2.1). Subsequently, the weighting factors for the objective funtions and constraints are given in Tab. A.12 and Tab. A.13 respectively. The former is differentiated between the optimization models to show the differences between the models.

Table A.11: Parameters of the DE algorithm

Parameter	Value
NP	100
F	0.75
CR	0.95
$it_{\min}$	25
ε	1e−3

Table A.12: Weighting factors for objective functions and constraints

Objective function	Study 1a	Study 1b	Study 2a	Study 2b
$N_{\text{cc,prev}}$	100		1,000	10
$N_{\text{cc,cur}}$	100		10	1,000
$C_{\text{redispatch}}$		1e−7		
$\lvert\Delta \boldsymbol{p}_{\text{VSC}}\rvert$		1e−5		

Table A.13: Weighting factors for objective functions and constraints

Constraint	Weighting factor
AC system P equilibrium	9
AC system Q equilibrium	3
DC system P equilibrium	5
VSC S limit	1
VSC P limit	2
VSC Q limit	5
VSC k_{droop} limit	5
Generator P limit	3
Generator Q limit	3
Grid booster P limit	3
Grid booster Q limit	3

continued on next page

Table A.13: *continued from previous page*

Constraint	Weighting factor
AC system voltage range	5
DC system voltage range	5
AC line PATL	5
DC line PATL	3

A.3.2 Test System

A.3.2.1 Topology

AC System

In the following, the parameters of the AC system are given. First, the bus data is presented in Tab. A.14 where the voltage range, control area and bus type is declared for each bus. For the bus types, the following naming convention is used: **SL**, **PQ** and **PV** for slack, load and voltage-control busses respectively.

Table A.14: Bus data of the AC system

No.	bus type	CA	v_{max} in pu	v_{min} in pu	No.	bus type	CA	v_{max} in pu	v_{min} in pu
1	SL	1	1.1	0.9	35	PQ	2	1.1	0.9
2	PQ	1	1.1	0.9	36	PV	2	1.1	0.9
3	PQ	1	1.1	0.9	37	PQ	2	1.1	0.9
4	PV	1	1.1	0.9	38	PQ	2	1.1	0.9
5	PQ	1	1.1	0.9	39	PQ	2	1.1	0.9
6	PQ	1	1.1	0.9	40	PQ	2	1.1	0.9
7	PQ	1	1.1	0.9	41	PV	2	1.1	0.9
8	PQ	1	1.1	0.9	42	PQ	2	1.1	0.9
9	PQ	1	1.1	0.9	43	PV	2	1.1	0.9
10	PV	1	1.1	0.9	44	PQ	2	1.1	0.9
11	PQ	1	1.1	0.9	45	PQ	2	1.1	0.9

continued on next page

Table A.14: *continued from previous page*

No.	bus type	CA	v_{max} in pu	v_{min} in pu	No.	bus type	CA	v_{max} in pu	v_{min} in pu
12	PQ	1	1.1	0.9	46	PQ	2	1.1	0.9
13	PV	1	1.1	0.9	47	PQ	2	1.1	0.9
14	PQ	1	1.1	0.9	48	PQ	2	1.1	0.9
15	PQ	1	1.1	0.9	49	PQ	2	1.1	0.9
16	PQ	1	1.1	0.9	50	PV	2	1.1	0.9
17	PQ	1	1.1	0.9	51	PQ	2	1.1	0.9
18	PV	1	1.1	0.9	52	PQ	3	1.1	0.9
19	PQ	1	1.1	0.9	53	PQ	3	1.1	0.9
20	PQ	1	1.1	0.9	54	PQ	3	1.1	0.9
21	PQ	1	1.1	0.9	55	PQ	3	1.1	0.9
22	PQ	1	1.1	0.9	56	PV	3	1.1	0.9
23	PQ	1	1.1	0.9	57	PQ	3	1.1	0.9
24	PQ	1	1.1	0.9	58	PQ	3	1.1	0.9
25	PV	1	1.1	0.9	59	PV	3	1.1	0.9
26	PQ	2	1.1	0.9	60	PQ	3	1.1	0.9
27	PQ	2	1.1	0.9	61	PQ	3	1.1	0.9
28	PQ	2	1.1	0.9	62	PQ	3	1.1	0.9
29	PV	2	1.1	0.9	63	PV	3	1.1	0.9
30	PQ	2	1.1	0.9	64	PV	3	1.1	0.9
31	PQ	2	1.1	0.9	65	PQ	3	1.1	0.9
32	PQ	2	1.1	0.9	66	PV	3	1.1	0.9
33	PV	2	1.1	0.9	67	ISO	4	1.1	0.9
34	PQ	2	1.1	0.9					

The transmission branches are modelled as 400 kV overhead transmission lines (OHTLs). Tab. A.15 shows the parameters that are chosen following the definitions of [211, 224]. Subsequently, Tab. A.16 gives information regarding the line connections and lengths of each branch.

Table A.15: Parameters of the AC lines, following [211, 224]

R' in Ω/km	X' in Ω/km	C' in nF/km	I_n in A	P_{PATL} in MW
0.03	0.26	13.5	3,500	1,000

Table A.16: Branch data of the AC system

No.	from	to	l in km	No.	from	to	l in km	No.	from	to	l in km
1	1	5	57	36	20	21	144	71	41	42	44
2	1	7	96	37	21	22	75	72	42	43	127
3	1	8	98	38	21	23	109	73	42	49	95
4	1	14	94	39	21	25	64	74	43	44	74
5	2	3	130	40	22	25	124	75	43	49	61
6	2	9	43	41	22	56	139	76	44	45	89
7	2	12	71	42	24	49	116	77	44	48	142
8	3	4	120	43	24	49	116	78	45	46	74
9	3	10	111	44	25	43	330	79	45	50	80
10	3	12	105	45	26	27	72	80	47	48	66
11	3	9	96	46	26	30	110	81	46	48	54
12	4	14	68	47	26	31	122	82	47	50	112
13	4	19	102	48	26	40	149	83	47	51	87
14	5	6	43	49	27	28	58	84	47	59	295
15	5	7	115	50	27	31	174	85	52	53	70
16	5	8	82	51	28	35	151	86	52	54	77
17	6	7	148	52	28	37	58	87	52	64	98
18	7	15	62	53	29	35	169	88	54	65	137
19	7	16	113	54	29	39	86	89	54	66	243
20	8	9	88	55	29	44	40	90	55	57	140
21	10	11	76	56	30	31	76	91	55	63	127
22	10	22	126	57	30	32	43	92	56	58	152

continued on next page

Table A.16: *continued from previous page*

No.	from	to	l in km	No.	from	to	l in km	No.	from	to	l in km
23	11	12	84	58	32	40	93	93	56	59	144
24	11	13	130	59	33	34	68	94	57	58	192
25	12	13	76	60	33	35	100	95	57	63	144
26	13	53	195	61	33	51	86	96	58	60	92
27	14	15	97	62	34	51	66	97	58	61	246
28	14	18	141	63	35	36	50	98	59	60	105
29	16	17	48	64	35	47	154	99	61	62	152
30	16	18	135	65	36	37	149	100	62	63	137
31	17	24	61	66	36	38	76	101	62	66	116
32	18	20	116	67	37	38	196	102	65	66	164
33	18	24	95	68	39	40	119	103	65	64	100
34	19	20	61	69	39	43	124	104	52	58	251
35	19	23	99	70	40	41	51				

Following the described changes on the generation landscape introduced in Section 4.1.1, Tab. A.17 presents the machine data for all conventional generating units. The data comprises the grid connection points, fuel type and power ratings. Subsequently, Tab. A.18 shows the data of the installed grid booster units.

Table A.17: Machine data of the test system

No.	AC bus	fuel type	v_m in pu	P_{max} in MW	P_{min} in MW	Q_{max} in Mvar	Q_{min} in Mvar	S_{rated} in MVA
1	1	Natural gas	1	560	180	250	-250	610
2	1	Natural gas	1	560	180	250	-250	610
3	4	Hard coal	1	630	225	350	-350	720
4	10	Natural gas	1	560	180	250	-250	610
5	13	Hard coal	1	630	225	350	-350	720
6	18	Lignite	1	850	360	250	-250	980

continued on next page

Table A.17: *continued from previous page*

No.	AC bus	fuel type	v_m in pu	P_{max} in MW	P_{min} in MW	Q_{max} in Mvar	Q_{min} in Mvar	S_{rated} in MVA
7	25	Pumped-storage	1	720	270	450	-450	850
8	29	Pumped-storage	1	720	270	450	-450	850
9	33	Pumped-storage	1	720	270	450	-450	850
10	36	Natural gas	1	560	180	250	-250	610
11	41	Natural gas	1	850	180	500	-500	980
12	43	Natural gas	1	560	180	500	-250	610
13	50	Pumped-storage	1	720	270	450	-450	850
14	56	Lignite	1	850	360	500	-500	980
15	59	Natural gas	1	560	180	250	-250	610
16	63	Lignite	1	850	360	500	-500	980
17	64	Natural gas	1	560	180	250	-250	610
18	66	Lignite	1	850	360	500	-500	980

Table A.18: Data of grid booster units in the test system

No.	AC bus	P_{max} in MW	P_{min} in MW	Q_{max} in Mvar	Q_{min} in Mvar	S_{rated} in MVA
1	16	250	-250	250	-250	350
2	24	250	-250	250	-250	350
3	42	250	-250	250	-250	350
4	49	250	-250	250	-250	350

DC System

Tab. A.19 shows the bus data of the embedded HVDC system. In contrast to the system proposed in [211], a bipolar HVDC system is used. Correspondingly, modifications were done. For once, the voltage was reduced from 500kV to ±250kV to keep the voltage difference the same compared to the monopolar system. Bus types are differentiated in three different types, indicated by the subscripts **0**, **+** and **-** for nodes on the neutral, positive and negative pole respectively.

Table A.19: Bus data of the DC system

No.	bus type	v_{max} in pu	v_{min} in pu	No.	bus type	v_{max} in pu	v_{min} in pu	No.	bus type	v_{max} in pu	v_{min} in pu
1	SL_0	1.05	-1.05	10	PQ_0	1.05	-1.05	19	PQ_0	1.05	-1.05
2	SL_+	1.05	0.95	11	PQ_+	1.05	0.95	20	PQ_+	1.05	0.95
3	SL_-	-0.95	-1.05	12	PQ_-	-0.95	-1.05	21	PQ_-	-0.95	-1.05
4	PQ_0	1.05	-1.05	13	PQ_0	1.05	-1.05	22	PQ_0	1.05	-1.05
5	PQ_+	1.05	0.95	14	PQ_+	1.05	0.95	23	PQ_+	1.05	0.95
6	PQ_-	-0.95	-1.05	15	PQ_-	-0.95	-1.05	24	PQ_-	-0.95	-1.05
7	PQ_0	1.05	-1.05	16	PQ_0	1.05	-1.05	25	PQ_0	1.05	-1.05
8	PQ_+	1.05	0.95	17	PQ_+	1.05	0.95	26	PQ_+	1.05	0.95
9	PQ_-	-0.95	-1.05	18	PQ_-	-0.95	-1.05	27	PQ_-	-0.95	-1.05

Following the change of the voltage level, the branch type is changed accordingly. The bipolar system uses ±200kV OHTL for branches with data according to [225] and given in Tab. A.20. Subsequently, the connectivity information follows in Tab. A.21.

Table A.20: Branch parameters of the DC system

R' in Ω/km	X' in Ω/km	C' in nF/km	I_n in A	P_{PATL} in MW
0.0133	0.26	13.9	3,000	750

Table A.21: Connectivity information of the DC branches

No.	from	to	l in km	Type	No.	from	to	l in km	Type
1	1	4	391	DMR	19	22	13	219	DMR
2	2	5	391	pos. pole	20	23	14	219	pos. pole
3	3	6	391	neg. pole	21	24	15	219	neg. pole
4	7	10	426	DMR	22	10	16	384	DMR
5	8	11	426	pos. pole	23	11	17	384	pos. pole

continued on next page

Table A.21: *continued from previous page*

No.	from	to	l in km	Type	No.	from	to	l in km	Type
6	9	12	426	neg. pole	24	12	18	384	neg. pole
7	10	13	346	DMR	25	4	10	394	DMR
8	11	14	346	pos. pole	26	5	11	394	pos. pole
9	12	15	346	neg. pole	27	6	12	394	neg. pole
10	16	19	125	DMR	28	13	19	613	DMR
11	17	20	125	pos. pole	29	14	20	613	pos. pole
12	18	21	125	neg. pole	30	15	21	613	neg. pole
13	1	7	190	DMR	31	7	25	276	DMR
14	2	8	190	pos. pole	32	8	26	276	pos. pole
15	3	9	190	neg. pole	33	9	27	276	neg. pole
16	4	22	209	DMR					
17	5	23	209	pos. pole					
18	6	24	209	neg. pole					

Lastly, Tab. A.22 shows the data of the VSCs, encompassing the power limits and grid connection point.

Table A.22: VSC data of the test system

Name	AC bus	P_{max} in MW	P_{min} in MW	Q_{max} in Mvar	Q_{min} in Mvar	S_{max} in MVA	S_{min} in MVA
VSC1_p	7	1,000	−1,000	1,000	−1,000	1,000	−1,000
VSC1_n	7	1,000	−1,000	1,000	−1,000	1,000	−1,000
VSC2_p	40	1,000	−1,000	1,000	−1,000	1,000	−1,000
VSC2_n	40	1,000	−1,000	1,000	−1,000	1,000	−1,000
VSC3_p	3	1,000	−1,000	1,000	−1,000	1,000	−1,000
VSC3_n	3	1,000	−1,000	1,000	−1,000	1,000	−1,000
VSC4_p	23	1,000	−1,000	1,000	−1,000	1,000	−1,000
VSC4_n	23	1,000	−1,000	1,000	−1,000	1,000	−1,000

continued on next page

Table A.22: *continued from previous page*

Name	AC bus	P_{max} in MW	P_{min} in MW	Q_{max} in Mvar	Q_{min} in Mvar	S_{max} in MVA	S_{min} in MVA
VSC5_p	48	1,000	−1,000	1,000	−1,000	1,000	−1,000
VSC5_n	48	1,000	−1,000	1,000	−1,000	1,000	−1,000
VSC6_p	54	1,000	−1,000	1,000	−1,000	1,000	−1,000
VSC6_n	54	1,000	−1,000	1,000	−1,000	1,000	−1,000
VSC7_p	57	1,000	−1,000	1,000	−1,000	1,000	−1,000
VSC7_n	57	1,000	−1,000	1,000	−1,000	1,000	−1,000
VSC8_p	27	1,000	−1,000	1,000	−1,000	1,000	−1,000
VSC8_n	27	1,000	−1,000	1,000	−1,000	1,000	−1,000
VSC9_p	67	750	-750	1,000	−1,000	1,000	−1,000
VSC9_n	67	750	-750	1,000	−1,000	1,000	−1,000

A.3.2.2 Scenarios

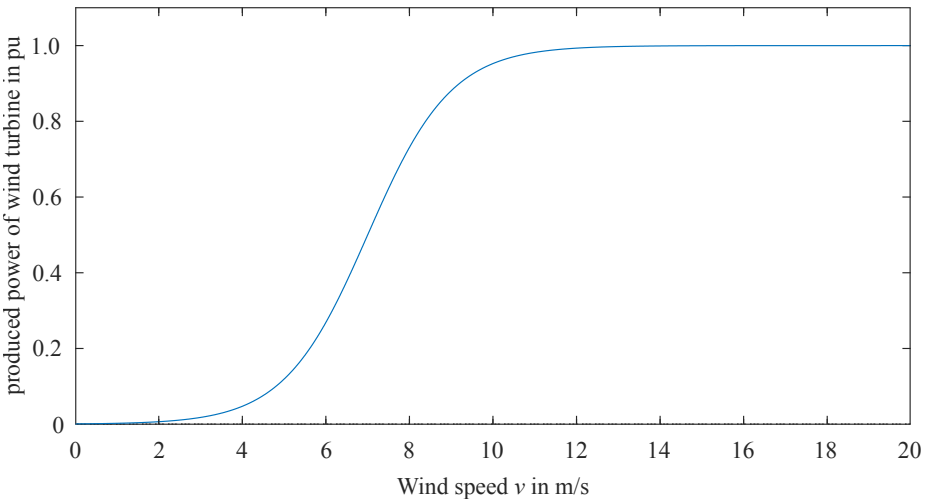

Figure A.1: Power curve of a wind turbine

The data shows positive active power as generation and negative power as demand. For the reactive power, negative reactive power indicates inductive reactive power whereas capacitive reactive power is shown with a positive sign.

Scenario 1 – High Load/High Wind

Table A.23: Generation and load data for scenario 1 (HL/HW)

Bus no.	v in pu	φ in °	P_{load} in MW	Q_{load} in Mvar	P_{gen} in MW	Q_{gen} in Mvar	P_{VSC} in MW	Q_{VSC} in Mvar
1	1.0000	0.00	0	0	995	-360	0	0
2	1.0182	2.79	1,650	100	0	0	0	0
3	1.0000	-2.25	0	0	0	0	-600	-270
4	1.0000	-4.26	0	0	480	-126	0	0
5	1.0121	0.67	1,320	100	0	0	0	0
6	1.0067	-1.20	-191	-76	0	0	0	0
7	0.9998	-5.15	0	0	0	0	-854	-76
8	1.0069	-0.39	-287	-74	0	0	0	0
9	1.0098	0.46	-186	-74	0	0	0	0
10	1.0000	-3.03	0	0	403	-182	0	0
11	1.0023	-2.84	-271	-55	0	0	0	0
12	1.0053	-1.13	-171	-87	0	0	0	0
13	1.0000	-1.83	0	0	492	-206	0	0
14	1.0006	-4.68	-199	-60	0	0	0	0
15	0.9994	-5.36	-113	-53	0	0	0	0
16	0.9982	-10.51	-38	-7	0	0	0	0
17	0.9930	-13.17	-275	-106	0	0	0	0
18	1.0000	-8.84	0	0	641	-179	0	0
19	1.0000	-9.93	-165	-46	0	0	0	0
20	1.0018	-10.25	-178	-83	0	0	0	0
21	1.0070	-10.34	0	0	0	0	0	0
22	1.0076	-9.02	-30	-7	0	0	0	0
23	1.0000	-13.33	0	0	0	0	-660	-15
24	0.9983	-15.03	-32	-7	0	0	0	0
25	1.0000	-9.66	0	0	463	-286	0	0
26	0.9864	-35.12	-395	-89	0	0	0	0

continued on next page

Table A.23: *continued from previous page*

Bus no.	v in pu	φ in °	P_{load} in MW	Q_{load} in Mvar	P_{gen} in MW	Q_{gen} in Mvar	P_{VSC} in MW	Q_{VSC} in Mvar
27	1.0000	-33.37	0	0	0	0	1,100	101
28	0.9909	-36.17	-665	-99	0	0	0	0
29	1.0000	-26.87	0	0	484	-54	0	0
30	0.9726	-36.54	-366	-100	0	0	0	0
31	0.9750	-38.46	-845	-119	0	0	0	0
32	0.9718	-34.48	-335	-137	0	0	0	0
33	1.0000	-32.08	0	0	481	72	0	0
34	0.9848	-34.08	-540	-158	0	0	0	0
35	1.0000	-32.77	-460	-97	0	0	0	0
36	1.0000	-33.04	0	0	455	-110	0	0
37	0.9884	-36.66	-451	-190	0	0	0	0
38	1.0030	-34.86	-150	0	0	0	0	0
39	0.9968	-27.52	-529	-87	0	0	0	0
40	1.0000	-27.23	0	0	0	0	1,100	87
41	1.0000	-25.70	0	0	242	60	0	0
42	0.9917	-25.32	-709	-180	0	0	0	0
43	1.0000	-22.58	0	0	488	-101	0	0
44	0.9961	-26.96	-474	-92	0	0	0	0
45	0.9893	-29.21	-668	-109	0	0	0	0
46	0.9882	-29.03	-614	-95	0	0	0	0
47	1.0042	-28.12	-81	50	0	0	0	0
48	1.0000	-25.81	0	0	0	0	1,100	-78
49	0.9994	-20.31	0	0	0	0	0	0
50	1.0000	-26.40	0	0	539	-56	0	0
51	0.9902	-32.71	-430	-123	0	0	0	0
52	1.0015	-13.86	-309	-102	0	0	0	0
53	1.0008	-11.21	-100	-30	0	0	0	0
54	1.0001	-13.90	0	0	0	0	60	-171

continued on next page

Table A.23: *continued from previous page*

Bus no.	v in pu	φ in °	P_{load} in MW	Q_{load} in Mvar	P_{gen} in MW	Q_{gen} in Mvar	P_{VSC} in MW	Q_{VSC} in Mvar
55	0.9929	-24.05	-303	-110	0	0	0	0
56	1.0000	-11.82	0	0	515	-227	0	0
57	1.0001	-24.16	0	0	0	0	-600	-56
58	1.0067	-18.43	-324	-157	0	0	0	0
59	1.0000	-15.49	0	0	399	-200	0	0
60	1.0042	-17.60	-115	-42	0	0	0	0
61	1.0091	-20.67	-187	-75	0	0	0	0
62	1.0013	-19.35	-319	-95	0	0	0	0
63	1.0000	-20.37	0	0	509	-149	0	0
64	1.0000	-12.84	0	0	310	-107	0	0
65	0.9999	-14.73	-315	-97	0	0	0	0
66	1.0000	-13.95	0	0	543	-223	0	0
67	1.0000	0.00	880	0	0	0	-880	0

Scenario 2 – High Load/Low Wind

Table A.24: Generation and load data for scenario 2 (HL/LW)

Bus no.	v in pu	φ in °	P_{load} in MW	Q_{load} in Mvar	P_{gen} in MW	Q_{gen} in Mvar	P_{VSC} in MW	Q_{VSC} in Mvar
1	1.0000	0.00	0	0	997	-355	0	0
2	1.0159	2.45	900	100	0	0	0	0
3	1.0000	-0.11	0	0	0	0	-330	-305
4	1.0000	-2.02	0	0	536	-150	0	0
5	1.0103	-0.38	720	100	0	0	0	0
6	1.0058	-1.82	-191	-76	0	0	0	0
7	1.0000	-4.23	0	0	0	0	-396	-112
8	1.0058	-0.69	-287	-74	0	0	0	0

continued on next page

Table A.24: *continued from previous page*

Bus no.	v in pu	φ in °	P_{load} in MW	Q_{load} in Mvar	P_{gen} in MW	Q_{gen} in Mvar	P_{VSC} in MW	Q_{VSC} in Mvar
9	1.0087	0.70	-186	-74	0	0	0	0
10	1.0000	0.50	0	0	468	-203	0	0
11	1.0024	0.35	-271	-55	0	0	0	0
12	1.0053	1.07	-171	-87	0	0	0	0
13	1.0000	2.29	0	0	539	-259	0	0
14	1.0008	-3.53	-199	-60	0	0	0	0
15	0.9995	-4.35	-113	-53	0	0	0	0
16	0.9936	-10.44	-38	-7	0	0	0	0
17	0.9862	-13.76	-275	-106	0	0	0	0
18	1.0000	-8.03	0	0	730	-86	0	0
19	1.0012	-6.51	-165	-46	0	0	0	0
20	1.0024	-7.33	-178	-83	0	0	0	0
21	1.0073	-5.97	0	0	0	0	0	0
22	1.0083	-4.13	-30	-7	0	0	0	0
23	1.0000	-7.98	0	0	0	0	-360	-72
24	0.9902	-16.44	-32	-7	0	0	0	0
25	1.0000	-5.67	0	0	594	-224	0	0
26	0.9852	-45.56	-395	-89	0	0	0	0
27	1.0000	-44.71	0	0	0	0	600	166
28	0.9898	-45.74	-665	-99	0	0	0	0
29	1.0000	-32.72	0	0	599	-33	0	0
30	0.9709	-46.63	-366	-100	0	0	0	0
31	0.9740	-48.93	-845	-119	0	0	0	0
32	0.9699	-44.21	-335	-137	0	0	0	0
33	1.0000	-37.81	0	0	598	104	0	0
34	0.9836	-39.77	-540	-158	0	0	0	0
35	0.9978	-39.73	-460	-97	0	0	0	0
36	1.0000	-40.56	0	0	481	-65	0	0

continued on next page

Table A.24: *continued from previous page*

Bus no.	v in pu	φ in °	P_{load} in MW	Q_{load} in Mvar	P_{gen} in MW	Q_{gen} in Mvar	P_{VSC} in MW	Q_{VSC} in Mvar
37	0.9871	-45.46	-451	-190	0	0	0	0
38	1.0023	-42.74	-150	0	0	0	0	0
39	0.9955	-33.93	-529	-87	0	0	0	0
40	1.0000	-36.20	0	0	0	0	600	221
41	1.0000	-32.43	0	0	429	108	0	0
42	0.9887	-30.85	-709	-180	0	0	0	0
43	1.0000	-27.14	0	0	489	117	0	0
44	0.9956	-32.71	-474	-92	0	0	0	0
45	0.9889	-35.22	-668	-109	0	0	0	0
46	0.9883	-35.77	-614	-95	0	0	0	0
47	0.9980	-33.58	-81	50	0	0	0	0
48	1.0000	-33.07	0	0	0	0	600	26
49	0.9927	-23.89	0	0	0	0	0	0
50	1.0000	-31.87	0	0	613	-24	0	0
51	0.9877	-38.36	-430	-123	0	0	0	0
52	1.0036	-2.35	-309	-102	0	0	0	0
53	1.0061	-1.64	-100	-30	0	0	0	0
54	1.0000	-1.38	0	0	0	0	30	-183
55	0.9927	-7.03	-303	-110	0	0	0	0
56	1.0000	-3.47	0	0	699	-276	0	0
57	1.0000	-7.33	0	0	0	0	-330	-111
58	1.0096	-7.25	-324	-157	0	0	0	0
59	1.0000	-8.75	0	0	467	-59	0	0
60	1.0060	-8.48	-115	-42	0	0	0	0
61	1.0100	-6.96	-187	-75	0	0	0	0
62	1.0015	-4.06	-319	-95	0	0	0	0
63	1.0000	-3.18	0	0	698	-168	0	0
64	1.0000	0.21	0	0	445	-131	0	0

continued on next page

Table A.24: *continued from previous page*

Bus no.	v in pu	φ in °	P_{load} in MW	Q_{load} in Mvar	P_{gen} in MW	Q_{gen} in Mvar	P_{VSC} in MW	Q_{VSC} in Mvar
65	0.9998	-1.37	-315	-97	0	0	0	0
66	1.0000	0.92	0	0	706	-241	0	0
67	1.0000	0.00	480	0	0	0	-480	0

Scenario 3 – Low Load/High Wind

Table A.25: Generation and load data for scenario 3 (LL/HW)

Bus no.	v in pu	φ in °	P_{load} in MW	Q_{load} in Mvar	P_{gen} in MW	Q_{gen} in Mvar	P_{VSC} in MW	Q_{VSC} in Mvar
1	1.0000	0.00	0	0	995	-573	0	0
2	1.0311	-1.05	1,650	100	0	0	0	0
3	1.0003	-6.43	0	0	0	0	-600	-848
4	1.0202	-7.77	0	0	0	0	0	0
5	1.0163	0.96	1,320	100	0	0	0	0
6	1.0133	-0.47	-76	-30	0	0	0	0
7	0.9998	-4.39	0	0	0	0	-854	-464
8	1.0149	-0.78	-115	-30	0	0	0	0
9	1.0206	-2.36	-74	-30	0	0	0	0
10	1.0401	-9.39	0	0	0	0	0	0
11	1.0393	-8.45	-108	-22	0	0	0	0
12	1.0301	-6.20	-68	-35	0	0	0	0
13	1.0392	-8.96	0	0	0	0	0	0
14	1.0193	-5.63	-80	-24	0	0	0	0
15	1.0091	-5.05	-45	-21	0	0	0	0
16	1.0381	-7.94	-15	-3	0	0	0	0
17	1.0442	-8.89	-110	-42	0	0	0	0
18	1.0475	-9.01	0	0	0	0	0	0

continued on next page

Table A.25: *continued from previous page*

Bus no.	v in pu	φ in °	P_{load} in MW	Q_{load} in Mvar	P_{gen} in MW	Q_{gen} in Mvar	P_{VSC} in MW	Q_{VSC} in Mvar
19	1.0258	-11.98	-66	-18	0	0	0	0
20	1.0416	-11.81	-71	-33	0	0	0	0
21	1.0563	-13.89	0	0	0	0	0	0
22	1.0690	-13.91	-12	-3	0	0	0	0
23	1.0001	-15.76	0	0	0	0	-660	-455
24	1.0536	-9.51	-13	-3	0	0	0	0
25	1.0711	-13.65	0	0	0	0	0	0
26	1.0052	-8.73	-158	-36	0	0	0	0
27	0.9985	-7.20	0	0	0	0	1,100	-578
28	1.0270	-11.16	-266	-40	0	0	0	0
29	1.0457	-11.84	0	0	0	0	0	0
30	1.0035	-9.58	-146	-40	0	0	0	0
31	1.0051	-10.00	-338	-48	0	0	0	0
32	1.0006	-9.07	-134	-55	0	0	0	0
33	1.0593	-14.74	0	0	0	0	0	0
34	1.0546	-15.42	-216	-63	0	0	0	0
35	1.0580	-13.49	-184	-39	0	0	0	0
36	1.0621	-13.39	0	0	0	0	0	0
37	1.0444	-12.66	-180	-76	0	0	0	0
38	1.0653	-13.51	-60	0	0	0	0	0
39	1.0364	-10.84	-212	-35	0	0	0	0
40	0.9988	-6.81	0	0	0	0	1,100	-708
41	1.0183	-8.63	0	0	0	0	0	0
42	1.0335	-10.13	-284	-72	0	0	0	0
43	1.0534	-11.04	0	0	0	0	0	0
44	1.0404	-11.86	-190	-37	0	0	0	0
45	1.0306	-12.78	-267	-44	0	0	0	0
46	1.0107	-11.63	-246	-38	0	0	0	0

continued on next page

Table A.25: *continued from previous page*

Bus no.	v in pu	φ in °	P_{load} in MW	Q_{load} in Mvar	P_{gen} in MW	Q_{gen} in Mvar	P_{VSC} in MW	Q_{VSC} in Mvar
47	1.0456	-13.04	-32	20	0	0	0	0
48	0.9989	-9.54	0	0	0	0	1,100	-935
49	1.0538	-10.26	0	0	0	0	0	0
50	1.0420	-12.92	0	0	0	0	0	0
51	1.0540	-14.89	-172	-49	0	0	0	0
52	1.0218	-19.01	-124	-41	0	0	0	0
53	1.0297	-16.55	-40	-12	0	0	0	0
54	1.0004	-19.91	0	0	0	0	60	-531
55	1.0252	-30.65	-121	-44	0	0	0	0
56	1.0921	-18.64	0	0	0	0	0	0
57	1.0010	-30.59	0	0	0	0	-600	-579
58	1.0776	-22.98	-130	-63	0	0	0	0
59	1.0989	-19.14	0	0	0	0	0	0
60	1.0911	-21.37	-46	-17	0	0	0	0
61	1.0846	-25.85	-75	-30	0	0	0	0
62	1.0625	-26.55	-128	-38	0	0	0	0
63	1.0399	-29.30	0	0	0	0	0	0
64	1.0000	-18.49	0	0	278	-343	0	0
65	1.0183	-20.79	-126	-39	0	0	0	0
66	1.0492	-23.41	0	0	0	0	0	0
67	1.0000	0.00	880	0	0	0	-880	0

Scenario 4 – Low Load/Low Wind

Table A.26: Generation and load data for scenario 4 (LL/LW)

Bus no.	v in pu	φ in °	P_{load} in MW	Q_{load} in Mvar	P_{gen} in MW	Q_{gen} in Mvar	P_{VSC} in MW	Q_{VSC} in Mvar
1	1.0000	0.00	0	0	1,037	-442	0	0
2	1.0221	-5.03	900	100	0	0	0	0
3	0.9982	-8.16	0	0	0	0	-260	-539
4	1.0097	-9.18	0	0	0	0	0	0
5	1.0135	0.28	720	100	0	0	0	0
6	1.0114	-0.37	-76	-30	0	0	0	0
7	0.9983	-1.56	0	0	0	0	783	-418
8	1.0112	-1.96	-115	-30	0	0	0	0
9	1.0146	-5.13	-74	-30	0	0	0	0
10	1.0000	-10.60	0	0	246	-250	0	0
11	1.0153	-10.39	-108	-22	0	0	0	0
12	1.0179	-8.76	-68	-35	0	0	0	0
13	1.0244	-11.17	0	0	0	0	0	0
14	1.0073	-6.41	-80	-24	0	0	0	0
15	1.0027	-3.63	-45	-21	0	0	0	0
16	1.0061	-10.89	-15	-3	0	0	0	0
17	1.0054	-13.94	-110	-42	0	0	0	0
18	1.0167	-12.94	0	0	0	0	0	0
19	1.0120	-14.07	-66	-18	0	0	0	0
20	1.0200	-14.63	-71	-33	0	0	0	0
21	1.0279	-16.99	0	0	0	0	0	0
22	1.0295	-16.76	-12	-3	0	0	0	0
23	0.9961	-17.25	0	0	0	0	-400	-291
24	1.0098	-17.21	-13	-3	0	0	0	0
25	1.0350	-17.97	0	0	0	0	0	0
26	1.0050	-36.28	-158	-36	0	0	0	0
27	0.9995	-36.90	0	0	0	0	-20	-226
28	1.0052	-37.13	-266	-40	0	0	0	0

continued on next page

Table A.26: *continued from previous page*

Bus no.	v in pu	φ in °	P_{load} in MW	Q_{load} in Mvar	P_{gen} in MW	Q_{gen} in Mvar	P_{VSC} in MW	Q_{VSC} in Mvar
29	1.0099	-30.68	0	0	0	0	0	0
30	1.0028	-36.31	-146	-40	0	0	0	0
31	1.0050	-37.60	-338	-48	0	0	0	0
32	0.9997	-34.98	-134	-55	0	0	0	0
33	1.0172	-34.87	0	0	0	0	0	0
34	1.0136	-35.33	-216	-63	0	0	0	0
35	1.0116	-34.55	-184	-39	0	0	0	0
36	1.0000	-34.69	0	0	237	-250	0	0
37	1.0069	-36.91	-180	-76	0	0	0	0
38	1.0094	-35.67	-60	0	0	0	0	0
39	1.0062	-30.11	-212	-35	0	0	0	0
40	0.9996	-30.94	0	0	0	0	224	-181
41	1.0000	-28.33	0	0	244	-39	0	0
42	1.0000	-27.09	-284	-72	0	0	0	0
43	1.0000	-25.88	0	0	238	-250	0	0
44	1.0053	-29.98	-190	-37	0	0	0	0
45	1.0011	-31.23	-267	-44	0	0	0	0
46	0.9980	-31.66	-246	-38	0	0	0	0
47	1.0125	-31.62	-32	20	0	0	0	0
48	0.9980	-30.74	0	0	0	0	250	-282
49	1.0056	-22.79	0	0	0	0	0	0
50	1.0000	-29.88	0	0	339	-176	0	0
51	1.0145	-34.50	-172	-49	0	0	0	0
52	1.0147	-20.49	-124	-41	0	0	0	0
53	1.0209	-18.24	-40	-12	0	0	0	0
54	0.9990	-21.27	0	0	0	0	22	-477
55	1.0217	-27.60	-121	-44	0	0	0	0
56	1.0327	-21.19	0	0	0	0	0	0

continued on next page

Table A.26: *continued from previous page*

Bus no.	v in pu	φ in °	P_{load} in MW	Q_{load} in Mvar	P_{gen} in MW	Q_{gen} in Mvar	P_{VSC} in MW	Q_{VSC} in Mvar
57	0.9984	-26.82	0	0	0	0	-140	-529
58	1.0383	-24.04	-130	-63	0	0	0	0
59	1.0000	-22.87	0	0	246	-250	0	0
60	1.0241	-23.73	-46	-17	0	0	0	0
61	1.0644	-25.91	-75	-30	0	0	0	0
62	1.0544	-25.93	-128	-38	0	0	0	0
63	1.0356	-26.86	0	0	0	0	0	0
64	1.0000	-20.02	0	0	237	-250	0	0
65	1.0171	-21.95	-126	-39	0	0	0	0
66	1.0455	-23.77	0	0	0	0	0	0
67	1.0000	0.00	480	0	0	0	-480	0

B Abbreviations

B2B	back-to-back
BESS	battery energy storage system
BLP	bilevel programming
CMM	congestion management measure
C2RT	close to real-time
CSCOPF	Corrective Security Constrained Optimal Power Flow
DACF	day-ahead congestion forecast
DE	differential evolution
DMR	dedicated metallic return
ENTSO-E	European Network of Transmission System Operators for Electricity
EnWG	Energy Industry Act (German: Energiewirtschaftsgesetz)
FACTS	fast AC transmission system
GNPC	grid national power consumption
HL	high load
HVDC	high voltage direct current
HW	high wind
IDCF	intraday congestion forecast
IQR	interquartile range
IGBT	insulated-gate bipolar transistor
KAI	Kurative Ausführungsinstanz
LL	low load
LCC	line commutated converter
LP	linear programming
LW	low wind
MIP	mixed-integer programming
MINLP	mixed-integer non-linear programming
MMC	modular multi-level converter
MT	multi terminal
NERC	North American Electric Reliability Corporation
NLP	non-linear programming
GUC	grid utilization case
NR	Newton-Raphson
OHTL	overhead transmission line
OPF	Optimal Power Flow
OWF	offshore wind farm
P2P	point-to-point
PATL	permanent admissible transmission loading
pp	percentage points
pRD1	preventive redispatch 1
PSCOPF	Preventive Security Constrained Optimal Power Flow

PST phase-shifting transformer
RES renewable energy source
ROSC regional operational security coordination
SCOPF Security Constrained Optimal Power Flow
SoC state of charge
SO GL system operation guideline
SpPS special protection scheme
SSA steady-state security assessment
STATCOM static synchronous compensator
TATL temporary admissible transmission loading
TSO transmission system operator
TTC total transfer capacity
TYNDP Ten-Year Network Development Plan
UCTE Union for the Co-ordination of Transmission of Electricity
VSC voltage source converter
WAPP week ahead planning process

C Nomenclature

Sets and indices

C	Set of all contingencies
C_{cur}	Set of all curative feasible contingencies
C_{prev}	Set of all preventive feasible contingencies
C_{viol}	Set of all infeasible contingencies
$\mathcal{X}$	Set of the upper level optimization variables
$\mathcal{X}_{\text{base}}$	Set of the base case feasible upper level optimization variables
$\mathcal{X}_{\text{viol}}$	Set of all infeasible upper level optimization variables
$\mathcal{Y}$	Set of the lower level optimization variables
d, e	Nodes in the AC system
m, n	Nodes in the DC system

Symbols

$\boldsymbol{u}$	Vector of state variables
$\boldsymbol{x}$	Vector of optimization variables
$\boldsymbol{y}$	Vector of the lower level optimization variables
λ	Step-size
$\underline{I}$	Current
$\underline{S}$	Apparent power
$\underline{y}_{de}$	Admittance of branch element between bus d and e
ε	Convergence criteria for the DE algorithm
ϑ	Temperature
a_0, a_1, a_2	Parameter of generator input costs
c	Contingency in set C
C_{DC}	Network capacitance of the DC system
CR	Cross-over rate of the DE algorithm
D	Dimension of the DE algorithm
F	Mutation step-width of the DE algorithm
$F(\boldsymbol{x}, \boldsymbol{y})$	Upper level objective function
$f(\boldsymbol{x}, \boldsymbol{y})$	Lower level objective function
$G(\boldsymbol{x}, \boldsymbol{y})$	Upper level equality constraint function
$H(\boldsymbol{x}, \boldsymbol{y})$	Upper level inequality constraint function
I	Current
$it_{\min}$	Minimum number of iterations for the DE algorithm to consider convergence

$k_{\text{droop},m}$	Parameter of the linear DC voltage control
$N_{\text{dof,CSCOPF}}$	Number of available degrees of freedom for the curative actions
$N_{\text{dof,PSCOPF}}$	Number of available degrees of freedom in the base case and preventive actions
$N_{\text{dof,total}}$	Number of available degrees of freedom for the bilevel optimization problem
$N_{\text{bus(,\{AC,DC\})}}$	Number of busses (in the {AC,DC} system)
$N_{\text{cc,\{base,opt\}}}$	Number of critical contingencies in the base, optimized case
$N_{\text{feas,\{prev,cur\}}}$	Number of {preventive, curative} feasible contingency cases
N_{gen}	Number of generators
N_{load}	Number of loads
N_{OF}	Number of objective functions
NC	Number of contingencies
NP	Population size of the DE algorithm
P	Active power
Q	Reactive power
SoC	State of charge of a battery system
t	Time
v	Voltage
$v_{\text{ref},m}$	Reference voltage of the DC voltage control
w_l	Weighting factor of the lth objective function
θ_{de}	Voltage angle difference of bus d and e
b_{de}	Susceptance of branch element between bus d and e
$f(\boldsymbol{x},\boldsymbol{u})$	Objective function of an optimization problem
$g(\boldsymbol{x},\boldsymbol{u})$	Equality constraint function of an optimization problem
g_{de}	Conductance of branch element between bus d and e
$h(\boldsymbol{x},\boldsymbol{u})$	Inequality constraint function of an optimization problem

Units

A	Ampere
Hz	Hertz
kV	Kilo volt
K	Kelvin
m/s	Meters per second
MVar	Mega volt-ampere reactive
MVA	Mega volt-ampere
MWh	Mega watt hours

MW	Mega watt
pp	Percentage points
pu	Per unit
TWh	Tera watt hours
t	Ton

D List of Figures

E List of Tables

universitätsverlag *ilmenau*

Sennewald: Coordinated Determination of Preventive and Curative Actions for Congestion Management in Power Systems

The energy transition is driving significant changes in Europe's transmission systems, emphasizing HVDC technology for long-distance transmission and necessitating the optimization of existing assets with new control. This thesis introduces an innovative approach for coordinating preventive and curative congestion management in electrical power systems.

It develops a novel optimization model that integrates preventive and curative measures through a SCOPF model using bilevel programming. A specialized hybrid solver based on the Differential Evolution algorithm addresses the model's computational challenges. Case studies evaluate the impact of combining curative actions with preventive measures, explore prioritization strategies, and assess cost and computational implications.

The research offers a framework to enhance the reliability and resilience of power systems, providing a valuable tool for operators and planners to manage the dynamic energy landscape efficiently and securely.

ISSN 2194-2838
DOI 10.22032/dbt.61594